

**Design, Synthesis and Characterization of Porous Silica Nanoparticles and
Application in Intracellular Drug Delivery**

Prabhakaran Munusamy

Dissertation submitted to the faculty of the Virginia Polytechnic Institute and State
University in the partial fulfillment of the requirements for the degree of

DOCTOR OF PHILOSOPHY

In

Materials Science and Engineering

Dr. Gary R. Pickrell, Chair
Dr. Nammalwar Sriranganathan
Dr. Elankumaran Subbiah
Dr. Carlos Suchicital

June 29, 2010
Blacksburg, Virginia

Keywords: sol-gel, porous silica, nanoparticles, solubility, bio-degradability, magnetic properties,
controlled drug delivery, template surfactants, intracellular pathogens.

Design, Synthesis and Characterization of Porous Silica Nanoparticles and their Applications as Intracellular Drug Delivery Carrier

Prabhakaran Munusamy

ABSTRACT

Nanoparticle mediated drug delivery approaches provide potential opportunities for targeting and killing of intracellular bacteria. Among them, the porous silica nanoparticles deserve special attention due to their multifunctional properties such as high drug loading, controlled drug release and targeting of organs/cells. A review of the functional requirements of an ideal drug delivery system is provided. A general comparison between different drug delivery carriers and key issues to be addressed for intracellular drug delivery is discussed. Acid catalyzed and acid-base catalyzed, sol-gel derived, silica xerogel systems were investigated for sustained release of an aminoglycosides antimicrobial against salmonella infection in a mouse model. The release of gentamicin from the inner hollow part of the carrier is delayed. Further, the higher porosity of the acid–base catalyzed silica xerogel allows for high drug loading compared to the acid catalyzed silica xerogel system. Efficacy of these particles in killing intracellular bacteria (salmonella) was determined by administering three doses of porous silica loaded gentamicin. This proved to be useful in reducing the salmonella in the liver and spleen of infected mice. Furthermore, the presence of silanol groups provides the ability to functionalize the silica xerogel system with organic groups, poly (ethylene glycol) (PEG), to further increase the hydrophilicity of the silica xerogel matrix and to modify the drug release properties. Increase in the hydrophilicity of the matrix allows for faster drug release rate.

In order to facilitate controlled drug release, magnetic porous silica xerogels were fabricated by incorporating iron particles within the porous silica. The particles were fabricated using an acid-

base catalyzed sol-gel technique. The in-vitro drug release studies confirm that the release rate can be changed by the magnetic field “ON-OFF” mechanism. This novel drug release methodology combined with the property of high drug loading capacity proves to be influential in treating salmonella intracellular bacteria. The potential application of any drug delivery carrier relies on the ability to deliver the requisite drug without adversely affecting the cells over the long term. We have developed silica/calcium nanocomposites and evaluated their solubility behavior. The solubility of particles was characterized by particle size measurements for different periods of time. It was found that the solubility behaviour of the silica/calcium particles was dependent on their calcium content. The results obtained demonstrate the potential to use mesoporous silica/calcium nano-composites for drug delivery applications.

The significant contribution of this research to drug delivery technology is on design and development of the novel porous core-shell silica nano-structures. This new core-shell nano-structure combines all the above mentioned properties (high drug loading, magnetic field controlled drug release, and solubility). The main aim of preparing these porous core-shell particles is to have a control over the solubility and drug release property, which is a significant phenomenon, which has not been achieved in any other drug delivery systems. The shell layer acts as a capping agent which dissolves at a controllable rate. The rate at which the shell layer dissolves depends on the composition of the particles. This shell prevents the drug “leakage” from the particles before reaching the target site. The core layer drug loading and release rate was modified by application of a magnetic field. Additionally, inclusion of the calcium ions in the core layer destabilizes the silica network and allows the particles to dissolve at an appropriate rate (which can be controlled by the concentration of the calcium ions).

Dedications

I would like to dedicate this dissertation to Nature, Family, Friends and All.

ACKNOWLEDGEMENTS

I would like to take this opportunity to say my heart full thanks and appreciation to many people for their great support provided to me during all these years.

First of all I would like to thank my major supervisor and primary advisor Professor. Dr. Gary R. Pickrell for being a mentor, teacher and as a guide for providing me his invaluable support throughout my research program. During my research stay I learned from him about critical thinking and proper planning as most essential part of any work. I am very grateful to him for all his helpfulness and support during difficult times.

I am also very grateful to all committee members, Professor. Dr. Nammalwar Sriranganathan, Professor. Dr. Carlos Suchicital and Professor. Dr. Elankumaran Subbiah for their valuable time, ingenious suggestions, excellent support and fruitful discussions.

My sincere thanks go to Professor. Dr. Bill Reynolds for his helpful discussions, Professor. Dr. Anbo Wang and Professor. Dr. Kathleen Meehan for providing their help in using their lab for my research.

I would also like to thank my co-workers Dr. Mohamed N. Seleem, Dr. Ke Wang, Mr. Brain Scott and Dr. V.S for their friendship and help. My special thanks and gratitude goes to Dr. Mohamed N. Seleem for his valuable comments and suggestions on my thesis work. Without his collaboration, this work wouldn't have been done.

I am also thankful to all the professors and friends in the Material Science and Engineering department and Institute for Critical Technology and Applied Science (ICTAS) for all their help in my research and personally during my stay in Virginia Tech.

Finally, I would like to express my appreciation to my family and friends for their helpful support. Special thanks to my wife Shanthi for being with me through all these years and for her invaluable patience and lovable support.

I am also very thankful to my friend K. Siva Kumar who has been instrumental for me to come across many milestones in my carrier. Personally I have to thank my father, mother and sister for supporting me and providing there valuable suggestions all through my life carrier.

TABLE OF CONTENTS

Title Page.....	i
Abstract.....	ii
Acknowledgements.....	V
Table of Contents.....	Vii
List of Figures.....	XiV
List of Tables.....	XXi

CHAPTER 1:

INTRODUCTION.....	1
1.1. Introduction to nanoparticles for targeted intracellular drug delivery.....	1
1.2. Dissertation overview.....	3
1.3. References.....	6

CHAPTER 2:

LITERATURE REVIEW.....	9
2.1 Functional requirements of drug delivery system.....	9
2.2 Classification of drug delivery materials.....	10
2.3 Design criteria of drug delivery carriers.....	13
2.3.1. Key issues in intracellular drug delivery.....	14
2.3.1.1. Particles size and shape.....	14

2.3.1.2.	Surface functionalization and zeta potential.....	15
2.3.1.3.	Biocompatibility and toxicity.....	16
2.3.1.4.	Controlled drug release.....	17
2.4	Silica nanoparticles as drug delivery carriers.....	19
2.5	Sol-gel derived porous silica drug delivery systems.....	27
2.6	References.....	32

CHAPTER 3:

TARGETED DRUG DELIVERY USING SILICA XEROGEL SYSTEMS TO TREAT DISEASES DUE TO INTRACELLULAR PATHOGENS..... 44

3.1	Abstract.....	44
3.2	Introduction.....	46
3.3	Experimental procedure.....	48
3.3.1	Preparation of sol-gel processed silica xerogel particles.....	48
3.4	Characterization.....	49
3.4.1	In-vitro drug release.....	49
3.4.2	Bacterial strain.....	50
3.4.3	Animal experiment (in-vivo infection assay).....	50
3.4.4	Histopathological effects of injected silica xerogel.....	51
3.4.5	Statistical analysis.....	51
3.5	Results.....	52
3.5.1	In-vivo infection assay.....	58
3.5.2	Histopathological effects of injected silica xerogel.....	59
3.6	Discussion.....	60

3.7	Conclusion.....	65
3.8	References.....	66

CHAPTER 4

SILICA-ANTIBIOTIC HYBRID NANOPARTICLES FOR TARGETING

INTRACELLULAR PATHOGENS..... 70

4.1	Abstract.....	70
4.2	Introduction.....	71
4.3	Materials and Methods.....	73
4.3.1	Preparation of antibiotics loaded xerogel and xerogel/PEG.....	73
4.3.2	Synthesis of fluorescein isothiocyanate-labeled porous silica materials.....	75
4.3.3	Cell culture and localization of xerogel FITC.....	75
4.4	Characterization and Instrumentation.....	76
4.4.1	In-vitro drug release of gentamicin.....	76
4.4.2	Drug release assay.....	77
4.4.3	Bacterial strain.....	77
4.4.4	Animal experiment (in-vivo infection assay).....	77
4.4.5	Statistical analysis.....	78
4.5	Results.....	79
4.5.1	Characterization of silica xerogels.....	79
4.5.2	Infrared spectroscopy analysis.....	79
4.5.3	N ₂ adsorption-desorption isotherm analysis.....	82
4.5.4	Scanning and transmission electron microscopy.....	82

4.5.5	Thermogravimetry analysis.....	83
4.5.6	<i>In vitro</i> release studies of entrapped gentamicin from xerogel and xerogel/PEG matrix.....	85
4.5.7	In-vivo infection assay.....	89
4.6	Discussion.....	90
4.7	References.....	94

CHAPTER 5

SYNTHESIS AND CHARACTERIZATION OF MAGNETIC SILICA XEROGELS CONTAINING ANTIMICROBIALS FOR TARGETING INTRACELLULAR PATHOGENS.....98

5.1	Abstract.....	98
5.2	Introduction.....	100
5.3	Experimental Details.....	102
5.3.1	Preparation of sol-gel processed magnetic silica xerogel particles.....	102
5.3.2	Synthesis of FITC-labeled porous magnetic silica xerogels particles.....	102
5.3.3	Cell culture and localization of magnetic silica xerogel-FITC.....	103
5.4	Characterization.....	104
5.4.1	Bacterial strain.....	104
5.4.2	Animal experiment (in-vivo infection assay).....	105
5.4.3	Statistical analysis.....	105
5.5	Results and Discussion.....	106
5.5.1	Magnetic field controlled drug release.....	114

5.5.2	Mechanism of magnetic-sensitive drug release behaviour.....	118
5.5.3	In-vivo infection assay.....	120
5.6	Conclusion.....	122
5.7	References and Notes.....	123

CHAPTER 6

IN-VITRO SOLUBILITY BEHAVIOUR OF MESOPOROUS SILICA/CALCIUM NANOCOMPOSITES FOR DRUG DELIVERY APPLICATIONS..... 123

6.1	Abstract.....	123
6.2	Introduction.....	124
6.3	Experimental procedure.....	126
6.3.1	Synthesis of mesoporous silica/calcium nano-composite.....	126
6.3.2	Characterization of mesoporous silica/calcium nano-composite.....	126
6.3.3	Solubility test: weight loss and pH measurements.....	131
6.3.4	MTS cell viability assay.....	128
6.4	Results.....	129
6.4.1	Cytotoxicity results.....	140
6.5	Discussion.....	142
6.6	Conclusion.....	145
6.7	References.....	146

CHAPTER 7

INFLUENCE OF TEMPLATE CONCENTRATION ON TEXTURE

PROPERTIES AND CONTROLLED DRUG RELEASE..... 151

7.1	Abstract.....	151
7.2	Introduction.....	152
7.3	Experimental procedure.....	153
	7.3.1 Synthesis of mesoporous silica nanoparticles.....	154
	7.3.2 Characterization of mesoporous silica nanoparticles.....	154
	7.3.3 Drug loading and drug release studies.....	155
	7.3.4 Cell culture and localization of mesoporous silica nanoparticles.....	156
7.4	Results and discussion.....	157
7.5	Conclusion.....	166
7.6	References.....	167

CHAPTER 8

MULTIFUNCTIONAL SILICA NANOCOMPOSITES FOR DRUG

DELIVERY APPLICATIONS..... 170

8.1	Abstract.....	170
8.2	Introduction.....	171
8.3	Experimental section.....	173
	8.3.1 Synthesis of silica/calcium/iron nano-composites.....	173
	8.3.2 Synthesis of core-shell silica/calcium/iron nano-composite	174

8.3.3	Drug storage studies.....	174
8.3.4	Magnetic field controlled drug release studies.....	175
8.3.5	Magnetic field controlled solubility studies.....	175
8.3.6	Characterization of magnetic mesoporous silica/calcium/iron.....	176
	nano-composite	
8.4	Results and discussion.....	178
8.5	Conclusion.....	188
8.6	References.....	189

CHAPTER 9

GENERAL CONCLUSIONS.....	192
---------------------------------	------------

APPENDIX: List of abbreviations.....	195
---	------------

LIST OF FIGURES

Chapter 2

Figure 2.1. Porous silica nano-device for imaging, magnetically controlling, and in-situ monitoring drug release. 21

(a) Coating with bio-degradable polymer/liposome allows for facile inclusion within the cells,

(b) Attachment of targeting moieties takes the nano-device towards the target site.

(c) Optical probe allows for non-invasive imaging of the nano-device site.

(d) Drug release rate within the target site can be modulated by magnetic field control.

Figure 2.2. Schematic representation of sol-gel synthesis of silica nanoparticles. 23

Initial hydrolysis steps leads to the formation of silicon alkoxide which undergoes further synthesis steps for formation of silica nanoparticles. Depending on the stage and process of drying a xerogel monolith or silica thin film can be formed.

Chapter 3

Figure 3.1. X-ray diffraction pattern of porous silica xerogel. 52

Figure 3.2. The N₂ adsorption-desorption isotherm of silica xerogel (volume of nitrogen as a function of relative pressure P/P_0). The isotherm features are typical for a type I isotherm (BDDT classification³¹) characteristic of a micro porous solid, that is, a solid with a large number of pores having radii equal to or below 2 nm. 54

Figure 3.3 Scanning electron micrographs of the prepared silica gel xerogels at (A) lower and (B) higher magnifications. The highly porous silica xerogel appears as a dense material with fine structure. 55

Figure 3.4. TG curves of (A) pure porous silica matrix and (B) porous silica matrix entrapped with gentamicin. 56

Figure 3.5. Gentamicin release from porous silica matrix as a function of immersion time in PBS.	57
Figure 3.6. EDX spectra of silica xerogel synthesized by acid catalysis process	58
Figure 3.7. Part of cumulative release versus square root of time.	63
 Chapter 4	
Figure 4.1. FTIR Spectra of silica xerogel and silica xerogel/PEG.	80
Figure 4.2. SEM images of (A) silica xerogel, (B) silica xerogel/PEG complex	82
Figure 4.3. TEM image of silica xerogel showing the agglomerations of spherical-like nanoparticle and disordered framework pores.	83
Figure 4.4. TGA curves of the silica xerogel/drug and silica xerogel/PEG–drug systems.	84
Figure 4.5. Cumulative release of gentamicin from silica xerogel and silica xerogel-PEG complex. In vitro release profiles of gentamicin immobilized in the silica xerogel and that in the xerogel-PEG matrix showed a higher release rate followed by a slower, steady release. There was a sustained release of gentamicin (57% in 33 h) from the silica xerogel network, while with the addition of 2% PEG, the gentamicin release rate reached 90% in 33 h.	85
Figure 4.6. (A) Cumulative release of gentamicin (Q) versus square root time profile (Higuchi model), (B) First-order plot of gentamicin released versus time.	86
Figure 4.7. Confocal fluorescence images of macrophage cells loaded with the (A) silica xerogel-FITC, (B) silica xerogel/PEG. (Left) transmitted image of cell lines, (Right) endocytosed green fluorescent image of silica xerogel particles.	88

Chapter 5

- Figure 5.1. Acid-base catalyzed magnetic silica xerogel monolith. 106
- Figure 5.2. X-ray diffraction patterns of porous silica 107
xerogels/iron complex. No diffraction peaks except for the broad band
assigned to the characteristic reflection of amorphous SiO₂ can be found ($2\theta = 22^\circ$).
- Figure 5.3. FTIR spectra for the (a) silica xerogel and (b) silica xerogel /iron 108
oxide complex. The group of bands observed corresponds well with the band
positions for silica xerogel. The smaller shoulder bands observed around 550 to
650 cm⁻¹ are assignable to Fe-O bonds in Fe-O-Fe systems.
- Figure 5.4. EDX pattern of Fe/silica xerogel particles 109
- Figure 5.5. High-magnification scanning electron micrographs for acid-base 110
catalyzed porous silica xerogel/iron oxide complex. The globular morphology
with the clusters of agglomerates is seen. The mesoporous result from organized
packing of globules in to large clusters.
- Figure 5.6. Nitrogen adsorption-desorption isotherms for acid-base catalyzed 111
silica xerogels. The lower adsorption pressure and gradual increase in
adsorption with increasing relative pressure which are characteristic for type
IV isotherm indicates less microporosity and broader distribution of larger pores
which are in the range of ~ 1 to 50nm.
- Figure 5.7. Pore distributions determined from the isotherms for 112
acid- base-catalyzed xerogel. Pore size distribution with average pore diameter
of ~173 Å (17.3nm). The shape of this distribution is consistent with a

microstructure composed of micropores and mesopores.

Figure 5.8. Confocal image of magnetic silica xerogel particles in macrophage cells after 1 h of uptake time; particles are tagged with FITC (green). 114

Figure 5.9. Cumulative drug release profile from magnetically controlled porous silica xerogel/Fe particles and the control group of silica xerogel particles without magnetic simulation. (Red line- Drug release profile from silica xerogel/Fe complex with magnetic simulation, Black line- Control group of silica xerogel/Fe complex without magnetic simulation). Drug loaded silica xerogel/Fe were actuated by applying magnetic field. Increase in the amount of drug release was observed in presence of magnetic excitation. 116

Figure 5.10. Mechanism for drug release from porous silica xerogel/Fe matrix. 118

During the application of the magnetic field, the silica matrix may undergo a structural change. The structural change (rearrangement of the particles in confined space) allows for open configuration of the silica xerogel/Fe complex which allows higher drug release.

Chapter 6

Figure 6.1. XRD pattern of silica/calcium nano-composites of different concentrations (a) silica/calcium-50/50, (b) silica/calcium-60/40 and (c) silica/calcium-90/10. 129

Figure 6.2. SEM image of silica/calcium nanocomposites 130

Figure 6.3. N₂ adsorption-desorption isotherm (A) measurements for (a) silica/calcium- 50/50, (b) silica/calcium- 60/40 and silica/calcium- 90/10 132

compositions and (B) pore size distribution.

Figure 6.4. EDX analysis for silica /calcium nano-composites, Inset- EDX 133

mapping analysis for silica/calcium-60/40 composition.

Figure 6.5. FTIR spectra for silica/calcium nano-composites. 135

Figure 6.6. Particle size measurements after solubility testing for 136

silica-calcium nano-composites. (a) Silica/Calcium -50/50, (b) Silica/Calcium-60/40,
(c) Silica/Calcium- 90/10.

Figure 6.7. N₂ adsorption isotherm measurements for silica-calcium 137

compositions before and after immersion in water.

Figure 6.8. Pore size distribution for silica/calcium compositions (A) 90-10 and 138

(B) 50-50 before and after immersion in water for two days.

Figure 6.9. Plot for weight loss percentage to dissolution time for 140

silica-calcium compositions. (a) Si/Ca -50/50, (b) Si/Ca-60/40, (c) Si/Ca- 90/10.

Figure 6.10 MTS assay of the cells incubated with silica/calcium 141

nano-composites (50/50 and 90/10) at a concentration of 15µg and 30µg.

Figure 6.11 Schematic representation of silica dissolution. (A) Silica network 143

modified and interrupted by Ca²⁺ ions which up on immersion in water gets
susceptible to nucleophilic attack and exchanges weakly bonded, network-modifying
Ca²⁺ for protons. (B) Further nucleophilic attack primarily by OH⁻ groups in water,
structurally deforms [SiO₄]₄ tetrahedral to five-coordinated intermediate which
further breaks down to Si(OH)₄.

Chapter 7

- Figure 7.1. (a) Molecular structure of ciprofloxacin, (b) Molecular structure of Cetyl trimethylammonium bromide (CTAB) (16 carbon chain). 153
- Figure 7.2. SEM image of mesoporous silica particles (MSN1). These materials are spherical particles with diameter in the range of 100-150nm. 157
- Figure 7.3. TEM image of mesoporous silica nanoparticles (MSN1). 158
- Figure 7.4. FTIR spectra of ciprofloxacin drug (a), MSN1-ciprofloxacin (b), MSN2-ciprofloxacin (c). 159
- Figure 7.5. TG curves of (A and B) Empty MSN1 and MSN2, (C and D) mesoporous silica nanoparticles MSN1 and MSN2 encapsulating ciprofloxacin drug. 160
- Figure 7.6. Nitrogen adsorption/desorption isotherms (A) and corresponding pore size distribution (B). MSN1-(a) and MSN2-(b). 161
- Figure 7.7. Cumulative release profiles for ciprofloxacin loaded on mesoporous silica particles of (a) MSN1, (b) MSN2. 164
- Figure 7.8. (Left) transmitted image of cell lines, (Right) endocytosed green fluorescent image of MSN/FITC. 165

Chapter 8

- Scheme 8.1. Mechanism for formation of mesoporous silica/calcium/iron nano-composites. Step 1: Surfactant molecules cluster together to form micelles, as their hydrophobic tails tend to congregate and their hydrophilic heads provide protection in water, Step 2: Addition of inorganic precursor materials (TEOS, calcium and iron) gets deposited on the surface of surfactant micelles and 179

condense to form -Si-O-Ca-O-Fe-O inorganic network. Step 3: Surface coating of mesosphere silica/calcium/iron with another layer silica/calcium/iron. The presence of silanol groups on the core particles facilitates further coating on the surface of inner core particles.

Figure 8.2 FTIR spectra for silica/calcium/iron nano-composites mesoporous silica (a), 181
mesoporous silica/calcium/iron-gentamicin (b), mesoporous silica/calcium/iron (c),
and neat gentamicin (d).

Figure 8.3. Nitrogen adsorption/desorption isotherms of (a) MSN1, (b) MSN2 183
and (c) drug-loaded MSN1 samples, pore size distribution of (a) MSN1, and (b) MSN2.

Figure 8.4. Particles size measurements for MSN2 particles. The solubility 185
of the particles was investigated with and without exposure of magnetic field.

Figure 8.5. Cumulative release of gentamicin drug from mesoporous 187
silica/calcium/iron nano-composites. The drug release rate was altered by exposing
the magnetic field to the particles. As a control group, the same particle without
magnetic simulation was shown. The particles exposed to magnetic field shows faster
drug release.

LIST OF TABLES

Chapter 2

Table 2.1.	The advantages and disadvantages of drug delivery carrier	12
------------	---	----

Chapter 3

Table 3.1.	Pore parameters of porous silica xerogels before and after adsorption of drug.	53
Table 3.2.	Efficacy of three doses of Silica xerogel –loaded gentamicin against infection with <i>Salmonella typhimurium</i> TL2 administered intraperitoneally.	59

Chapter 4

Table 4.1.	The structural parameters of the silica xerogel and silica xerogel/PEG.	81
Table 4.2.	Correlation coefficients of different mathematical models for gentamicin -loaded silica and PEG/silica xerogels.	88
Table 4.3.	Efficacy of two doses of Silica-antibiotic hybrid against infection with <i>S.typhimurium</i> .	89

Chapter 5

Table 5.1.	Physical properties of porous silica xerogel and Fe/Silica xerogel from N ₂ adsorption-desorption isotherms, ^a Calculated by the BJH method.	113
Table 5.2.	Efficacy of two doses of Silica-antibiotic hybrid against infection \with <i>S.typhimurium</i>	119

Chapter 6

Table 6.1.	Textural properties of mesoporous silica-calcium compositions	132
Table 6.2.	Textural properties of silica-calcium compositions after immersion in water	138

Chapter 7

Table 7.1.	Structure parameters of mesoporous silica nanoparticles (MSN1 and MSN2).	163
Table 7.2.	Structure parameters of mesoporous silica nanoparticles (MSN1 and MSN2) after drug loading.	163

Chapter 8

Table 8.1.	Textural parameters of MSN1, MSN2 and gentamicin drug loaded MSN1 particles.	184
------------	--	-----

CHAPTER 1

INTRODUCTION

1.1. Nano-particle mediated controlled drug delivery

Drug delivery systems metamorphosized from the life of leaves, barks and roots of plants to present-day controlled-release systems (CRS) gradually [3]. This became centric to many modern new drug discoveries with large molecular sizes, higher dose sensitivities, and often poor stabilities in biological environments. This necessitates newer methods for the development of efficient encapsulation and new controlled-release technologies.

CRS gained considerable interest and special attention due to better clinical efficacy and patient compliance. In addition, economical considerations played a vital role, since CRS could decrease the frequency and cost of administrating the drug [4, 5], the drive for creating new versatile and high performance systems. Controlled drug release technology (CRT) is the most advancing and fastest growing area in the pharmaceutical market in US with 10% annual growth, approximately [5].

Controlled drug delivery technology (CRT)

As used in this context, controlled drug delivery (CDD) means that a remote control can be exercised over the rate at which the drug is being released. It is not only limited to the drug release rate, but would also imply that the control over the delivery of drug at specific target site (specific location/organs). Hence, CDD is a method to control the distribution of the drug both in space and time [6, 7, 8].

Nanoparticles as drug delivery carrier

The main advantage of the CDD system is the increased efficacy of the drug achieved by controlling the drug concentration in the body within the optimum therapeutic range and avoiding systemic toxicity. Most of the commercially available drugs in the market are labeled toxic due to their indiscriminate delivery and killing of normal flora. The non-selective partitioning of the drug between healthy and diseased cells can be overcome by nano-particle mediated drug delivery. Nanoparticle mediated drug delivery utilize particles in the nanometer size range and the optimum size of particle differs based on the type of administration and the targeted organs or cells.

Numerous materials including liposomes, micelles (polymers), and dendrimers have been designed, developed and tested as nanoparticle mediated drug delivery systems [9, 10, 11, 12]. Although each of them offers unique properties and advantages, several characteristics limit their potential use as ideal drug-delivery carriers. Liposome's and micelles are limited due to their poor chemical stability which restricts their route of administration and a self-life. The ability to design micelles and liposomes to achieve control over the drug release rate is also limited [13, 14, 15]. The other major hurdle is the toxic effects of *in-vivo* degradation products, specifically with synthetic polymers [16, 17]. Natural polymers such as chitosan and agar, lack control over monomer purity limiting their release profiles reproducibility.

In contrast to organic systems, inorganic materials including amorphous silica provide numerous advantages for use as controlled drug delivery carriers [18, 19]. Hence, the main goal of this research was to design and develop a porous silica nanoparticle system for intracellular drug delivery applications that can provide the requisite drug loading, allow for magnetically controlled drug release, and allow for dissolution of the particles after drug delivery. Amorphous

silica is non-toxic, and is used regularly in food additives and as components in vitamin supplements [20]. Additionally, the biocompatibility of silica particles has been shown by encapsulating enzymes, bacteria and mammalian cells within the porous silica. The metabolic activities of silica encapsulated bacteria and cells were retained their normal activity which confirmed the high compatibility of silica with biological systems [21, 22, 23]. Further, the silanol groups on the surface of silica provide easy functionalization for a wide variety of targeting applications [24, 25] and required functional properties can be imparted using sol-gel technology [26, 27]. Furthermore our research aims to improve the silica nanoparticle as efficient drug delivery carrier. The results of this research are likely to yield new insights into the intracellular drug delivery technology.

The specific objectives of this research are to:

1. Design highly porous silica nanoparticles for high drug loading capacity.
2. Design a magnetic field controlled drug release system.
3. Design and develop a degradable silica nanoparticle system.

1.2. Dissertation Organization

There are 9 chapters in this dissertation. Chapter 1 gives brief introduction to nanoparticles mediated drug delivery. Chapter 2 is a detailed literature review section, where the first part is about functional requirements and design criteria of the drug delivery carriers. The second part discusses silica nanoparticles and their applications as drug delivery carrier. Chapters 3 to 6 and chapter 8 are journal articles; where chapters 3, 4, 5 are already published. The chapter 6 and 8 has been submitted for publication and final chapter 9 gives the overall conclusions and significance of the research done in this dissertation. Future research directions are also included.

The second chapter gives a review of nanoparticles used for drug delivery applications. The main focus is on detailing the design criteria and key issues to be followed for developing a drug delivery carrier. The second part of this chapter includes the fundamentals of sol-gel process, synthesis of silica nanoparticles by template and non-templating sol-gel approach, and putting together potential applications of porous silica nanoparticles in content of platform for new intracellular drug delivery carrier. Chapter 3 is a study on the synthesis and applications of a silica xerogel system as drug delivery vehicle. Characterization of the silica xerogel is also provided in terms of porosity and drug release. The application of this carrier was successfully demonstrated in the treatment of *Salmonella* bacteria in the mouse model.

Chapter 4 discusses two different silica nanoparticle systems. Influence of the sol-gel synthesis conditions, specifically the pH, on porosity was determined. Another novel feature of this system is the surface functionalization of the particles proved to be useful in modifying the drug release rate. The high loading and efficient release is useful in intracellular drug delivery applications. The efficacy of this silica nanoparticle system was tested against *Salmonella* bacteria by *in-vivo* studies.

One of the important criteria for any drug delivery carrier is to release the drug in a time- and site controlled fashion. In Chapter 5, design and characterization of magnetic porous silica nanoparticles is discussed. The attractive property of this material is the stimuli-response controlled release by an externally applied magnetic field. The efficacy of these particles is tested successfully in *in-vivo* mice studies against salmonella.

Solubility or bio-degradation at a required rate is an important aspect of a drug delivery carrier. Chapter 6 mainly discusses about modifying the structure-property of silica nanoparticles

to provide controlled solubility. Addition of modifying cations, such as Ca^{2+} , proves to be useful in controlling the solubility rate.

Though many different nanomaterials are being investigated for drug delivery applications, silica nanoparticle offers the advantage that they can be engineered to provide multifunctional properties, such as targeting, imaging and controlled drug release. Chapter 8 discusses the synthesis and characterization of the core-shell silica/Ca/Fe nano-composite particles. The core-shell particles were designed to provide multifunctional properties such as magnetic field controlled drug release, controlled solubility and control over the drug release until reaching their target site. The particles were characterized in terms of solubility of shell layer to control drug release, and application of magnetic field to regulate the drug release rate.

Chapter 9 provides the overall general conclusions and potential future directions.

1.3. References

- [1] R. C. Srimol, B. N. Dhawan.1973. Pharmacology of Diferuloyl Methane (Cur cumin). A Non-steroidal Anti-inflammatory Agent. *J. Pharm. Pharmacol.* **25**: 447-452.
- [2] J. R. Robinson. In *Controlled drug delivery* (Ed: K. Park), ACS, Washington DC 1997, ch.1.
- [3] A. C. Ross, R. J. MacRae, M. Walther, H.N.Stevens.2000.Chronopharmaceutical drug delivery from a pulsatile capsule device based on programmable erosion. *J. Pharm Pharmacol.* **52**: 903-909.
- [4] D. L. Wise, *Handbook of Pharmaceutical Controlled Release Technology*, 2000.
- [5] S. K. Sahoo, V. Labhasetwar. 2003. Drug discovery today. **24**: 1112.
- [6] D. R. Radu, C. Y. Lai, K. Jeftinija, E. W. Rowe, S. Jeftinija, V.S.-Y.Lin. 2004. A polyamidoamine Dendrimer-Capped Mesoporous Silica Nanosphere-Based Gene Transfection Reagent. *J. Am. Chem. Soc.* **126**: 13216-13217.
- [7] J. K. Vasir, M. K. Reddy, V. D. Labhasetwar. 2005. Nanosystems in drug targeting: opportunities and challenges. *Curr. Nanosci.* **1**: 47–64.
- [8] R. Gref, P. Couvreur. Nanocapsules: preparation, characterization and therapeutic applications, in: V.P. Torchilin (Ed.), *Nanoparticulates as Drug Carriers*, Imperial College Press, London, 2006, pp. 255–276.
- [9] T. C. Whitehead, A. M. Lovering, I. M. Cropley, P. Wade, R. N. Davidson. 1998. Kinetics and toxicity of liposomal and conventional amikacin in a patient with multidrug-resistant tuberculosis. *Eur. J. Clin. Microbiol. Infect. Dis.* **17**: 794–797.
- [10] H. Pinto-Alphandary, A. Andremont, P. Couvreur. 2000. Targeted delivery of antibiotics using liposomes and nanoparticles: research and applications. *Int. J. Antimicrob. Agents.* **13**: 155–168.

- [11] S. Prior, C. Gamazo, J. M. Irache, H. P. Merkle, B. Gander. 2000. Gentamicin encapsulation in PLA/PLGA microspheres in view of treating Brucella infections. *Int. J. Pharm.* **196**: 115–125.
- [12] T. Dutta, N. K. Jain, N. A. J. McMillan, H. S. Parekh. 2010. Dendrimer nanocarriers as versatile vectors in gene delivery. *Nanomedicine: Nanotechnology, Biology and Medicine.* **6**: 25-34.
- [13] A. Martini, C. Ciocca. 2003. Drug delivery system for cancer drugs. *Expert Opin. Ther. Patents.* **13**: 1801-1807.
- [14] D. L. Emerson. 2000. Liposomal delivery of camptothecins. *Pharm. Sci. Technol. Today.* **3**: 205-209.
- [15] C. Oussoren, G. Storm. 2001. Liposomes to target the lymphatic's by subcutaneous administration. *Adv. Drug Delivery Rev.* **47**: 143-156.
- [16] P. Couvreur, C. Dubernet, F. Puisieux. 1995. Controlled drug delivery with nanoparticles Current possibilities and future trends. *Eur. J. Pharm. Biopharm.* **41**: 2-13.
- [17] R. Abu-Rmaileh, D. Attwood, A. D'Emanuelle. 2003. *Drug Delivery Syst. Sci.* **3**: 65-68.
- [18] C. Barbé, J. Bartlett, L. Kong, K. Finnie, H. Q. Lin, M. Larkin, S. Calleja, A. Bush, G. Calleja. 2004. Silica particles: A novel drug delivery system. **16**: 1959-1966.
- [19] S. H. Hu, K. T. Kuo, W. L. Tung, D. M. Liu, S. Y. Chen. 2009. A Multifunctional Nano-device Capable of Imaging, Magnetically Controlling, and In Situ Monitoring Drug Release. **19**: 3396-3403.
- [20] http://en.wikipedia.org/wiki/Silicon_dioxide.
- [21] K. S. Finnie, J. R. Bartlett, J. L. Woolfrey. 2000. Encapsulation of sulfate-reducing bacteria in a silica host. *J. Mater. Chem.* **10**: 1099-1101.

- [22] I. Gill, A. Ballesteros. 1998. Encapsulation of biologicals within silicate, siloxane, and hybrid sol-gel polymers: an efficient and generic approach. *Journal of the American Chemical Society*. **120**: 8587-8598.
- [23] S. Boninsegna, P. Bosetti, G. Carturan, G. Dellagiacomma, R. Dal Monte, M. Rossi. 2003. *Journal of Biotechnology*. **100**:277-286.
- [24] M. Tsotsalas, M. Busby, E. Gianolio, S. Aime, L. De Cola. 2008. *Chem. Mater.* **20**: 5888-5893.
- [25] J. Andersson, J. Rosenholm, S. Areva, M. Lindn. 2004. *Chem. Mater.* **16**: 4160-4167.
- [26] G.W. Scherer, C.J. Brinker, *Sol-gel science*, Academic press, New York 1990.
- [27] I.I. Slowing, J.L. Vivero-Escoto, C.W. Wu, V.S.-Y. Lin. 2008. Mesoporous silica nanoparticles as controlled release drug delivery and gene transfection carriers. *Advanced Drug Delivery Reviews*. **60**: 1278–1288.

CHAPTER 2

LITERATURE REVIEW

2.1 Functional requirements of a drug delivery system to treat intracellular pathogens

For treating intracellular pathogens, several prerequisites of a material need to be incorporated.

This can be divided into nine carrier requirements [1-15].

- 1) Biocompatibility: The material should be biocompatible.
- 2) Drug loading capacity: High loading/encapsulation of desired drug molecules.
- 3) Controlled drug release: Controlled release of drug molecules with a proper rate of release to achieve therapeutic levels at the site of infection over long periods of time. Zero premature release, i.e., no leaking of drug molecules under *in-vivo* conditions.
- 4) Drug toxicity: Must be able to increase the therapeutic index of the drug, decreasing its toxicity and maintaining its therapeutic efficacy [15-16]. The therapeutic index (also known as therapeutic ratio), is a comparison of the amount of a therapeutic agent that causes the therapeutic effect to the amount that causes death.
- 5) Site directing ability: Once in the bloodstream, they must be rapidly recognized and withdrawn from the circulation by the phagocytic cells, where the pathogen is located and to reach elevated drug concentrations in the target cells [17-18].
- 6) Size and Shape: Should be more than 200 nm as sizes lower than this may escape phagocytosis. For microspheres, the maximum phagocytosis was observed when the size range was between 1-2 μm [14, 20].

7) Surface functionalization and zeta potential: Surface functionalisation helps to target specific cell types and even the nucleus. This, in general, involves multi-modification, multi-component loading and/or multicomponent combination into one species. While the Zeta potential, as a critical parameter, indicates the strength of the electrostatic interaction [13, 21].

2.2 Classification of drug delivery materials

Many drug delivery carriers have been developed and studied extensively and can be generally classified into three major groups: viral carriers, liposomes, polymer particles and inorganic nanoparticles. The advantages and disadvantages of each carrier type are listed in Table 2.1.

Viral carriers: A part of the original gene segment is eliminated to leave space for the gene to be inserted and delivered [22, 23]. A variety of viruses including cowpea mosaic virus, cowpea chlorotic mottle virus, canine parvovirus, and bacteriophages have been developed for biomedical and nanotechnology applications that include tissue targeting and drug delivery. A number of targeting molecules and peptides can be displayed in a biologically functional form on their capsid surface using chemical or genetic means. Therefore, several ligands or antibodies including transferrin, folic acid, and single-chain antibodies have been conjugated to viruses for specific tumor targeting *in-vivo* [110].

Liposome: are the microscopic vesicles composed of one or more concentric lipid bilayers, separated by water or aqueous buffer compartments with a diameter ranging from 25 nm to 100 μm . According to their size, liposomes are known as Small Unilamellar Vesicles (SUV) (10-100 nm) or Large Unilamellar Vesicles (LUV) (100-3000 nm). If more than one bilayer is present, then they are referred to as Multilamellar Vesicles (MUV). Liposomes are formed when thin

lipid films or lipid cakes are hydrated and stacks of liquid crystalline bilayers become fluid and swell. During agitation hydrated lipid sheets detach and self associate to form vesicles, which prevent interaction of water with the hydrocarbon core of the bi-layer at the edges [24-26].

Polymeric Nanoparticles: Colloidal carriers based on biodegradable and biocompatible polymeric systems have largely influenced the controlled and targeted drug delivery concept. Nanoparticles are sub-nanosized colloidal structures composed of synthetic or semi-synthetic polymers that vary in size from 10-1000 nm. Biodegradable polymeric nanoparticles, typically consisting of polylactic acid (PLA), polyglycolic acid (PGA), polylactic- glycolic acid (PLGA), and polymethyl methacrylate (PMMA) are being investigated for the delivery of proteins, genes and DNA [27-31]. Polymers such as albumin, chitosan, and heparin occur naturally and have been a material of choice for the delivery of oligonucleotides, DNA, and protein, as well as drugs. Recently, a nanoparticle formulation of paclitaxel, in which serum albumin is included as a carrier nanometer-sized albumin-bound paclitaxel (Abraxane has been applied in the clinic for the treatment of metastatic breast cancer). Besides metastatic breast cancer, Abraxane has also been evaluated in clinical trials involving many other cancers including non-small-cell lung cancer (phase II trial) and advanced nonhematologic malignancies (phase I and pharmacokinetics trials) [110]. Recently, pluronic based core-shell polymer nanostructures encapsulating gentamicin have been designed for treatment of Salmonella bacteria [111].

Inorganic nanoparticles: Inorganic nanoparticles as new non-viral carriers have attracted much attention, only recently. Inorganic nanoparticles generally possess versatile properties suitable for cellular delivery, including wide availability, rich functionality, good biocompatibility, potential capability of targeted delivery (e.g. selectively destroying cancer cells but sparing normal tissues) and controlled release of carried drugs. These particles provide the complete

protection to the entrapped molecules such as proteins, enzymes and drugs against the denaturizing effects of external pH and temperature [10, 32-35].

The major advantages of ‘sol gel silica’ compared to other carrier type are: a) Sol gel processed silica can form a highly porous network based on the appropriate preparation conditions, which can have high drug loading capacity up to 90% in the case of aerogels [36, 37] and b) general functional requirements like size, charge, surface property etc can be fulfilled by the sol-gel processing of silica. However, achieving the combined requirements is still a challenge for material scientists.

Table 2.1.The advantages and disadvantages of drug delivery carriers [110,111, 33].

Carrier Type	State of Art	Advantages	Disadvantages
Viral	Clinical trials	Highly efficient	Expensive Immunogenicity
Cationic Compounds	Commercial	Easily prepared	High toxicity Low drug loading
Inorganic silica nanoparticles	Laboratory	Low toxicity High loading Easily Prepared Size controllable Ready functionality	Low efficiency

2.3 Design criteria of drug delivery carriers for treating intracellular pathogens

Proper functional requirements are the key to meet the demands of an intracellular drug delivery. Silica generally possesses versatile properties suitable for the intracellular controlled delivery of drugs such as wide availability, rich functionality, good biocompatibility and the potential capability of targeted delivery. Therefore, high loading/encapsulation of the desired drug molecules and controlled/sustained release of the drug molecules with a proper rate of release are a high priority for a drug delivery carrier design. By developing a method which possesses high drug loading capacity and sustained drug delivery rate, the effective delivery of the required dosage of the appropriate drug can be achieved to target a specific disease causing bacteria. This method of effective delivery of the required drug within the cells may allow us to achieve an effective local concentration, while at the same time increase the amount of drug delivered to the specific bacteria.

Drug delivery carrier design is generally based on the properties of the particular carrier system. The properties of the drug delivery carrier include hydrophobicity, surface charge, size and loading capacity. Hydrophobicity, charge and functionalization are referred to as the surface property in drug delivery systems. The functionalisation or modification depends, to a large degree, on the types of nanoparticles that provide specific functional groups on the surface. In section 2.3.1 a more detailed exposition of these considerations is presented.

2.3.1. Key issues in intracellular drug delivery using nanoparticles

2.3.1.1. Particle size and shape

The size of the particles used in drug delivery range from 50 nm to 2-3 μm in size. The suggested size in treating intracellular pathogens is >200 nm. Sizes lower than this may escape the phagocytosis process. In the case of microspheres, the maximum phagocytosis occurred in size range between 1-2 microns [47-52]. There is no clear conclusion as to what size is the most suitable for cellular uptake without disrupting the cytoskeleton structure and cytochemistry in human tissue. This issue has not been resolved yet in the literature. The silica particles of the size range around 200 nm have been used in gene transfection in a DNA-transfection agent-silica tertiary system. Radu et.al[53, 54] reported using silica as gene-delivery system attached with polyamidoamine dendrimers, the size of these particles were greater than 200-300 nm and higher transfection efficiency was observed with these particles in neural glial cells, human cervical cancer cells, and Chinese hamster ovarian cells. Volker et.al [55] reported about using polymer nanoparticles made of polyhexylcyanoacrylate(PHCA) or human serum albumin with a diameter of 200 nm for targeting antiviral substances such as azidothymidine to macrophages[55].

In addition to the particle size, the other important property which can mediate the phagocytic process is the particle shape. The particle shapes such as spherical, tubular, sheet and rod have been used in cell culture studies [3, 48, 35, 49, 56-58]. Although different shapes have been used, further investigation is needed to determine whether different particle shapes result in different process of endocytosis. Hence, it is important to conclude that particle size and shape is one of the important criteria in designing drug delivery carriers for medical applications.

2.3.1.2. Surface functionalization and zeta potential

Another important property for efficient intracellular drug delivery is the state of surface functionalization. Surface functionalization acts like a driving force for transfection such as electrostatic, hydrophobic and hydrophilic (polar) forces, to carry the cargo into the cells and deliver the drug. The electrostatic force/attraction could play a major role in adhesive interaction between the drug delivery carrier and the cell membrane and this property acts as an impulsive force to drive the nanoparticles to approach the cell membrane [1, 4, 6, 59, 60, 12, 13, 53, 61]. Other than the electrostatic force, the hydrophilic and hydrophobic interactions between drug delivery carrier and cellular compartment are responsible for the recognition of specific domains of cell surface.

In drug delivery system characterization, the electrostatic interaction is identified by a critical parameter called Zeta potential. Physically, zeta potential represents development of a net charge at the particle surface which affects the distribution of ions in the surrounding medium, resulting in an increased concentration of counter ions close to the surface. Hence, there exists an electric double layer around each particle called stern layer, where the ions are strongly bound and an outer diffuse region where they are less firmly bound. Within these two layers, there is a boundary inside where ions and particles form a stable entity. The electric potential that exists at this boundary is known as the Zeta potential.

Zeta potential is represented by a numerical value which can range between -50 to +50 and relates to how fast/slow a drug delivery carrier can move towards the cell membrane. A higher zeta potential represents a higher driving force, where there will be a fast approach and quick adhering of drug delivery carrier on to the surface of the cells. The force or speed at which particles adhere to the cell surface can be slow at lower zeta potential. This sometimes may be

disadvantageous since the drug delivery carrier flow away from the targeted cells during circulation. The Zeta potential can vary based on the ambient condition and applications. There may be an optimum zeta potential for the intracellular drug delivery of nanoparticles to specific cells.

Surface functionalization plays a vital role in targeting of the cells or even nucleus. This is generally accomplished by multi-modification, multicomponent loading and/or multicomponent combination in one species. By appropriate surface functionalization, many objectives can be accomplished such as increasing the biocompatibility of the drug delivery carrier, increasing the uptake by specific cells and it can also help in targeting the cellular localization in cells and organs and increase the therapeutic efficiency [18, 57, 62, 63]. As an example, targeting of porous silica nanoparticles to cancer cells have been achieved by surface functionalizing of silica nanoparticles with poly (ethylene amine) and with fluorescent and targeting moieties. They have shown that the total number of particles internalized by the cancer cells was about an order of magnitude higher than the total number of particles internalized by normal cells [32]. Nevertheless, targeted delivery is still a great challenge at present time for intracellular bacteria.

2.3.1.3. Biocompatibility and cytotoxicity

Biocompatibility is an important criterion for drug delivery design. Since the drug delivery carrier will be in direct contact with the biological environment it should not cause any adverse effects in the individual who undertakes the treatment. The biocompatibility of any drug delivery carrier can be determined only by understanding how it interacts with the biological system. By knowing this, their diagnostic sensitivity, payload or therapeutic efficiency. By appropriate modification, the carrier leads to moderate or lower cytotoxicity. The

biocompatibility is normally classified based on their level as lethal dose, LD 50 or LD 80. In general, inorganic carriers like silica, iron and other inorganic species have a higher LD 50 at a concentration level of 1mg/ml while cationic organic carriers have a much lower level, about 10 mg/ml. For example, silane modified silica nanoparticles of size 16-50 nm were toxic (LD 50 > 1mg/ml) for COS-1 cells while LD 50 of poly (lysine) –modified silica nanoparticles (~20nm) for HNEI cells is decreased to 0.2-0.5mg/ml [131-133]. Various *in-vitro* studies have demonstrated the importance of the size and surface chemistry of the drug delivery carrier on their interaction with the biological environment; for example cellular uptake, toxicity and molecular response [18, 67, 68]. However, there is no direct comparison between the *in-vivo* and the *in-vitro* environments, since the *in-vivo* environment is far more complex and the limited studies available for the *in-vivo* studies of the behavior of engineered nano-carriers. Moreover, the drug delivery carrier should be stable in all environmental conditions. This is necessary so that their physicochemical properties can be kept unchanged during the whole delivery process.

2.3.1.4. Controlled drug release

An effective intracellular drug delivery carrier should have the potential to load large quantities of the cargo and deliver it at the appropriate site and concentration inside the cells. Currently, several drug delivery systems are employed which include several organic materials such as polymeric nanoparticles, dendrimers, and liposome's. These materials have been classified as Smart drug delivery systems, whereby the release of the drug in aqueous solution is based upon the structural degradation of the carrier [69, 70, 14, 25, 27, 28, 53]. The drug release rate is influenced by various chemical factors, such as pH, under physiological conditions. The drug release rate cannot be controlled efficiently for these drug delivery system which remains as a main drawback. However, the main disadvantage among these materials are the low drug

loading capacity and the premature release of matrix entrapped drug molecules from source material. This presents a major problem in the treatment of intracellular pathogens where premature release of toxic drugs can have adverse effects on normal flora and the probability of bacteria becoming drug resistant increase. The other problems with premature release have to do with release of the cargo of enzymes, DNAs and RNAs which can easily get denaturized before reaching the target site.

Hence for the treatment of intracellular pathogens, it is necessary that the drug carrier does not degrade or leak until it reaches the target site and then it must release a high enough concentration of the appropriate drug at the target site to kill the bacteria effectively. Control over the drug release rate can be achieved in a passive way, such as using a magnetic field response. For example, introduction of a magnetic susceptible coating in the porous silica can allow control of the release rate of the drug from the carrier material. In the case of the bioactive glasses, the appropriate glass chemistry can also be engineered in order to achieve efficient and controllable release of the drug, since degradability of the carrier material can be controlled over a period of time.

2.4 Silica nanoparticles as new drug delivery carriers

For the past few decades, several different nanomaterials were investigated for drug delivery applications. Two main categories of drug delivery carriers are (a) organic nano-carriers and (b) inorganic nano-carriers. Organic nano-carriers include liposomes, polymers and dendrimers [70]. These organic carriers have the ability to release the drug under physiological conditions. Among inorganic nanoparticles, gold and carbon nano-tubes have been extensively studied for biomedical applications. Recently, other nanoparticles such as semiconductor nano-crystals, super-paramagnetic nanoparticles, silicon-, and silica based nano-systems are being investigated for drug delivery applications [71].

Among all these inorganic and organic nano-systems, porous silica nanoparticles have attractive drug delivery characteristics and provide special properties in the field of biotechnology and biomedicine. Silica from pure glass forming oxides does not have the required properties to function as a drug delivery carrier [38]. For example low efficiency of delivery, not biodegradable and toxic at high concentrations. However, the desired properties of silica can be tailored by designing the sol-gel process such as the hydrolysis and condensation reactions including the activity of the metal alkoxide, the water/alkoxide ratio, the solution pH, the temperature, and the nature of the solvent and additive. Another consideration is that catalyst that is frequently added to help control the rate and the extent of hydrolysis [39-46]. By varying these processing parameters, materials with different microstructure and surface chemistry can be obtained which can also control the particle size, distribution, surface property, drug loading capacity, and the capability for functionalization and for sustained drug release at controlled duration for an extended period.

Sol-gel derived silica can provide porous matrix which contains many empty channels (pores) in the form of a regular arrangement. Some of the attractive properties of the sol-gel derived silica include high surface area, pore volume, stable porous structure and tunable pore diameter [72]. Furthermore, open pore arrangements of silica provide two functional surfaces for attachment of biomolecules or drugs. Additionally, the sol-gel synthesis step allows control over particle morphology i.e. size and shape as per requirements [73, 74]. One of the important aspects of porous silica particles is the high surface area and pore volume which provides the opportunity to achieve a high drug loading capacity. Furthermore, the diffusion drug release profile from the porous nature of the particles can be modified to release an appropriate drug concentration at the required target site. This allows maintaining regulated drug release and avoids drug associated systemic toxicity. Additionally, inclusion of drugs, imaging agents, and enzymes within the pores of silica allows protecting the loaded cargo from harsh environments such as the stomach or intestine, and avoids leakage of pharmaceutical cargos until reaching the required target site. Another important property of porous silica particles is the surface functionalization. Porous silica particles possess a high amount of silanol group on its surface. This allows for easy attachment of functional groups on its surface. Additionally, with its open pore arrangement, the particles can be surface functionalized either on the exterior or interior of the nano-channels.

By appropriate surface functionalization, different stimuli-response tethers could be attached to the open end of the nanoparticles. The type of external stimuli-response molecules could be gold, quantum dots (QD), and iron oxide [75]. Furthermore, these nanoparticles can act as a gate keeper, where once the porous silica nanoparticle reaches the designated target site, they can be removed by external or internal cellular triggers such as the change in pH, the

reducing environment, the enzymatic activity, light, the magnetic field or ultrasound which allows drug molecules to escape the pores at the tunable rate [76-78].

The targeting ability or biocompatibility of the porous silica nanoparticles can also be improved by surface modification of the silica which allows attachment to cells with specific moieties/ligands such as peptides, targeting agents or antibodies. Figure 2.1. Illustrates the ability of porous silica nanoparticles as intracellular drug delivery carrier.

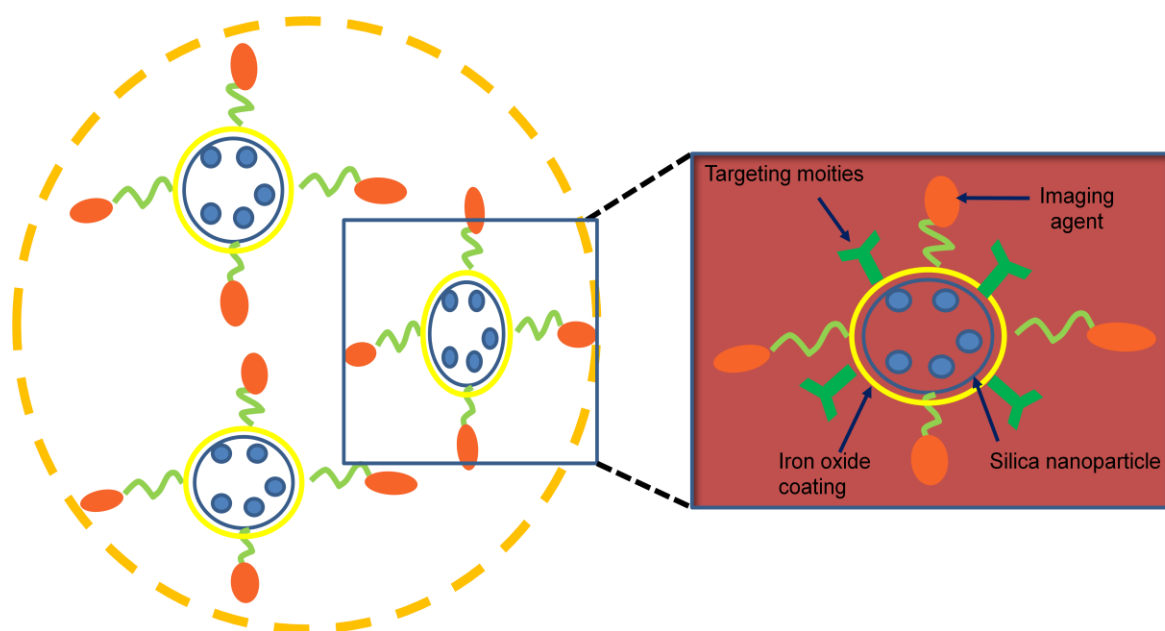


Figure 2.1. Porous silica nano-device for imaging, magnetically controlling, and *in-situ* monitoring of drug release. (a) Coating with bio-degradable polymer/liposome allows for facile inclusion within the cells, (b) Attachment of targeting moieties takes the nano-device towards the target site. (c) Optical probe allows for non-invasive imaging of the nano-device site. (d) Drug release rate within the target site can be modulated by magnetic field control.

Sol-gel process

Sol-gel is a simple inorganic polymerization process used for preparation of various inorganic materials. The primary material produced by sol-gel process includes glasses and ceramics of high purity. It can be a two step catalyst process where the first step involves formation of the liquid “sol” (colloidal suspension of solid particles in a liquid) which undergoes transition to form the solid “gel” phase. The sol-gel chemical transition occurs at room temperature under appropriate chemical conditions such as, in water or organic solvents and in a wide range of pH/ionic strength. This property allows for encapsulation of sensitive bio-molecules within the inorganic hosts and widens the application of the sol-gel process in the biomedical field. Several authors have shown the biocompatibility of sol-gel derived silica for encapsulation of enzymes and yeast cells [79, 80]. Importantly, these enzymes and yeast retain their normal catalytic activity after immobilization within the sol-gel silica and this shows the biocompatibility of the sol-gel derived silica. In addition to enzymes and yeast, other bio-molecules such as antibodies, DNA, and phospholipids have also been successfully encapsulated within the silica network [81, 82].

Sol-gel chemistry of silica

Sol-gel synthesis of silica is a multistep process. The steps involved in the synthesis can be classified as forming a solution, gelation, aging, drying and densification. For the formation of sol-gel derived silica, the commonly used main precursor is a silicon alkoxide ($\text{Si}(\text{OR})_n$) such as tetramethylorthosilicate (TMOS) or tetraethylorthosilicate (TEOS). As a first step in the formation of silica, water and a mutual solvent, ethanol or methanol, will be added to the silica precursor (TMOS or TEOS) to form a solution. This solution undergoes the hydrolysis process with elimination of alcohol molecules to form Si-OH silanol groups.

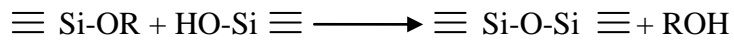
Hydrolysis:

The formed silanol group's act as intermediates and the alcohol produced during the hydrolysis step evaporates and silanol groups further undergo condensation to form siloxane Si-O-Si groups.



Alcohol condensation:

Extension of the condensation reaction increases the viscosity of the “sol” and it ceases to flow, forming a gel which finally yields to SiO₂ particle formation.



H₂O condensation:

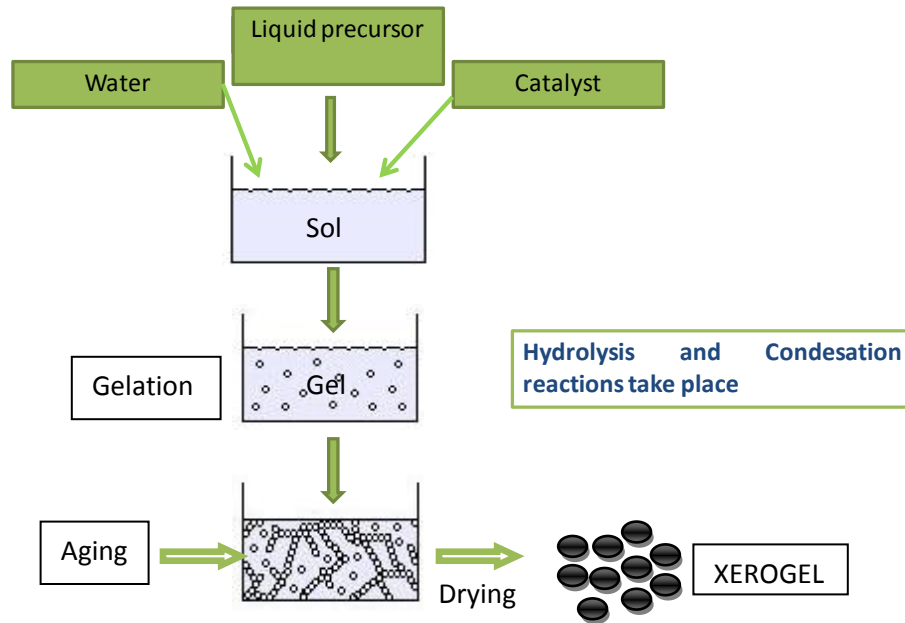
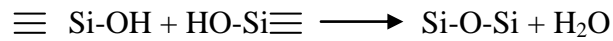


Figure 2.2. Schematic representation of sol-gel synthesis of silica xerogel. Initial hydrolysis steps leads to the formation of silicon alkoxide which undergoes further synthesis steps for formation of silica nanoparticles. Depending on the stage and process of drying a xerogel

monolith or silica thin film can be formed. Aerogels are another kind of sol-gel silica material with lowest bulk density. Aerogels are produced by extracting the liquid component of a gel through supercritical drying. This allows the liquid to be slowly drawn off without causing the solid matrix in the gel to collapse from capillary action, as would happen with conventional evaporation.

Sol-gel derived silica xerogel

Xerogel is a type of porous silica obtained by conventional drying or ambient drying for removal or evaporation of solvent during the sol-gel process. Silica xerogels can be non-toxic and biocompatible *in-vivo*. Silica xerogel degrade as silicic acid ($\text{Si}(\text{OH})_4$) and is eliminated through the kidney without any adverse reaction. There are several sol-gel parameters which determine the final structure of the xerogels. The reactivity of the alkoxide towards hydrolysis/condensation reactions can be modified, which can alter the final xerogel structure. This can be accomplished by modifying the molecular ratio of the H_2O to alkoxide by the type of catalyst or by the thermal treatment of the obtained silica xerogels. Based on the type of catalyst used, the xerogel synthesis can be broadly classified in to (a) acid catalyzed silica xerogel and (b) acid-base catalyzed silica xerogel.

Acid catalyzed silica xerogel

In the acid catalyzed sol-gel process, the final material obtained will have very weak branched systems. The weak branched system occurs due to low condensation rate during the acid catalyzed sol-gel process and this free moving system tend to overlap (interwoven) at the gel point. Due to free interpenetrating structure, there exist weak excluded volume effects. With weak excluded volume effect and low condensation rate, the final structure obtained shrinks freely with respect to solvent removal. The final dried xerogel structure obtained will be a

contracted and distorted version of the structure originally formed in solution. With acid-catalyzed process, a dense microporous silica network will be obtained. The size of the pores is limited to <2 nm.

Acid-base catalyzed silica xerogels

With an acid-base catalyzed process, highly branched structures will be formed. In contrast to acid-catalyzed system, the branched structures in the acid-base system are prevented from interpenetration due to strong intercluster and steric screening effects. During the solvent removal process, individual clusters undergo shrinkage and rearrangement to achieve higher coordination numbers. This allows to form mesoporous particulate xerogel where the pore size ranges between $2\text{nm} < \text{pore size} < 50\text{nm}$.

Sol-gel derived mesoporous silica

For the synthesis of mesoporous silica nanoparticles, charged (cationic or anionic) or neutral surfactants are employed as templates. The presence of appropriate surfactants leads to direct formation of the meso-phase by electrostatic attraction (for charged) and hydrogen bonding (neutral) interactions.

Ionic surfactant template

The first use of a charged surfactant was by Mobil technology [85]. They mainly used long-chain quaternary ammonium surfactants for their synthesis of porous silica. These surfactants under appropriate sol-gel condition minimize their energy in the solution by forming micelles. Based on the synthesis condition, the micelles can rearrange to form a rod-like shape and can also organize themselves to long-range hexagonal arrays. The possible explanation provided for formation of the hexagonal array is due to a steric effect where charged head groups point toward the solution and the hydrophobic long carbon chains point towards the centre of micelle. The

main parameters which adjust the formation of micelle rods and hexagonal arrays are surfactant alkyl chain lengths, the concentration of the surfactant, the nature of the halide counter-ion and the temperature of the solution [86-88].

Meso-phase silica formation can be achieved by addition of a silicate precursor to the above solution. At a suitable concentration, the added silica precursor undergoes hydrolysis and condensation process which leads to the attachment of negatively charged silica species (I^-) on the surface of the positively charged micelles (S^+), which then leads to the corresponding hexagonal S^+I^- organic-inorganic complex. Finally, the surfactant can be removed by a calcinations process, forming an open porosity. The open porosity replicates the initial organization of the organic phase and different mechanistic pathways have been proposed for the formation of the ordered nano-phase structure in the form of hexagonal, cubic or lamellar [90].

Neutral surfactant templates

The mesoporous silica particles have also been prepared using neutral surfactants as templates. With neutral surfactants, the mesoporous materials prepared provide improved stability. It is possible to modify the pore size of the mesopores by the chain length of the surfactants. The main mechanism proposed for formation of the mesophase with the neutral surfactant is the hydrogen bonding interactions and self-assembly between neutral primary amine micelles (S^0) and the neutral inorganic precursor (I^0). The wall thickness measured for the mesoporous materials prepared using the neutral surfactants was higher (1.5-3 nm) which is also the reason for the higher thermal stability [91]. The higher wall thickness was due to the absence of any electrostatic or charge matching effects.

2.5 Sol-gel derived porous silica drug delivery systems

Sol-gel derived silica materials have been widely studied as drug delivery carriers for biomedical applications. Unger et.al [92] first reported about the use of sol-gel materials for drug delivery applications. Similarly, Sieminska et.al [93] studied the use of sol-gel silica for the release of steroids. In this study the samples of porous sol-gel glass were impregnated with progesterone, estradiol, and hydrocortisone. Diffusion coefficients for those steroids inside the pores filled with pure ethanol, ethanol-water mixture or physiological solution were determined. It is shown that permeability is favored for steroids having fewer hydroxyl and carbonyl groups. Solvents that readily dissolve steroids increase the diffusion rate and thus the amount of delivered material. Bottcher et.al [94] reported about the use of silica gel system for the delivery of calcium antagonist nifedipine. It is shown that the release rate is affected by the grain size of the particle and is increased by the addition of penetration agents such as sorbitol, but is inversely proportional to particle size and is decreased by modification of the silica matrix with methyl-triethoxysilane. As part of our research on the effect of surface functionalization of silica on its drug release profile, we also explored the possibility of surface modifying the silica matrix i.e., by addition of PEG, a swelling agent, which modifies the texture property and increases the hydrophilicity of the matrix which allows for easy penetration of dissolution media and faster drug release.

Sol-gel silica have also been used for delivery of recombinant human growth factors- β 1 (TGF- β 1) for the repair of osseous defects [95-a]. The release of TGF- β 1 was extended to over seven days by modifying the degree of drying. Other than sol-gel synthesis condition dose dependent drug release properties were investigated by Radin et.al [95-b]. In this study, Vanomycin was used as a model drug and the drug release rate was modified from 2 -3 weeks to 6 weeks with

load increase from 2.2 to 11.1 mg/g. Ahola et.al [96] studied the loading and release rate of heparin, powerful anticoagulant used for the prophylaxis of both surgical and medical thrombosis, from silica xerogel. The influence of various chemical sol–gel parameters (the properties of reaction precursors, catalyst and final moisture content of the gel and heparin concentration) was studied. The release of heparin was proportional to the drug load in the concentration range between 6.8 and 13.6 wt%. It has been reported that the catalyst used for the preparation of the gel and the final moisture content of silica xerogel network have an influence on the release rate of heparin. Our group has investigated the influence of pH condition, acid and acid-base catalyzed process, in modifying the silica xerogel structure (texture property) and in controlling the drug release.

In addition to being a drug delivery carrier, silica xerogel has also been used as implant materials, where after subcutaneous implantation, the toremifene citrate loaded silica xerogel released the drug over forty days of duration. In addition to that, the release of drug occurs by erosion of silica gel itself within the implant site [97]. The biocompatibility of implanted silica was shown by histopathological studies. Furthermore the eroded silica gel formed a fibrotic capsule which proves the resorbable property of sol gel silica [97].

From the above studies it is well understood that major factors which could contribute to the differential drug release kinetics are

- (a) Tailoring the gel micro-structure utilizing the sol-gel synthesis conditions.
- (b) Modification of nature of pore surface to hydrophilic/hydrophobic.
- (c) Controlling drug diffusion through introduction of soluble or swelling penetration agents

Texture properties

Further advancement in the sol-gel synthesis process leads to formation of mesoporous silica nanoparticles with the aim to modify the size and organization of the pores. Studies have shown the influence of pore properties on loading and controlling the drug diffusion from the pores. Qu et.al [101] prepared a series of mesoporous silica materials with different morphologies and variable pore geometries. Ibuprofen was used as model drug and the drug release profile was related to the particles size and particle morphology. The influence of pore morphology (pore connectivity and pore geometry) on the drug release rate has been reported [102]. The choice of carrier matrix with particular pore connectivity and pore geometry along with diffusion controlled release process, have greater influence in drug release rate. [102]. P. Horcajada et.al [103] prepared a series of mesoporous particles with different pore sizes ranging from 3.6 to 2.5 nm. The analgesic ibuprofen was used as model drug and its delivery rate has been measured and compared with the delivery from different pore sized particles. This study has revealed that the delivery rate of ibuprofen decreases as the pore size decreases in the range of 3.6–2.5 nm. From all these studies, it is clear that modifying the particle morphology and using different surfactants chain length have influences in the drug release kinetics [103-104]. Additionally, the drug loading efficiency is also affected by modifying the texture properties but at the expense of modifying the particle size or particle morphology.

We further demonstrated a new method to improve the texture properties of silica particles without any modification of their size or pore morphology. Here we used CTAB surfactant (chain length-16 carbon) as template for synthesis of porous silica particles. By modifying the surfactant concentration to the silica precursor ratio, we were able to increase the pore volume and surface area of the particles.

Stimuli-response controlled drug release

The surfactant template sol-gel synthesis processes have provided ample opportunities for design and development of ordered mesoporous silica materials for drug delivery applications. In all these systems the release of adsorbed drug molecules usually follows sustained kinetic mechanism i.e., by diffusion of adsorbed drug molecules from the interior channels of the pores of the silica matrix. Hence, the release kinetics can be explained based on characteristics of the drug molecules being loaded and the carrier silica matrix. However for certain medical applications, like cancer treatment where mostly toxic drugs are employed, release of the drug has to be modulated by external stimuli. This allows for controlling any drug leakage before reaching the targeted cells or tissues. Therefore external or chemical stimuli-response controlled drug delivery systems are being widely investigated. Stimuli response systems includes light, magnetic field, heat, reducing environment, enzymatic activity or ultrasound. The mesoporous materials can be surface functionalized with certain functional groups which allows responding to environmental changes and consequently modifying the adsorption and release characteristics. Xiao et.al [106] have designed pH-responsive silica nanocarriers in which polycations are grafted to anionic, carboxylic acid modified silica by ionic interactions. The polycations act as closed gates to store the drug within the mesopores [105]. Lai et.al incorporated cadmium selenide nanoparticles within the porous silica which act as a capping agents and prevents leakage of drug molecules. As a stimuli-response agent, presence of disulfide-reducing agent breaks down the S-S bridge and triggers the CdS particles diffusion and of the silica nanoparticles [106]. Similarly, iron oxide particles were tested for killing cancer cells by the so-called hyperthermia treatment [107]. With respect to light-sensitive particles, gold is being given special consideration due to its

property of absorbing light over a broad spectral range from visible to the near infra-red light, which can acts as a optically tunable carriers for diagnostics.

In all these studies, there is a general trend of functionalizing the silica surface with many organic functional groups such as photosensitive organic groups for light sensitive property, addition of pH sensitive poly-cations etc. Though all these properties looks attractive for drug delivery *in-vitro*, there is a strong limitation in using these carriers for *in-vivo* studies. Most of the organic functional groups employed for designing the stimuli-response system could induce the toxicity at different concentrations. To overcome this limitation we have newly designed magnetically controlled soluble core-shell silica/calcium/iron drug release system. Basically the silica particles are made susceptible to magnetic field by inclusion of iron within the silica. Iron plays an important role in biology, forming complexes with dioxygen as hemoglobin and myoglobin; these two compounds are common oxygen transport proteins in vertebrates [108]. Furthermore the silica particles are made degradable by inclusion of metallic cations [Ca^{2+}] which eliminates the problem of accumulation during long-term treatment. Calcium is essential for living organisms, particularly in cell physiology, where movement of the calcium ion Ca^{2+} into and out of the cytoplasm functions as a signal for many cellular processes. As a major material used in mineralization of bones and shells, calcium is the most abundant metal by mass in many animals [109]. The core-shell structure allows for controlling the drug release until reaching the required target site.

2.5 REFERENCES

- [1] E. Briones, C.I.C José, M. Lanao. 2008. Delivery systems to increase the selectivity of antibiotics in phagocytic cells. *Journal of Controlled Release*. **125**: 210-227.
- [2] H. Pinto-Alphandary, P. Couvreur. 2000. Targeted delivery of antibiotics using liposomes and nanoparticles: research and applications. *Int. J. Antimicrob. Agents*. **13**: 155-168.
- [3] P. Lutwyche, D.J. Wiseman, M. St-Louis, M. Uh, M.J. Hope, M.S. Webb, B.B. Finlay. 1998. Intracellular delivery and antibacterial activity of gentamicin encapsulated in pH-sensitive liposomes. *Antimicrob. Agents Chemother*. **42**: 2511-2520.
- [4] T.Yamamoto, M. Hosaka, H. Fukuda, Y.Oomori, H. Shinoda. 1996. Uptake and intracellular activity of AM-1155 in phagocytic cells. *Antimicrob. Agents Chemother*. **40**: 2756-2759.
- [5] A. Mukhopadhyay, Intracellular delivery of drugs to macrophages. 2003. *Adv. Biochem. Engin/Biotechnol*. **84**: 183-209.
- [6] A.E. Aneed. 2004. An overview of current delivery systems in cancer gene therapy. *J Controlled Release*. **94**: 1-14.
- [8] D. Arcos, A. Lo´pez-Noriega, E. Ruiz-Herna´ndez, O. Terasaki, M. Vallet-Reg¹. 2009. *Chem. Mater*. **21**: 1000–1009.
- [9]D. Avnir, O Lev, J Livage. 2006. Recent bio-applications of sol–gel materials. *J. Mater. Chem*, 2006. **16**: 1013-1030.
- [10] H. Bottcher, W. Suss. 1998. Sol-gel carrier systems for controlled drug delivery. *Journal of sol-gel science and technology*. **13**: 277-281.
- [11] V. Sokolova. 2008. Inorganic Nanoparticles as Carriers of Nucleic Acids into Cells. *Ang.Chem.Int.edition*. **47**: 1382 - 1395.

- [12] B.G. Trewyn, I.I. Slowing, V. S.-Y. Lin. 2007. Mesoporous silica nanoparticle based controlled release, drug delivery, and biosensor systems. *Chem. Communications*. **31**: 3236-3245.
- [13] T. Chung, M. Yao, C.W. Lu, Y.S. Lin, Y. Hung, C.Y. Mou., Y. Chen, D.M. Huang. 2007. The Effect of Surface Charge on the Uptake and Biological Function of Mesoporous Silica Nanoparticles in 3T3-L1 Cells and Human Mesenchymal Stem Cells. *Biomaterials*. **28**: 2959-2966.
- [14] E.F. Craparo, M.L. Bondi, D. Mandracchia, G. Giammona. 2006. PEGylated Nanoparticles based on a polyaspartamide. preparation, physico-chemical characterization, and intracellular uptake. *Biomacromolecules*. **7**: 3083-92.
- [15] J.K. Vasir, V.D. Labhasetwar. 2005. Nanosystems in drug targeting: opportunities and challenges. *Curr. Nanosci.* **1**: 47-64.
- [16] A.J.S Pasqua, Y.L. Shi, B.B Toms, W. Oullette, J.C. Dabrowiak, T. Asefa. 2008. Cytotoxicity of Mesoporous Silica Nanomaterials. *J. Inorg. Biochem.* **102**: 1416-1423.
- [17] J.L. Lu, J.I. Zink, F. Tamanoi. 2007. Mesoporous Silica Nanoparticles as a Delivery System for Hydrophobic Anticancer Drugs. *Small*. **3**: 1341-1346.
- [18] J.M.A. Saul, R.V. Bellamkonda. 2006. A Dual-Ligand Approach for Enhancing Targeting Selectivity of Therapeutic Nanocarriers. *J. Controlled Release*. **114**: 277-287.
- [19] E.F. Craparo, M.L. Bondi, D. Mandracchia, G. Giammona. 2006. PEGylated Nanoparticles based on a polyaspartamide. preparation, physico-chemical characterization, and intracellular uptake. *Biomacromolecules*. **7**: 3083-92.
- [20] H.G. Vallhov, M. Strømme, A. Schydenius, A.E. Garcia-Bennett. 2007. Mesoporous Silica Particles Induce Size Dependent Effects on Human Dendritic Cells. *Nano Lett.* **7**: 3576-3582.

- [21] J.M.D Rosenholm, M. Lindén. 2008. Hyperbranching Surface Polymerization as a Tool for Preferential Functionalization of the Outer Surface of Mesoporous Silica. *Chem. Mater.* **20**: 1126-1133.
- [22] A. Aris, A. Villaverde. 2004. Modular protein engineering for non-viral gene delivery. *Trends in Biotechnology.* **22**: 371-377.
- [23] T. Azzam, A.J. Domb. 2004. Current development in gene transfection agents. *Current Drug Delivery.* **1**: 165-193.
- [24] A. K. Agrawal. 2000. Tuftsin-bearing liposomes in treatment of macrophage-based infections. *Adv. Drug Deliv. Rev.* **41**: 135-146.
- [25] R.H. Müller, S. Gohla. 2000. Solid lipid nanoparticles (SLN) for controlled drug delivery-a review of the state of the art. *Eur. J. Pharm.Biopharm.* **50**: 161-177.
- [26] A. Smith. 1986. Evaluation of poly (lactic acid) as a biodegradable drug delivery system for parenteral administration. *Int. J.Pharm.***30**: 215-220.
- [27] A.O. Eniola, D. A. Hammer. 2003. Artificial polymeric cells for targeted drug delivery. *J Control Release.* **87**:15-22.
- [28] N. Murthy, J. Campbell, N. Fausto, A.S. Hoffman, P.S. Stayton. 2003. Bioinspired pH-Responsive Polymers for the Intracellular Delivery of Biomolecular Drugs. *Bioconjug Chem.* **14**: 412-9.
- [29] M. Otsuka, T. Kokubo, S. Yoshihara, T. Nakamura, T. Yamamura. 1995. Drug release from a novel self-setting bioactive glass bone cement containing cephalexin and its physicochemical properties. *J Biomed Mater Res.* **29**:33-38.

- [30] S. Suárez, M. Kazantseva, C.E. Newcomer, R. Hopfer, D.N. McMurray, A.J. Hickey. 2001. Respirable PLGA microspheres containing rifampicin for the treatment of tuberculosis: screening in an infectious disease model. *Pharm. Res.* **18**: 1315-1319.
- [31] J.M.D. Rosenholm, E. Peuhu, R. Niemi, J.E. Eriksson, C. Sahlgren, M. Lindén. 2009. Targeting of Porous Hybrid Silica Nanoparticles to Cancer Cells. *ACS NANO.* **3**: 197-206.
- [32] R. Mortera, I.I. Slowing, E. Garrone, B. Onida, V. S.-Y. Lin. 2009. Cell-induced intracellular controlled release of membrane impermeable cysteine from a mesoporous silica nanoparticle-based drug delivery system. *Chem. Commun.* **1**: 3219-3221.
- [33] J.M.D. Rosenholm. 2008. Towards Establishing Structure-Activity Relationships for Mesoporous Silica in Drug Delivery Applications. *J. Controlled Release.* **128**: 157-164.
- [34] U. Maver, A. Godec, M. Bele, O. Planinšek, M. Gaberšček, S. Srčič, J. Jamnik. 2007. *International Journal of Pharmaceutics.* **330**: 164–174.
- [35] Z.K. Novak. 2003. Adsorption of Water Vapor on Silica, Alumina, and Their Mixed Oxide Aerogels. *Langmuir.* **19**: 8521-8525.
- [36] A.C.P. Pajonk. 2002. Chemistry of Aerogels and Their Applications. *Chem. Rev.* **102**: 4243-4265.
- [37] M. Vallet-Regí, A. J. Salinas. 2003. Glasses with Medical Applications. *Eur. J. Inorg. Chem.* **2003**:1029-1042.
- [38] Y. Wei, Q. Feng, H. Dong, M. Lin. 2000. Encapsulation of enzymes in mesoporous host materials via the nonsurfactant-templated sol-gel process. *Mater. Lett.* **44**: 6-11.
- [39] S. Radin, T. Kamplain, B. H. Tan. 2001. Silica sol-gel for the controlled release of antibiotics. I. Synthesis, characterization, and in vitro release. *J Biomed Mater Res.* **57**: 313-320.

- [40] W. Xia. 2006. Well-ordered mesoporous bioactive glasses (MBG): A promising bioactive drug delivery system. *Journal of Controlled Release*. **110**:522 - 530.
- [41] M.M. Motohiro Uo, Y. Kuboki, A. Makishima, F. Watari. 1988. Properties and cytotoxicity of water soluble $\text{Na}_2\text{O-CaO-P}_2\text{O}_5$ glasses. *Biomaterials*. **19**: 2277-2284.
- [42] S. Lowell, M. A. Thomas, M. Thommes. Characterization of porous solids and powders: surface area, pore size and density. Particle Technology Series. 2004, Kluwer Academic Publishers: Dordrecht/Boston/London. 73.
- [43] S. Radin, M. H. Lee, P. Ducheyne. 2002. In vitro bioactivity and degradation behavior of silica xerogels intended as controlled release materials. *Biomaterials*. **23**: 3113-3122.
- [44] B.G. Trewyn, S. Giri, H.T.Chen, V.S.-Y. Lin. 2007. Synthesis and Functionalization of a Mesoporous Silica Nanoparticle Based on the Sol-Gel Process and Applications in Controlled Release. *Acc.Chem.Res.* **40**: 846-853.
- [45] X. Wang, G. Zhu, S. Qiu, D. Zhao, B. Zhong. 2004. Effects of ammonia/silica molar ratio on the synthesis and structure of bimodal mesopore silica xerogel. *Microporous and Mesoporous Materials*. **71**: 87-97.
- [46] S. Ye. 2007. Nanoparticle-Mediated Drug Delivery and Gene Therapy. *Biotechnol.Progress*. **23**: 32-41.
- [47] Z.P. Xu, G. Q. Lu, A. Yu. 2006. Inorganic nanoparticles as carriers for efficient cellular delivery. *Chemical Engineering Science*. **61**: 1027-1040.
- [48] T.M. Allen, P.R. Cullis. 2004. Drug delivery systems: entering the mainstream. *Science*. **303**: 1818-1822.
- [49] M. Ahola, I. Kangasniemi, J. Kiesvaara, A. Yli-Urpo. 2000. Silica xerogel carrier material for controlled release of toremifene citrate. *International Journal of Pharmaceutics*. **195**: 219-227.

- [50]. N. Roveri, B. Palazzo, B. Parma, L. Vivi. 2005. Silica xerogels as a delivery system for the controlled release of different molecular weight heparins. *Anal Bioanal Chem.* **381**: 601-606.
- [51] P. Korteso, S. Karlsson, I. Kangasniemi, A. Yli-Urpo, J. Kiesvaara. 2000. Silica xerogel as an implantable carrier for controlled drug delivery-evaluation of drug distribution and tissue effects after implantation. *Biomaterials.* **21**:193-198.
- [52] D.R. Radu, K. Jeftinija, E.W. Rowe, S. Jeftinija, V.S.Y. Lin. 2004. A polyamidoamine dendrimer-capped mesoporous silica nanosphere-based gene transfection reagent. *J. Amer. Chem. Soc.***126**: 13216-13217.
- [53] D. Luo, E. Han, N. Belcheva, W.M. Saltzman. 2004. A self-assembled, modular DNA delivery system mediated by silica nanoparticles. *Journal of Controlled Release.* **95**: 333-341.
- [54] V. Schafer, R. Andreesen, A.M. Steffan, C. Rother, S. Troster, J. Kreuter, H. Rubsamen-Waigmann. 1992. Phagocytosis of Nanoparticles by Human Immunodeficiency Virus (HIV)-Infected Macrophages: A Possibility for Antiviral Drug Targeting. *Pharmaceutical Research* **9**: 541-546.
- [55] O. Balland, A. Viron, E. Puvion, A. Andremont, P. Couvreur. 1996. Intracellular distribution of ampicillin in murine macrophages infected with *Salmonella typhimurium* and treated with (3H) ampicillin-loaded nanoparticles. *J. Antimicrob. Chemother.* **37**: 105-115.
- [56] A.K. Salem, P.C. Searson, K.W. Leong. 2003. Multifunctional nanorods for gene delivery. *Nature Materials.* **2**: 668-671.
- [57] Y.Z. Shi. 2007. A mesoporous core-shell structure for pH-controlled storage and release of water-soluble drug. *Microporous and Mesoporous Materials.* **103**: 243-249.
- [58] A. Vinu, K. Ariga. 2005. Recent Advances in Functionalization of Mesoporous Silica. *Journal of Nanoscience and Nanotechnology.* **5**: 347-371.

- [59] S.W. Song, S. Kawi. 2005. Functionalized SBA-15 Materials as Carriers for Controlled Drug Delivery: Influence of Surface Properties on Matrix-Drug Interactions. *Langmuir*. **21**: 9568-75.
- [60] I. Slowing, V.S.Y. Lin. 2006. Effect of Surface Functionalization of MCM-41-Type Mesoporous Silica Nanoparticles on the Endocytosis by Human Cancer Cells. *J. Am. Chem. Soc.* **128**: 14792-14793.
- [61] F. Torney, V.S.Y. Lin, K.Wang. 2007. Mesoporous silica nanoparticles deliver DNA and chemicals into plants. *Nat. Nanotech.* **2**: 295-300.
- [62] J.C. Doadrio, I. Izquierdo-Barba, A.L. Doadrio, J. Perez-Pariente, M.Vallet-Regi Maria. 2006. Functionalization of mesoporous materials with long alkyl chains as a strategy for controlling drug delivery pattern. *J. Mater. Chem.* **16**: 462-466.
- [63] C. Kneuer, M. Sameti, U. Bakowsky, T. Schiestel, H. Schirra, H. Schmidt, C.S. Lehr. 2000. A nonviral DNA delivery system based on surface modified silica-nanoparticles can efficiently transfect cells in vitro. *Bioconjugate Chemistry*. **11**: 926-932.
- [64] C. Kneuer, M. Sameti, E.G. Haltner, T. Schiestel, H. Schirra, H. Schmidt, C.S. Lehr. 2000. Silica nanoparticles modified with aminosilanes as carriers for plasmid DNA. *International Journal of Pharmaceutical*. **196**: 257-261.
- [65] S.G. Zhu, J.J. Xiang, X.L. Li, S.R. Shen, H.B. Lu, J. Zhou, W. Xiong, B.C. Zhang, X.M. Nie, M. Zhou, K. Tang, G.Y. Li. 2004. Poly (L-lysine)-modified silica nanoparticles for the delivery of antisense oligonucleotides. *Biotechnology of Applied Biochemistry*. **39**: 179-187.
- [66] F. Cengelli, F. Tschudi-Monnet, X. Montet, A. Montoro1, H. Hofmann, S. Hanessian, L. Juillerat-Jeanneret. 2007. Surface Functionalization of Nanoparticles For Cell-Targeted Drug Delivery. *European Cells and Materials*. **14**: 117.

- [67] M.L. Liong, M. Kovoichich, T. Xia, S.G. Ruhem, A.E. Nel, F. Tamanoi, J.I. Zink. 2008. Multifunctional Inorganic Nanoparticles for Imaging, Targeting, and Drug Delivery. *ACS Nano* **2**: 889-896.
- [68] A.K. Agrawal. 2000. Tuftsin-bearing liposomes in treatment of macrophage-based infections *Adv. Drug Deliv. Rev.* **41**: 135-146.
- [69] C.B. Miller, H.G. Klingemann, M.C. Dignani, E.J. Anaissie, P.J. Cagnoni, P. McSweeney, P.R. Fleck, S.M. Frutchman, J. McGuirk. 2004. Lipid formulations of amphotericin B preserve and stabilize renal functions in HCST recipients. *Bone Marrow Transplant.* **33**:543-548.
- [70] S. Jin, K. Ye. 2007. Nanoparticle-Mediated Drug Delivery and Gene Therapy. 2007. *Biotechnol. Prog.* **23**: 32-41.
- [71] C. Loo, A. Lowery, N. Halas, J. West, R. Drezek. 2005. Immunotargeted Nanoshells for Integrated Cancer Imaging and Therapy. *Nano Lett.* **5**: 709-711.
- [72] A.B. Fuertes. 2004. Synthesis of mesostructured silica with tailorable textural porosity and particle size. *Materials Letters.* **58**: 1494– 1497.
- [73] S.B. Hartono, S.Z. Qiao, K. Jack, B.P. Ladewig, Z. Hao, G. Qing(Max)Lu. 2009. Improving Adsorbent Properties of Cage-like Ordered Amine Functionalized Mesoporous Silica with Very Large Pores for Bioadsorption. *Langmuir.* **25**: 6413-6424.
- [74] G. Zhou, Y. Chen, J. Yang, S. Yang. 2007. From cylindrical-channel mesoporous silica to vesicle-like silica with welldefined multilamella shells and large inter-shell mesopores. *J. Mater. Chem.* **17**: 2839-2844.
- [75] S.H. Hu, K.T. Kuo, W.L. Tung, D.M. Liu, and S.-Y. Chen. 2009. A Multifunctional Nanodevice Capable of Imaging, Magnetically Controlling, and In Situ Monitoring Drug Release. *Adv. Funct. Mater.* **19**: 3396- 3403.

- [76] M. Arruebo, M. Galan, N. Navascues, C. Tellez, C. Marquina, M.R. Ibarra. 2006. Development of magnetic nanostructured silica-based materials as potential vectors for drug-delivery applications. *Chem Mater.* **18**: 1911–9.
- [77] C.Y. Lai, B.G. Trewyn, D.M. Jeftinija, K. Jeftinija, S. Xu, S. Jeftinija. 2003. A mesoporous silica nanosphere-based carrier system with chemically removable CdS nanoparticle caps for stimuli-responsive controlled release of neurotransmitters and drug molecules. *J Am Chem Soc.* **125**: 4451–9.
- [78] H.J. Kim, H. Matsuda, H.S. Zhou, I. Honma. 2006. Ultrasound-triggered smart drug release from a poly (dimethylsiloxane)-mesoporous silica composite. *Adv Mater.* **18**: 3083.
- [79] S. Kohler, S. Belkin, R.D. Schmid, Fresenius. 2000. Reporter gene bioassays in environmental analysis. *J. Anal. Chem.* **366**: 769-79.
- [80] L. Inama, S. Dire, G. Carturan, A. Cavazza. 1993. Entrapment of viable microorganisms by SiO₂ sol-gel layers on glass surfaces: Trapping, catalytic performance and immobilization durability of *Saccharomyces cerevisiae*. *J. Biotechnol.* **30**: 197-210.
- [81] R.P. Liang, H.D. Qiu, P.X. Cai. 2005. A novel amperometric immunosensor based on three-dimensional sol-gel network and nanoparticle self-assemble technique. *Anal. Chim. Acta.* **534**: 223.
- [82] J.M. Liu, G.H. Zhu, Z.M. Rao, C.J. Wei, L.D. Li, C.L. Chen, Z.M. Li. 2005. Determination of human IgG by solid substrate room temperature phosphorescence immunoassay based on an antibody labeled with nanoparticles containing dibromofluorescein luminescent molecules. *Anal. Chim. Acta.* **528**: 29.
- [83] T. Coradin, M. Boissière, J. Livage. 2006. Sol-gel Chemistry in Medicinal Science. *Current Medicinal Chemistry.* **13**: 99-108.

- [84] C.J. Brinker, G.W. Scherer. Sol-gel science: The physics and chemistry of sol-gel processing. Academic Press: San Diego, **1990**.
- [85] S. Inagaki, Y. Fukushima, K. Kuroda. 1996. Adsorption isotherm of water vapor and its large hysteresis on highly ordered mesoporous silica. *J. Colloid Interface Sci.* **180**: 623–624.
- [86] A.S. Poyraz, O. Dag. 2009. Role of Organic and Inorganic Additives on the Assembly of CTAB-P123 and the Morphology of Mesoporous Silica Particles. *J. Phys. Chem. C.* **113**: 18596–18607.
- [87] J.H. Sun, M.O. Coppens. 2002. A hydrothermal post-synthesis route for the preparation of high quality MCM-48 silica with a tailored pore size. *J. Mater. Chem.* **12**: 3016–3020.
- [88] W. Zhao, J. Shi, H. Chen, L. Zhang. 2006. Particle size, uniformity, and mesostructure control of magnetic core/mesoporous silica shell nanocomposite spheres. *J. Mater. Res.* **21**: 3080-3089.
- [89] J.S. Beck, J.C. Vartuli, W.J. Roth, M.E. Leonowicz, C.T. Kresge, K.D. Schmitt, C.T.W. Chu, D. H. Olson, E.W. Sheppard, S.B. McCullen, J.B. Higgins, J.L. Schlenker. 1992. *J. Am. Chem. Soc.* **114**: 10834.
- [90] C.T. Kresge, M.E. Leonowicz, W.J. Roth, J.C. Vartuli, J.S. Beck. 1992. Ordered mesoporous molecular sieves synthesized by a liquid-crystal template mechanism. *Nature.* **359**: 710-712.
- [91] P.T. Tanev, T.J. Pinnavaia. 1995. A Neutral Templating Route to Mesoporous Molecular Sieves. *Science.* **267**: 865-867.
- [92] K. Unger, H. Rupprecht, B. Valentin, W. Kircher. 1983. The use of porous and surface modified silicas as drug delivery and stabilizing agents. *Drug Dev. Ind.Pharm.* **9**: 69-91.

- [93] L. Sieminska, T.W. Zerda. 1996. Diffusion of Steroids from sol-gel glass. *J. Phys. Chem.* **100**: 4591-4597.
- [94] H. Böttcher, U. Soltmann, M. Mertig, W.J. Pompe. 2004. Biocers: ceramics with incorporated microorganisms for biocatalytic, biosorptive and functional materials development. *J. Mater. Chem.* **14**: 2176-2188.
- [95] (a) S.B. Nicoll, S. Radin, E.M. Santos, R.S.Tuan, P. Ducheyne. 1997. In vitro release kinetics of biologically active transforming growth factor- β 1 from a novel porous glass carrier. *Biomaterials.* **18**: 853. (b) S. Radin, P. Ducheyne, T. Kamplain, B. H. Tan. 2001. Silica sol-gel for the controlled release of antibiotics. I. Synthesis, characterization, and *in vitro* release. *J Biomed Mater Res.* **57**: 313–320.
- [96] M.S. Ahola, E.S. Sakilynoja, M.H. Raitavuo, M. M. Aahtio, J.I. Salonen, A.U.O. Yli-Urpo. 2001. In vitro release of heparin from silica xerogels. *Biomaterials.* **22**: 2163-2170.
- [97] I. Roy, T.Y. Ohulchansky, D.J. Bharali, H.E. Pudavar, R.A. Mistretta, N. Kaur, P.N. Prasad. 2005. Optical tracking of organically modified silica nanoparticles as DNA carriers: a nonviral, nanomedicine approach for gene delivery. *Proc. Natl. Acad. Sci.* **102**: 279-284.
- [98] T. Czuryzkiewicz, J. Ahvenlammi, P. Kortueso, M. Ahola, F. Kleitz, M. Jokinen, M. Lindén, J.B. Rosenholm. 2002. Drug release from biodegradable silica fibers *J. Non-Cryst.Solids.* **306**: 1-10.
- [99] P. Kortueso, M. Ahola, M. Kangas, I. Kangasniemi, A. Yli-Urpo, J. Kiesvaara. 2000. In vitro evaluation of sol-gel processed spray dried silica gel microspheres as carrier in controlled drug delivery. *Int. Jnl. Pharm.* **200**: 223-229.
- [100] C. Barbé, J. Bartlett, L. Kong, K. Finnie, H.Q. Lin, M. Larkin, S. Calleja, A. Bush, G. Calleja. 2004. Silica particles: A novel drug delivery system. *Adv. Mater.* **16**: 1959-1966.

- [101] F. Qu, G. Zhu, H. Lin, W. Zhang, J. Sun, S. Li, S. Qiu. 2006. A controlled release of ibuprofen by systematically tailoring the morphology of mesoporous silica materials. *Journal of Solid State Chemistry*. **179**: 2027–2035.
- [102] Jenny Andersson, Jessica Rosenholm, Sami Areva, and Mika Lindeén. 2004. Influences of Material Characteristics on Ibuprofen Drug Loading and Release Profiles from Ordered Micro- and Mesoporous Silica Matrices. *Chem.Mat.* **16**: 4160-4167.
- [103] P. Horcajada, A. Rámila, J. Pérez-Pariente, M. Vallet-Regí. 2004. Influence of pore size of MCM-41 matrices on drug delivery rate. *Microporous and Mesoporous Materials*. **68**:105-109.
- [104] S.-W. Song, K. Hidajat, S. Kawi. 2005. Functionalized SBA-15 Materials as Carriers for Controlled Drug Delivery: Influence of Surface Properties on Matrix-Drug Interactions. *Langmuir*. **21**: 9568-9575.
- [105] Qing Yang, Shichao Wang, Peiwei Fan, Lifeng Wang, Yan Di, Kaifeng Lin, Feng-Shou Xiao. 2005. pH-Responsive Carrier System Based on Carboxylic Acid Modified Mesoporous Silica and Polyelectrolyte for Drug Delivery. *Chem.Mat.* **17**: 5999-6003.
- [106] C.Y. Lai, B.G. Trewyn, D.M. Jeftinija, K. Jeftinija, S. Xu, S. Jeftinija, V.S.Y Lin. 2003. A Mesoporous Silica Nanosphere-Based Carrier System with Chemically Removable CdS Nanoparticle Caps for Stimuli-Responsive Controlled Release of Neurotransmitters and Drug Molecules *J. Am. Chem. Soc.* **125**: 4451-4459.
- [107] A. Ito, H. Honda, T. Kobayashi. 2006. Cancer immunotherapy based on intracellular hyperthermia using magnetite nanoparticles: a novel concept of “heat-controlled necrosis” with heat shock protein expression. *Cancer Immunol Immunother.* **55**: 320–328.
- [108] <http://en.wikipedia.org/wiki/Iron>
- [109] <http://en.wikipedia.org/wiki/Calcium>

CHAPTER 3

TARGETED DRUG DELIVERY USING SILICA XEROGEL SYSTEMS TO TREAT DISEASES DUE TO INTRACELLULAR PATHOGENS

Material Science and Engineering C

2009, 29, 2313-2318

**Authors: Prabhakaran Munusamy, Mohamed N. Seleem, Hamzeh Alqublan, Ron Tyler Jr.,
Nammalwar Sriranganathan and Gary Pickrell**

3.1 ABSTRACT

Treatment and eradication of intracellular pathogens are difficult since infections are localized within phagocytic cells and most antibiotics, although highly active *in-vitro*, do not actively pass through the cellular membranes. Thus an optimum strategy to treat these infections should address targeting of active drugs to the intracellular compartments where the bacteria replicate, and should prolong release of the antibiotics so that the number of doses and associated toxicity can be reduced. The recently developed sol-gel technique offers new possibilities for embedding organic compounds within a porous silica matrix and for controlling their release from the host matrix into a surrounding medium. As yet, such sol-gel carrier systems for drug delivery are not widely known, despite their obvious advantages. We investigated a sol-gel derived silica matrix as a delivery system for the prolonged release of gentamicin for treatment of *Salmonella* infection in a mouse model. The release of gentamicin from the inside hollow part of the porous carrier can last a comparatively long time, leading to

a delayed release of drug (90% of gentamicin released in 5 days). Administration of three doses of porous silica loaded with gentamicin reduced the colony forming unit (CFU) of *S. typhimurium* in livers of infected mice by 0.48 log compared to 0.13 log with free drug. This new approach, utilizing sol-gel carrier systems for drug delivery, should improve our capability for targeting intracellular pathogens.

3.2 INTRODUCTION

Treatment of intracellular pathogens is difficult since infections are localized within phagocytic cells and most antibiotics, although highly active *in-vitro*, do not actively pass through cellular membranes, and hence, it is difficult to achieve the relatively high concentrations of the drugs within the infected cells [1-3]. Thus, an optimum strategy to treat these infections should address targeting of active drugs to the intracellular compartment where the bacteria replicate [1, 2, 4, 5]. Especially in treating intracellular pathogens, the premature release of guest molecules is a challenging problem and ideally requires “zero-release” before reaching the targeted cells. There have been numerous systems developed for drug release. However, there have been very few studies about using silica based xerogel materials as drug delivery agents for treating intracellular pathogens [2, 6, 7]. The recently developed sol-gel technique offers new possibilities for embedding antibiotics within silica and for controlling their release from the host matrix into a surrounding medium [8-11]. As of yet, such sol-gel carrier systems for drug delivery are not widely known, despite their obvious advantages. The particular sol-gel procedures employed have utilized room temperature synthesis to produce nanoporous silicon oxide material for use in drug delivery applications [12-14]. The first step in the synthesis process is the hydrolysis of tetraethylorthosilicate followed by gelation, aging, and drying. The resulting gels are termed xerogels. The encapsulation of the drug is obtained by adding the drug (dissolved in water or other solvent) to the sol which is in liquid state. This leads to uniform distribution of the drug in the solids. It has already been reported that these drugs or antibiotics retain their biological activity within the silica sol-gel material [9, 15]. The main advantage in using sol-gel materials is that they can be used as the host for various natural or synthetic therapeutic agents for controlled drug

delivery applications [8, 12-14, 16-19]. This can be accomplished by tailoring the specific sol-gel chemistry over a wide range of potential compositions.

In the sol-gel process, the drug molecules can be easily entrapped within the silica matrix with no chemical bonding. Also, they remain in a biologically active form after entrapment in matrix. Since the physical and chemical properties will be a function of the processing conditions, the desired properties can be engineered in the silica xerogel particles [13-15]. Xerogel silica offers unique features, such as stable porous structures, large surface areas, tunable pore sizes and volumes, and well-defined surface properties for site-specific delivery and for hosting guest molecules with various sizes, shapes, and functionalities [20]. Sol-gel silica materials have been shown to be biocompatible *in-vivo* as they are readily degradable inside the body [21], which eliminates the problem of accumulation of the particles used for drug delivery which remains as a major drawback for many other nano-particle delivery systems. The various glass compositions cause no adverse tissue reactions and are easily eliminated from the body through the kidneys as they degrade into Si (OH)₄ [20, 22, 23]. Porous silica xerogel particles have the drug molecules encapsulated in one large reservoir and by means of dissolution and diffusion mechanisms, the loaded drug molecules get released from any of these interconnected pores in the sol-gel matrix.

In the present study, we investigated the capability of porous, sol-gel derived, silica particles as a carrier for antibiotics. The efficacy of the treatment was compared to the free form of the same drug against *Salmonella typhimurium*, a leading cause of human gastroenteritis, and frequently used in a mouse model of human typhoid fever [3]. We describe the synthesis of gentamicin drug containing porous silica sol-gel particles and discuss the *in-vitro* release properties, its characterization and the bactericidal efficacy of the released drug.

3.3 EXPERIMENTAL PROCEDURES

3.3.1 Preparation of sol-gel processed silica xerogel particles

Silica xerogels were prepared at room temperature by acid hydrolysis of TEOS and water [12]. The molar ratio of water to TEOS was fixed at 8. The weight ratio of gentamicin to silica was 10%. Briefly, 10.4g of TEOS was slowly added to 7.2g of a solution of distilled water and HNO₃ with a pH value of 2.0. The resulting solution was magnetically stirred at 300 rpm for 1 h at room temperature. After stirring for 1 h, 0.3 gm of gentamicin powder was dissolved in the solution with the magnetic stirring continuing for an additional 1h at the same speed as before the gelation process occurred. The resulting drug loaded sol was allowed to gel and was subsequently dried at room temperature for 3 days. The air-dried gentamicin loaded xerogel was then crushed and refined into powder with an average particle size of less than 5µm.

3.4 CHARACTERIZATION

The morphologies of the synthesized silica xerogel particles were examined using field emission scanning electron microscopy (FE-SEM, JEOL-6500). Prior to FE-SEM analysis, the particles were sputter coated with gold. Texture property analysis was performed using nitrogen gas adsorption isotherms at 77 K and specific surface area and porosity parameters were calculated by the Barrett-Joyner-Halenda (BJH) technique[24]. Surface analysis for xerogels was performed before and after drug loading. Before surface analysis, the samples were crushed and degassed at 200°C for 2 h. X-Ray diffraction (XRD) measurements were carried out on crushed samples using a Siemens D-4000 diffractometer with Cu K α radiation at 40 Kv and 30 Ma. XRD was used to identify the nature of porous silica xerogel particles, at a scanning rate of 0.05 degrees per minute over a range of 2 theta from 0 to 100. Thermogravimetric (TGA) analysis was carried out with a TGA analyzer under air atmosphere at a programmed heating rate of 10°C/min. To calculate the amount of drug adsorbed, the powder samples were used for TGA analysis. The energy dispersive X-ray (EDX) analysis was performed to check for chemical composition of obtained silica xerogel and to confirm absence of unreacted reagents.

3.4.1 *In-vitro* drug release

A typical *in-vitro* drug release experiment was performed as follows:

Approximately 0.18g of silica xerogel particles were immersed in 100 ml of phosphate buffered saline (PBS), pH 7.4 at 37°C with stirring at a rate of 300 RPM. The release medium (3.0ml) of sample was removed at given time intervals using a syringe and replaced with the same volume of fresh PBS. The collected medium was then filtered and the gentamicin content in the filtered solution was analyzed by UV-Vis spectroscopy(UV-Vis) at a wavelength of 246 nm[11]. The

calibration curve of gentamicin was determined by taking the absorbance vs. gentamicin concentration between 0 and 100mg per 3ml of solution as the standard parameters. The cumulative drug release was determined by comparing the total amount of drug released at time t to the total amount of drug present in the drug loaded silica used in the experiment.

3.4.2 Bacterial Strain:

Salmonella typhimurium strain LT2 [3] was routinely grown at 37°C in tryptic soy broth (TSB) or on tryptic soy agar (TSA, Difco).

3.4.3 Animal experiment (*in-vivo* infection assay)

To study activities of the porous silica xerogel loaded antibiotic *in vivo*, 6 month old female AJ 646 mice (Charles River Laboratories, MA) were used. A total of 15 mice were inoculated intraperitoneally with 1000 colony forming units (CFU) of *S. typhimurium*. After 24 h, one group of mice (number of mice, $n = 5$) was kept untreated as a control and the remaining two groups ($n=5$) were administrated three doses of: (i) Silica xerogel (50 μ g gentamicin), (ii) free gentamicin 50 μ g, on days 2, 3 and 4 post-infection(PI). The animals were euthanized 48 h after administration of the last dose, the animals were euthanized. The spleen and liver were collected and bacterial colony forming units (CFU) per individual organ were determined by plating a series of 10-fold serial dilutions of the organ homogenates on TSA plates. The number of colonies was determined after incubation for 24 h at 37°C.

3.4.4 *In-vivo* tissue response study

An *in vivo* tissue response study was performed by exposing mice to intraperitoneally injection of porous silica xerogel. Sixteen, 12-week-old, female, CD-1 mice were divided into four groups (4 mice each). Two groups were used as the control exposed to a single 300 μ l dose of sterile saline. Two groups were used as the test groups exposed to a single dose 18 mg of porous glass suspended in 300 μ l PBS and were sacrificed with the control groups at 5 and 10 days post administration. Immediately before euthanasia of mice, blood was collected and complete blood counts were performed for each mouse. Major organs (brain, heart, lung, liver, pancreas, spleen, stomach, small intestine and large intestine) were harvested and placed in 10% buffered formaldehyde. Tissues were then trimmed, processed, and stained with hematoxylin and eosin for histopathology. Tissues were scored on a scale from 0 to 4, based on severity of histopathologic changes.

0 = unremarkable, 1 = minimal changes, <10% of organ affected, 2 = mild, 10-30 % of organ affected, 3 = moderate, 30-60% of organ affected, 4 = marked, >60% of organ affected.

3.4.5 Statistical Analysis

All statistical analyses for bacterial clearance from organs were performed using the Student two-tailed t test using Microsoft Excel. P values ≤ 0.05 were considered significant. One way ANOVA test was used for analysis of the blood count.

3.5 RESULTS

The porous silica xerogel with gentamicin are transparent, glassy and crack-free monoliths. The transparency and the absence of any cloudiness indicated that the gentamicin was homogeneously distributed throughout the xerogel. XRD analysis of the material showed an amorphous nature of the silica xerogels (Figure 3.1).

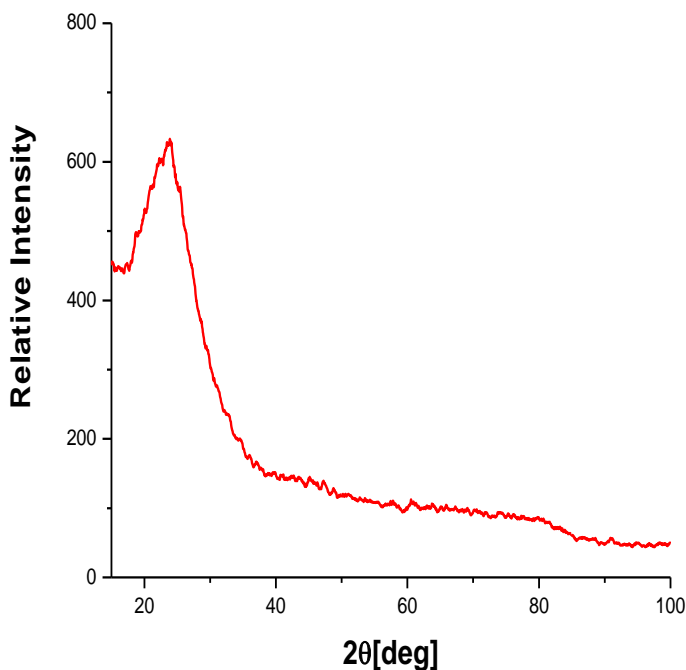


Figure 3.1. X-ray diffraction pattern of porous silica xerogel. A broad peak between 20 to 35 degrees indicates the amorphous nature of silica xerogel.

The N₂ adsorption–desorption isotherms of silica xerogel samples are shown in Figure 3.2. and the data of surface area, pore volumes and pore sizes are listed in Table 3.1. The isotherms were recorded at a constant temperature over a wide temperature range of relative pressures (P/P₀) from 0 to 1. According to Brunauer, Deming, Deming, and Teller (BDDT) classification [25, 26], the isotherm indicated absorption was high at very low pressure values of P/P₀. This is a

typical characteristic for type I isotherm which is a micro porous solid. This is further confirmed by the plateau observed at intermediate pressure and virtual lack of hysteresis in the desorption branch. The lack of hysteresis suggests that the pores are smooth and cylindrical. These materials had relatively lower pore radii in the range of <2nm. Isotherms of xerogels containing gentamicin was similar. The physical properties of xerogels tested were similar to those reported for acid-catalyzed silica xerogels. The size of the gentamicin molecules are in the range of 1.53*0.52nm [11] which was smaller than the pore size of porous silica, which is about 1.9nm. This allows gentamicin molecules to diffuse through the pore channels.

Table 3.1. Pore parameters of porous silica xerogels before and after adsorption of drug.

Parameters of Porous Structure: Langmuir Surface Area (SA, m²/g), Pore Diameter (PD, nm) and pore volume (PV, cm³/g)

Material	SA (m²/g)	PD(nm)	PV(cm³/g)
Xerogel	507.7	1.82	0.02
Xerogel/Gentamicin	854.8	1.82	0.08

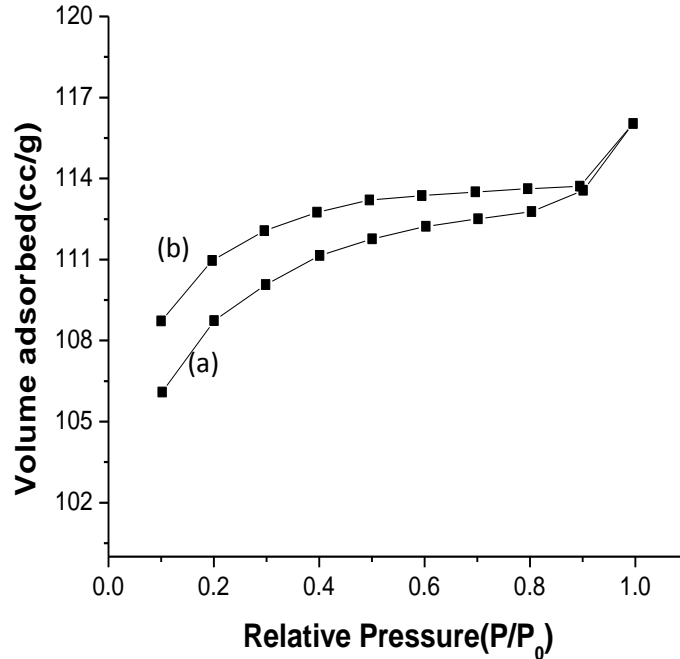


Figure 3.2. The N_2 adsorption-desorption isotherm of silica xerogel (volume of nitrogen as a function of relative pressure P/P_0). The isotherm features are typical for a type I isotherm (BDDT classification³¹) characteristic of a microporous solid, that is, a solid with a large number of pores having radii equal to or below 2 nm. (a) adsorption and, (b) desorption branch.

High magnification SEM micrographs of prepared xerogels are shown in figure 3.3. The particles show a rough surface and very fine structure. This indicates the presence of nano-sized pores. Indeed, N_2 adsorption experiments showed an average pore diameter of about 2 nm (Table 3.1). Individual silica particles cannot be resolved, suggesting that the textural pores are integral part of the final solid.

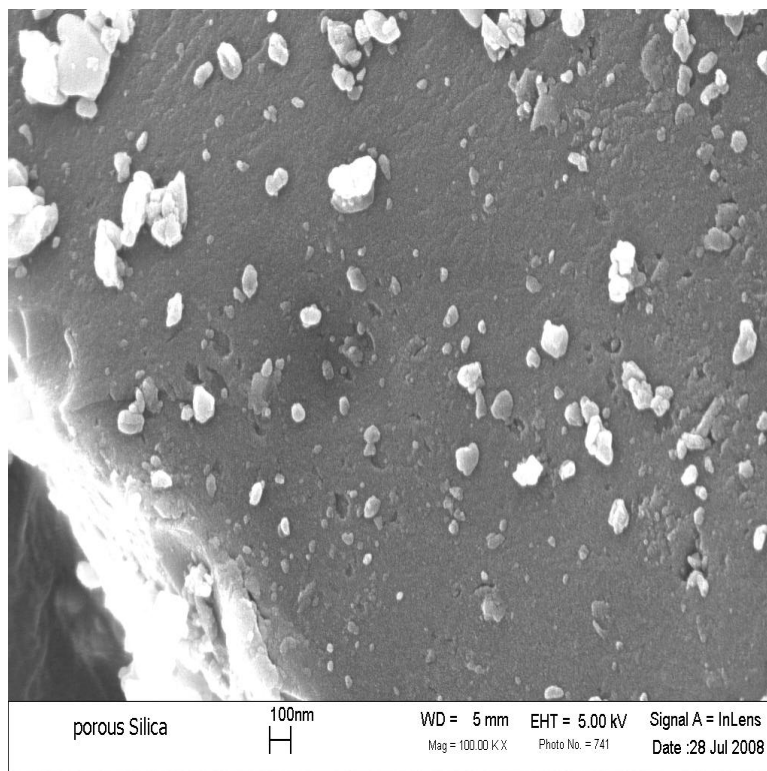


Figure 3.3. Scanning electron micrographs of the prepared silica xerogels. The highly porous silica xerogel appears as a dense material with fine structure.

Thermogravimetric analysis was carried out in an air atmosphere at a programmed heating rate of 10°C/min. The amount of drug adsorbed was monitored by thermogravimetry (TG). TG curves of porous silica with and without gentamicin are illustrated in Figure 3.4. By the comparison of curve (a) with curve (b), it can be concluded that the weight loss in curve (b) resulted mainly from the volatilization and decomposition of gentamicin. Since gentamicin gets entrapped within the pores of the silica xerogel, it was more difficult to volatilize and the volatilization of gentamicin occurs over a wide temperature range.

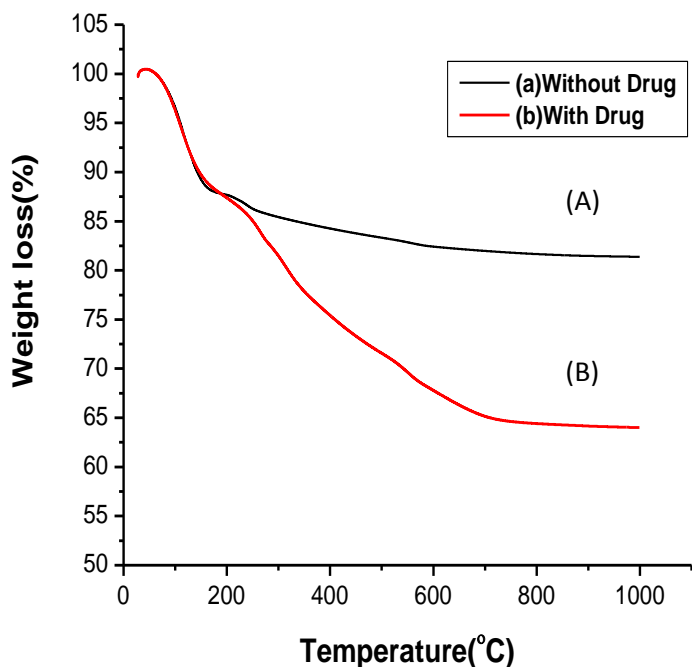


Figure 3.4. TG curves of (A) pure porous silica matrix and (B) porous silica matrix entrapped with gentamicin.

The release of gentamicin from the carriers is presented in Figure 3.5. A relatively fast release of the drug was observed during the first 20 h after particle immersion, reaching gentamicin release values of about 80%. This is followed by a slower release rate stage with the remaining approximately 20% being released between 20h and 140h. This change in release rate might arise from the release of gentamicin from different areas within the porous carrier and should allow control of the release rate by tailoring the characteristics of the porous carrier structure.

Furthermore, the UV-Vis spectra of the drug released from the matrices did not reveal any differences in shifts of peaks attributed to the drug, which could possibly indicate physicochemical changes in the drug structure. This confirmed that the sol/gel synthesis yields gel

matrices, which only encapsulate gentamicin drug without reactions that could possibly result in the formation of oligomers of drug or other species of gentamicin.

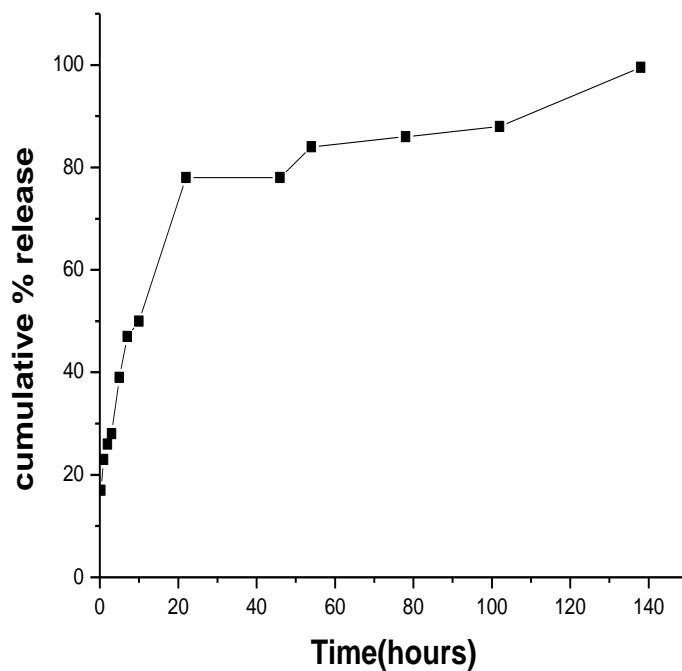


Figure 3.5. Gentamicin release from porous silica matrix as a function of immersion time in PBS.

Figure 3.6. shows the EDX analysis for the obtained silica xerogel samples. The results obtained revealed major peaks, attributed to the Si and O. This show the purity of the silica xerogel samples obtained by sol/gel synthesis.

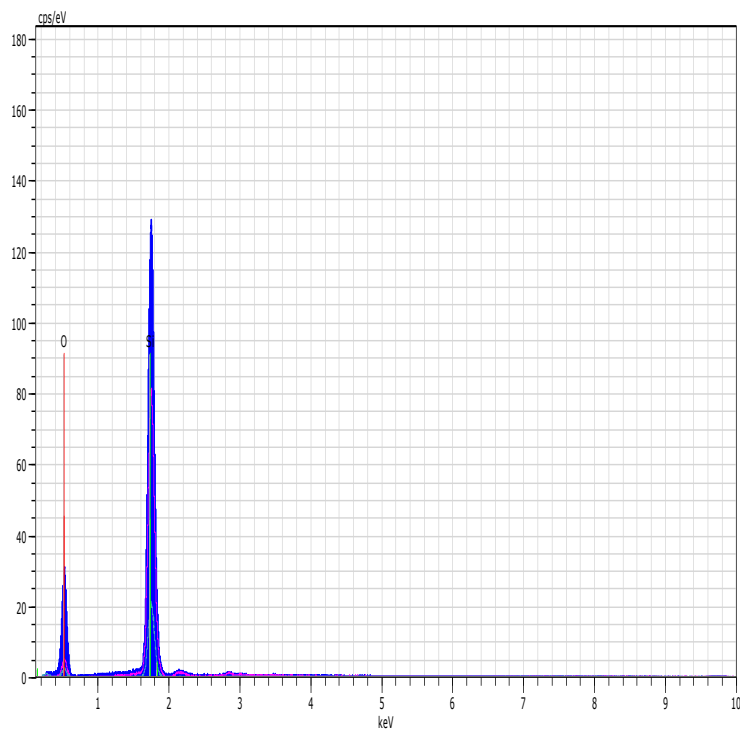


Figure 3.6. EDX spectrum of silica xerogel synthesized by acid catalysis process.

3.5.1 *In-vivo* infection assay

The efficacy of silica-loaded antibiotic versus the free form of the same drug was tested in AJ 646 mice. The treatment of mice started one day after infection with *S. typhimurium*. The mice received three doses of free drugs or antibiotic-loaded silica xerogel the animals were euthanized 24 h after administration of the last dose and the CFU in the liver and spleen were assayed. The results are summarized in Table 3.2. The silica xerogel loaded antibiotic was more effective in reducing the infection than free drug in the liver where a 0.48 log reduction in the log CFU of *S. typhimurium* compared to 0.13 log with free drug but, the results were not statistically significant. The silica and the free drug did not reduce *S. typhimurium* in the spleen.

Table 3.2. Efficacy of three doses of porous silica xerogel loaded gentamicin against infection with *Salmonella typhimurium*TL2 administered intraperitoneally.

Treatment	Log CFU±SD/ (spleen)	Reduction (log)	Log CFU±SD (liver)	Reduction (log)
Untreated	3.27 ±0.29	0.00	2.86 ±0.06	0.00
Silica-gentamicin	3.32 ±0.25	+0.05	2.38 ±0.035	0.48
Free gentamicin	3.48 ±0.13	+0.21	2.73 ±0.06	0.13

3.5.2 Tissue response study-Silica xerogel

There were no statistical differences between white blood cells counts of the injected groups compared to the control groups and white blood cell levels were within normal limits (1000-5000 cells/ μ l). Histopathology of the tissues revealed no significant changes in the silica xerogel groups compared to control mice.

3.6 DISCUSSION

Building on the previous knowledge regarding the bioactive behavior of silica sol-gels, the materials tested in this study are designed to function as a delivery agent for treating intracellular pathogens. The present study is the first to report the synthesis and testing of a porous sol-gel-derived material as a controlled release carrier of antibiotics for use in control of *S. typhimurium*, an intracellular pathogen. The synthesis of the silica xerogel/ antibiotic composite is a simple, room temperature process and provides easily reproducible xerogel properties. The synthesis route followed here guarantees that the maximum amount of drug can be added during the synthesis process and is uniformly distributed in the liquid phase. This allows the antibiotics to become encapsulated in the resulting glassy solid. The porous silica xerogel formed are optically transparent which gives a good indication that the channels are much smaller than the wavelength of light. The uniform distribution of the drug was confirmed by the absence of cloudiness and transparency of the composites. We used gentamicin antibiotic in this study, since it was shown to be a good model drug for controlling of intracellular pathogens, which in this case was *Salmonella*.

Highly branched network structures which are typical for sol-gel derived polymeric materials are advantageous as they provide gradual, time-dependent release. The parameters potentially of interest in determining the drug release kinetics are: pore size and total pore volume, surface area available for outward diffusion, initial quantity/concentration of loaded drug, physical characteristics of the drug (size, shape and charge), and the possible interaction between the drug and the xerogel (e.g. drug interactions with pore walls). The silica xerogel particles had a large surface area and were nanoporous. The physical and chemical properties of silica xerogel weren't affected by incorporation of the drug to the material. Upon immersion into

the solution, the drugs were released out of the pore structure of the room-temperature synthesized sol-gels (xerogels) in a time-dependent manner. The experiment was designed this way such that the drug release would follow a diffusion-controlled mechanism where surrounding fluid penetrates the porous structure formed by extensive network of interconnecting channels. This allows for dissolving the incorporated molecules and the loaded drug molecules elute from the matrix to the surrounding fluid. The dissolution data showed a gradual, sustained release of gentamicin for the total experimental duration of 3 days. For immersion duration up to 25 hours, the cumulative release varied between 20 and 40%, depending on the original drug amount in porous silica xerogels. This rate of drug release is advantageous for applications that require drug release duration of days for the full biological effect to be realized. In total, about 90 % release of the original load of the drug was realized after full duration of the elution study. If antimicrobials could be delivered into the phagocytic cells where the bacteria reside, clearance of the organisms can be achieved in a higher efficiency than using the free form of the same drug. The sustained release of the drugs will avoid systemic toxicities associated with the high and repeated dosages that are currently employed using free form of the drugs, and hence provide a safe treatment option.

Many materials have been tested as controlled drug delivery materials. The important prerequisite was one to develop biocompatible and resorbable delivery systems, which have the ability to transport drugs to the targeted site, released in sustained manner, and to maintain its bactericidal concentrations of loaded drug long enough at the target site. For many drug delivery systems the dissolution process occurs by diffusion process and release rate of the material was controlled by the rate at which carrier material gets degraded. For example in polymer drug delivery systems, the drug release is based on hydrolysis-induced erosion of the carrier matrix [3,

23]. The main disadvantage in using these materials would be in cases where there is an immediate need for large concentrations of drug. Since slow release kinetics leads to prolonged time lag in drug release. Many bioactive ceramics have also been tried as drug delivery materials. These material posses the properties of biodegradability and have been shown to be advantageous for bone re-growth [3, 27-29]. The main problems associated with these materials are the release of encapsulated compounds immediately upon dispersion of these composites in water, being referred to as “burst release” in many cases. Ideally, for drug delivery treatment to be most effective, the delivery of toxic drugs requires “zero release” before reaching the targeted cells, and release of an initial large concentration of the drug after reaching the target site. This will be followed by long-term steady state release. The other disadvantages which have been reported in using polymer drug delivery systems and other biodegradable materials are the role of organic solvents used during the synthesis step which could lead to adverse modifications of the structure and/or denaturation of the drug molecules [1, 3, 23]. The results from our studies and from previous reports have shown that these sol-gel derived silica xerogel materials are biocompatible and resorbable drug delivery materials [2, 18, 30, 31].

The cumulative release profile was plotted versus the square root of time (in hours) where a linear relationship that was observed in part of curve (Figure 3.6.) indicates this part of the process occurred by first-order release kinetics which also suggests the possibility for a burst effect i.e., faster release of the drug from the xerogel samples. When the cumulative release versus time curve shows some linearity, that part of the process is considered as near-zero-order. The long term dissolution showed a two-stage release where after day 1 the first order release was followed by slow near-zero-order of release. The process of transition from the first-to the zero order was observed when about 75% of the drug had been released. These release profiles may be

beneficial to kill intracellular pathogens as the required profile may need immediate supply of drug followed by steady long term delivery for certain applications [1, 2].

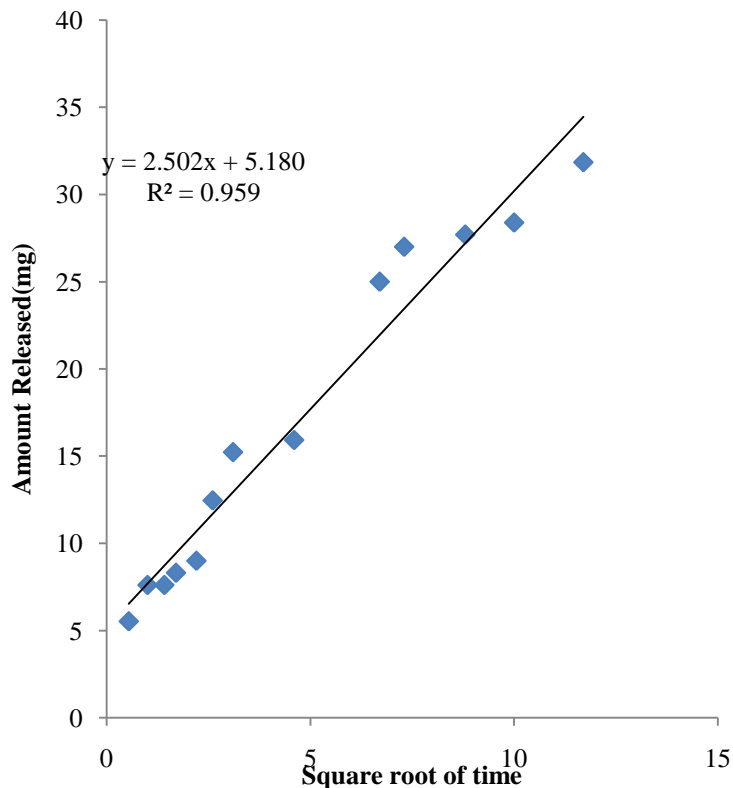


Figure 3.7. Part of cumulative release versus square root of time. A linear relationship that was observed in part of curve indicates this part of the process occurred by first-order release kinetics. N_2 adsorption-desorption reveals cylindrical shape of the pores and with such a pore geometry the loaded drug molecules cannot escape through the walls, but only through the cylindrical openings, where the release will be near zero-order since the opening has a fixed area.

The sol-gel silica materials showed a very good recovery of loaded antibiotics. The main problem associated with many polymeric drug delivery systems is the large loss of drugs or denaturation associated with fabrication. The amount of drug release was more than 90% for silica xerogel samples, while only about 4% of the drug was released even after 8 weeks of

elution for some drug loaded polymeric materials. The good recovery of loaded antibiotic indicates that there was no significant loss during the synthesis and the amount added to the sol was largely incorporated in the xerogel. It also indicated that the antibiotics were not chemically bonded to the materials. The biological activity of the released drug was confirmed by reduction in the log CFU of *S. typhimurium* in comparison to the free drug in the livers of infected mice. The present data confirms that the biological properties of the drug were not altered by room temperature sol-gel method of synthesizing silica.

In vivo biocompatibility of silica xerogel has been proven by using as implantation material subcutaneously and by the production of bioactive composite scaffolds for tissue engineering [32]. It has been widely reported about the formation of a biological apatite-like layer on the surface of the silica material while in contact with stimulated body fluid. The formation of apatite surface layer has been widely investigated for applications in bone-integration [27, 28, 30, 32].

Our current studies have shown the beneficial properties of xerogels as controlled drug release material for antibiotic delivery to intracellular pathogens. It is possible to tailor the release kinetics of xerogels over a wide range for specific therapeutic applications by changing the sol-gel synthesis parameters such as tailoring the texture properties, surface modification etc, including in this case, for treating intracellular pathogens. Mechanisms can be designed to provide a decrease or no drug release until the drug delivery carrier reaches the targeted site. Once it reaches the particular targeted site, the release profile can be changed from faster to slower steady release rate or vice versa.

3.7 CONCLUSION

In the present study, we investigated the applicability of sol-gel processed silica xerogel particles as a carrier for gentamicin, and the efficacy of treatment compared to the free drug against murine salmonellosis. Determination of the efficiency of the silica xerogel loaded antibiotic for elimination of *Salmonella* from the spleen and liver of infected mice was assessed after three doses. The release of gentamicin from the inner hollow part of porous carrier can last comparatively a long time, leading to a delayed release of the drug (90% of gentamicin released in 5 days). The initial release kinetics was of first order followed by steady release of near zero-order. i.e., cumulative release versus time curve shows linearity. The silica xerogel achieved a 0.48-log reduction in the liver, while for the free drugs the reduction was 0.13-log, indicating that the silica xerogel was more effective in reducing the bacteria in the liver compared to the same dose of free drugs

Our tissue response study did not show any trend or pronounced inflammatory response in the tested mice after injecting with 18 mg of the silica xerogel particle construct intraperitoneally. These results suggest that this particular construct of xerogel is more inert and does not stimulate a pronounced inflammatory reaction at a dosage of 18 mg per mouse. This new approach utilizing sol-gel carrier systems for drug delivery should improve our capability for targeting intracellular pathogens. Our current investigation demonstrated the biocompatibility of prepared silica xerogel materials as promising carriers for the controlled release of antibiotics in treatment of intracellular pathogens. Considerable research will be required to reach a statistically significant clearance of the infection by increasing the concentration of the antibiotics loaded in the xerogel.

3.8 REFERENCES

- [1] E. Briones, C. Colino, J.M. Lanao. 2008. Delivery systems to increase the selectivity of antibiotics in phagocytic cells. *J.Controlled Release*. **125**: 210-227.
- [2] Z.P. Xu, Z.Q. Hua, G.Q. Lu GQ, A.B.Yu. 2006. Inorganic nanoparticles as carriers for efficient cellular delivery *Chemical Engineering Science*. **61**: 1027-1040.
- [3] Y. Liu, H. Miyoshi, M. Nakamura. 2007. Nano-medicine for drug delivery and imaging: A promising avenue for cancer therapy and diagnosis using targeted functional nanoparticles. *International Journal of Cancer*.**120**: 2527-2537.
- [4] J. Zhou, W. Wu, D. Caruntu, M.H. Yu, A. Martin, J.F. Chen, C.J. O'Connor, W.L. Zhou. 2007. Synthesis of porous magnetic hollow silica nanospheres for nanomedicine application. *J.Phys.Chem*. **111**: 17473-17477.
- [5] V. Sokolova, M. Epple. 2008. Inorganic nanoparticles as carriers of nucleic acids in to cells. *Ang.Chem.Int.edition*. **47**: 1382-1395.
- [6] S. Jin, Y. Ye. 2007. Nanoparticle-mediated drug delivery and gene therapy. *Biotechnol.Progress*. **23**: 32-41.
- [7] J.E. Fuller, G.T. Zugates, L.S. Ferreira, H.S. Ow, N.N. Nguyen, U. B. Wiesner, R.S. Langer. 2008. Intracellular delivery of core-shell fluorescent silica nanoparticles. *Biomaterials*. **29**: 1526-1532.
- [8] P. Korteso, M. Ahola, S. Karlsson, I. Kangasniemi, J. Kiesvaara, A.Yli-Urpo. 1999. Sol-gel-processed sintered silica xerogel as a carrier in controlled drug delivery. *J Biomed Mater Res*. **44**: 162-167.

- [9] F. Qu, G. Zhu, H. Lin, W. Zhang, J. Sun, S. Li, S. Qiu. 2006. A controlled release of ibuprofen by systematically tailoring the morphology of mesoporous silica materials. *J. Solid State Chemistry*. **179**: 2027-2035.
- [10] B.G.S. Trewyn, I.I. Stowing, S. Giri, H.T. Chen, V.S.Y. Lin. 2007. Synthesis and Functionalization of a Mesoporous Silica Nanoparticle Based on the Sol–Gel Process and Applications in Controlled Release. *Acc.Chem.Res.* **40**: 846-853.
- [11] Y. Zhu, J. Shi, Y. Li, H. Chen, W. Shen, X. Dong. 2005. Hollow mesoporous spheres with cubic pore network as a potential carrier for drug storage and its *in vitro* release kinetics. *J.Mat.Res.* **20**: 54-61.
- [12] J.M. Xue, C.H. Tan, D. Lukito. 2006. Biodegradable polymer-silica xerogel composite microspheres for controlled release of gentamicin. *J.Biomed Mater Res Part B*. **78**: 417-422.
- [13] U. Maver, A. Godec, B. Marjan, O. Planinlek, M. Gaberscek, S. Srcic, J. Jamnik. 2007. Novel hybrid silica xerogels for stabilization and controlled release of drug *International journal of pharmaceutics*. **330**: 164-174.
- [14] S. Radin, P. Ducheyne, T. Kamplain, B.H. Tan. 2001. Silica sol-gel for the controlled release of antibiotics. I. Synthesis, characterization, and *in vitro* release. *J Biomed Mater Res*. **57**: 313-320.
- [15] S.W. Song, K. Hidajat, S.Kawi. 2007. pH-Controllable drug release using hydrogel encapsulated mesoporous silica. *Chem.Communications*. **1**: 4396-4398.
- [16] J. Yang, J. Lee, J. Kang, K. Lee, J. Suh, H. Yoon, Y. Huh, S. Haam. 2008. Hollow Silica Nano-containers as Drug Delivery Vehicles. *Langmuir*. **24**: 3417-3421.

- [17] L. Meseguer-Olmo, M. Ros-Nicolas, M. Clavel-Sainz, V. Vicente-Ortega, M. Alcaraz-Banos, A. Lax-Perez, D. Arcos, C.V. Ragel, M. Vallet-Regi. 2002. Biocompatibility and *in vivo* gentamicin release from bioactive sol-gel glass implants. *J Biomed Mater Res.* **61**: 458-465.
- [18] M. Otsuka, M. Yoshihisa, T. Kokubo, S. Yoshihara, T. Nakamura, Y. Takao. 1995. Drug release from a novel self-setting bioactive glass bone cement containing cephalexin and its physicochemical properties. *J Biomed Mater Res.* **29**: 33-38.
- [19] L.R Christina, T.G. Leong, B. Noy, H. Gracias, H. David. 2007. 3D lithographically fabricated nanoliter containers for drug delivery. *Adv. Drug Deliver Reviews.* **59**: 1547-1561.
- [20] L.X. Wen, H. Ding, J.X. Wang, J.F. Chen. 2006. Porous Hollow Silica Nanoparticles as Carriers for Controlled Delivery of Ibuprofen to Small Intestine. *Journal of Nanoscience and Nanotechnology.* **6**: 3139-3144.
- [21] P.Kortesuo, M.Ahola, S.Karlsson, I.Kangasniemi, A.Yli-Urpo, J. Kiesvaara. 2000. Silica xerogel as an implantable carrier for controlled drug delivery—evaluation of drug distribution and tissue effects after implantation. *Biomaterials.* **21**: 193-198.
- [22] M. Ahola, P. Kortesuo, I. Kangasniemi, J. Kiesvaara, A. Yli-Urpo. 2000. Silica xerogel carrier material for controlled release of toremifene citrate. *International Journal of Pharmaceutics.* **195**: 219-227.
- [23] B.G.S. Trewyn, S. Giri, I.I. Slowing, V.S.Y. Lin. 2007. Mesoporous silica nanoparticle based controlled release, drug delivery, and biosensor systems. *Chem. Communications.* 31, 3236-3245.
- [24] Y. Zhu, J. Shi. 2007. A mesoporous core-shell structure for Ph-controlled storage and release of water-soluble drug. *Microporous and Mesoporous Materials.* **103**: 243-249.
- [25] C.J. Brinker, G.Schere, Sol-gel science. The physics and chemistry of sol-gel processing, Academic Press limited, United Kingdom, 1990: p. 906.

- [26] S. Brunauer, W.S. Deming, E. Teller. 1940. On a Theory of the van der Waals Adsorption of Gases. *J Am Chem. Soc.* **62**: 1723-1732.
- [27] R. Mortera, B. Onida, S. Fiorilli, V. Cauda, C. Vitale Brovarone, F. Baino, E. Vernè, E. Garrone. 2008. Synthesis and characterization of MCM-41 spheres inside bioactive glass–ceramic scaffold. *Chem.Engg.Journal.* **137**: 54-61.
- [28] A.M. Gatti, G.Valdre, O.H. Anderson. 1994. Analysis of the *in vivo* reactions of a bioactive glass in soft and hard tissue. *Biomaterials.* **15**: 208-212.
- [29] M. Itokazu, T. Matsunaga, S. Kumazawa, Y.Wenyi. 1995. A novel drug delivery system for osteomyelitis using porous hydroxyapatite blocks loaded by centrifugation. *J Appl Biomat.* **6**: 167-169.
- [30] C.N. Cornell, D. Tyndall, S. Waller, J.M. Lane, B.D. Brause. 1993. Treatment of experimental osteomyelitis with antibiotic-impregnated bone graft substitute. *J Orthop Res.* **11**: 619-626.
- [31] L. Meseguer-Olmo, M. Ros-Nicolas, V. Vicente-Ortega, M. Alcaraz-Ban, M. Clavel-Sainz, D. Arcos, C.V. Ragel, M. Vallet-Reg, C. Cleseguer-Ortiz. 2006. A bioactive sol-gel glass implant for *in vivo* gentamicin release. Experimental model in Rabbit. *J Orthop Res.* **24**: 454-460.
- [32] S. Radin, G. El-Bassyouni, E.J. Vresilovic, E. Schepers, P. Ducheyne. Tissue reactions to controlled release silica xerogels carriers. In: LeGeros RZ, LeGeros JP, editors. *Bioceramics*, vol. 11. New York: World Scientific; 1998. p. 529–32.

CHAPTER 4
SILICA-ANTIBIOTIC HYBRID NANOPARTICLES FOR TARGETING
INTRACELLULAR PATHOGENS

Antimicrobial Agents and Chemotherapy

2009, 53, 4270-4274

Authors: Mohamed N. Seleem, Prabhakaran Munusamy, Ashish Ranjan, Hamzeh

Alqublan, Gary Pickrell, Nammalwar Sriranganathan

4.1 ABSTRACT

We investigated the capability of acid-base catalysed silica xerogel as a novel carrier of antibiotic and the efficacy of treatment compared to the same dose of free drug against murine salmonellosis. The drug molecules entrapped (57%) in the sol-gel derived silica xerogel matrix remained in biologically active form and the bactericidal effect was retained upon its release. The *in vitro* drug release profiles of the gentamicin from the silica xerogel/PEG were distinctly different at pH 7.4 where a delayed release of gentamicin was observed from silica xerogel/PEG (2%) network where the release rate reached 90% in 33 h. Administration of two doses of the silica xerogel significantly reduced the *Salmonella typhimurium* load in the spleen and liver of infected AJ 646 mice. The silica xerogel/PEG achieved statistically significant 1.15-log reduction in the liver of infected mice, while for the free drug the reduction was a non-significant value of 0.07 log respectively. This new approach utilizing room temperature synthetic route for incorporating therapeutic drugs into silica xerogel matrix should improve our capability for targeting intracellular pathogens.

4.2 INTRODUCTION

Targeting intracellular pathogens like *Salmonella*, *Brucella* and *Mycobacterium* remains a medical challenge. They can cause persistent infection due to their ability of maintaining infections in mammalian hosts even in the presence of inflammation, specific antimicrobial mechanisms and a robust adaptive immune response [13]. Some individuals who are infected with *Salmonella typhirium* become life-long carriers, periodically shedding large numbers of bacteria [12]. In host-adapted salmonellosis such as typhoid fever, the *Salmonella*-infected phagocytes gain access to the lymphatics and bloodstream allowing the bacteria to spread to the liver and the spleen [20]. Treatment and eradication are difficult since infections are localized within phagocytic cells, and it is difficult to achieve the optimum relatively high concentration of therapeutics within the infected cells [16]. Thus an optimum strategy to treat these infections should address targeting of active drugs to the intracellular compartment where the bacteria replicate, and should prolong the release of the antibiotics so that the number of doses and associated drug toxicity can be reduced. The associated problems with delivering free antibiotics to intracellular spaces have led to investigations of improved drug carriers for treating intracellular pathogens, including antibiotics loaded into liposomes, microspheres, polymeric carriers and nanoplexes [16].

The success of any approach for drug delivery to intracellular pathogens depends on the ability to construct a biocompatible carrier with high loading capacity of therapeutic drugs with no or minimum premature release of the cargo before reaching the replicative niche of the bacteria. The recently developed sol-gel technique offers new possibilities for embedding antibiotics within silica xerogel and for their controlled release from the host matrix into the surrounding medium and has shown great promise for biomedical applications [14, 17, 19, 23].

For controlled release applications, it has been shown that silica is able to store and gradually release therapeutically relevant drugs like antibiotics [18]. The composition of silica xerogels that can be tuned and the fabrication method at low temperature enable them to carry biologically active agents and be useful as a drug delivery system [9]. Sol-gel silica materials have been shown to be biocompatible *in vivo* as they are readily degradable inside the body [7], which eliminates the problem of accumulation which remains as main drawback for many other nanoparticle delivery systems. The various glass compositions cause no adverse tissue reactions and are easily eliminated from the body through the kidneys as they degrade in to Si(OH)_4 [1, 2, 21].

Also, the size, zeta potential, pore structure and the surface characteristics of silica xerogel make it a suitable carrier for therapeutics to target the replicative niche of intracellular pathogens. Gentamicin although exhibits several characteristics that makes it useful antimicrobial agent *in vitro*, does not kill intracellular *Salmonella* due to the polar nature of the drug and the associated low level of intracellular penetration. The usefulness of gentamicin seems therefore limited to eradication of the extracellular pathogens. In the present study, we investigated the capability of sol-gel processed silica xerogel as a carrier for gentamicin, and the efficacy of treatment compared to the free form of the same drug against *Salmonella typhimurium*, a leading cause of human gastroenteritis, and is used as a mouse model of human typhoid fever [11].

4.3 MATERIALS AND METHODS

All chemicals were purchased from Sigma-Aldrich Chemicals. Tetraethylorthosilicate (TEOS), gentamicin sulfate, polyethylene glycol (PEG; molecular weight, 8,000), ammonium hydroxide (NH₄OH), and hydrochloric acid (HCl) were used as received. Distilled, ionized water was used to make all aqueous solutions.

4.3.1 Preparation of antibiotics loaded silica xerogel and silica xerogel/PEG

The antibiotic loaded porous silica xerogel nanoparticles were prepared at room temperature by hydrolysis and polycondensation of tetraethoxysilane (TEOS) with water and catalyst contents [5]. Silica xerogel was prepared by two-phase catalysis with HCl and NH₃. Immobilization of antibiotic in the silica xerogels was carried out by mixing antibiotic solution with prehydrolyzed TEOS sol. 11 ml of TEOS were added to 9 ml of deionized water at room temperature to form a homogenous solution. The pH of the sol was adjusted by addition of nitric acid as catalyst followed by addition of ammonium hydroxide base. To control the hydrolysis process of TEOS, the temperature was kept under 20 °C. After 1 h of hydrolysis 750 mg of gentamicin dissolved in 3 ml water were added into the reaction. The resulting solution was stirred for 3 h and covered with a parafilm and left for gelation for 72 hours. After gelation, holes were pinned in the parafilm and the gels were allowed to continue aging and drying under ambient condition. During the drying process, evaporation of solvents and reaction by-products occurred from the interconnected pore network to reach constant weight and the so-called xerogels were obtained. The silica xerogel/PEG was fabricated using above mentioned procedure except with the addition of 2 % PEG. The silica xerogel/PEG was rinsed with deionized water to

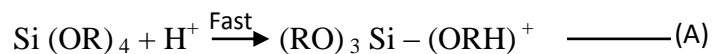
remove un-reacted reagents. The obtained silica xerogels were crushed into powder by ball milling, and powders were sieved to less than ~ 1µm in size for further characterization.

Two step acid-base catalyzed sol-gel synthesis process:

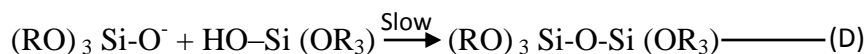
During the initial hydrolysis step, formation and distribution of partially hydrolyzed and un-hydrolyzed monomers form. The condensation step acts as an intermediate step in rearrangement of formed monomers to chainlike or cyclic polymers. Now, during the condensation reaction with addition of base catalyst the pH of the reaction solution increases, which primarily allows the reaction to take place between the end and middle of the chains. This step favors the formation of highly cross-linked clusters [24].

Reaction Mechanism [25]:

The TEOS is firstly hydrolyzed in a strong acidic medium (HCl), at such pH values that condensation reactions are very slow, according to the following mechanism given in Equations (A) and (B):



The sol is then neutralized with NH_4^+OH^- to promote the condensation reaction under a base catalyzed mechanism, as shown in Equations (C) and (D).



Where R represents (C_2H_5) .

In presence of PEG: $(\text{H (OCH}_2\text{CH}_2)_n\text{OH})$ [28]



4.3.2 Synthesis of fluorescein isothiocyanate(FITC)-labeled porous silica materials

For loading FITC to silica xerogel samples, 3ml of FITC solution of (5 mg/ml) ethanol was stirred in the presence of 50 mg of silica xerogel samples. The reaction mixture was vigorously stirred for 3 h at room temperature. The resulting solid was filtered, washed thoroughly with ethanol and dried under in air for 24 h.

4.3.3 Cell culture and localization of xerogel FITC

To study the ability of the FITC tagged Silica xerogel and PEG/silica xerogel particles to enter cells, macrophage cell line J774. A1 was used for this study. The J774A.1 cells were routinely grown as monolayers in 75 cm² tissue culture Flask (Corning Corporation Inc.) in a humidified 5% CO₂ atmosphere at 37°C. The cells were cultured and maintained in Dulbecco's modified Eagle's medium (DMEM) supplemented with 10% fetal bovine serum (FBS). At 90% confluency the cells were gently scrapped, seeded in six-well plates at density of 0.5x10⁶ cells/well and incubated for 24 h in a humidified 5% CO₂ atmosphere at 37°C to allow for attachment. Before the experiment, the culture media was discarded from each well, 200 µl (1.5mg/ml) silica xerogel-FITC or silica xerogel/PEG-FITC in DMEM supplemented with 10 % FBS were added to each well. After 1 h of incubation at 37°C, cells on cover slips were washed three times with phosphate buffered saline (PBS) and fixed in 4% paraformaldehyde for 1 hour, washed twice with PBS before mounting with Flouromount-G fluid (Southern Biotechnology Associates Inc.). Intracellular localization of silica xerogel was visualized using a Zeiss LSM 510 laser scanning microscope.

4.4 CHARACTERIZATION AND INSTRUMENTATION

The particle size of the silica xerogels was analyzed in a Malvern Zetasizer Nano Series HT. For the analysis, the particles were suspended in PBS at a concentration of 1 mg/3 ml and sonicated in a glass vial with no heating (Branson 1510) for 30 min. The suspension was transferred to a polystyrene cuvette and the particles size was measured, and the results were processed with DTS software version 4.20 (Malvern Zetasizer). The microstructure parameters such as pore size, specific surface area, and pore volume was determined from N₂ sorption isotherms at 77K with a Autosorb-1 MP (Quantachrome Co.). Prior to the measurements, the samples were degassed at 25°C and 1 Pa overnight. The infrared (IR) spectra of both silica xerogel and silica xerogel/PEG were recorded on a Fourier transform infrared spectrophotometer (FTIR) (PerkinElmer model 1600). Scanning electron micrographs were recorded using an FE-SEM (JEOL- 6500). The samples were deposited on a sample holder with an adhesive carbon foil and sputtered with gold. The thermogravimetric (TGA) analysis was carried out under air atmosphere at a programmed heating rate of 10° C/min. For transmission electron microscopy measurements, an aliquot of the powder was sonicated in nanopure water for 15 min. A single drop of this suspension was placed on a lacey carbon coated copper TEM grid and dried in air.

4.4.1 *In-vitro* release of gentamicin

The profiles of gentamicin release from silica xerogel and xerogel/PEG matrix were studied using suspensions (50µg/ml) of the antibiotic-loaded xerogel and xerogel-PEG in PBS. The suspensions were kept at room temperature, and the release was determined by taking aliquots at different time points. At the end of each time point, 1 ml of the solution was removed

for sampling and replaced immediately with an identical volume of PBS. The aliquots were centrifuged, and the absorbance value of the gentamicin sulfate antibiotic in the supernatant was measured [23]. The quantitative measurement in each elution sample was performed using a UV/VIS spectrophotometer (Perkin-Elmer). The analytical wavelength $\lambda=246$ nm, corresponding to the absorbance maximum, was selected for the determination of the drug. The drug-PBS standard solutions were used for calibration. The calibration curve of gentamicin was determined by taking absorbance versus drug concentration between 0 and 100 mg/ml.

4.4.2 Drug release assay

The quantitative measurement of gentamicin sulfate in each elution sample was performed using a UV/VIS spectrophotometer (Perkin Elmer). The analytical wavelength $\lambda=246$ nm corresponding to the absorbance maximum was selected for the determination of the drug[19]. The drug-PBS standard solutions were used for calibration. The calibration curve of gentamicin was determined by taking absorbance versus drug concentration between 0 and 100mg/ml as parameters.

4.4.3 Bacterial strain

Salmonella typhimurium strain LT2 [11] was routinely grown at 37 °C in tryptic soy broth (TSB) or on tryptic soy agar (TSA, Difco).

4.4.4 Animal experiment (*in-vivo* infection assay)

To study efficacy of the silica xerogel/PEG loaded antibiotic *in vivo*, female AJ 646 mice (Charles River Laboratories MA) 6 weeks old were used. Groups of five mice each were infected intraperitoneally with *S. typhimurium* (4×10^3 CFU/mouse). The animals received two

doses of (1) silica xerogel control, (2) free gentamicin 150 μg , (3) silica xerogel/PEG, (4) gentamicin 150 μg , and (5) PBS at days 3 and 5 post-infection animals were euthanized. 48 h after administration of the last dose, the animals were euthanized. The spleen and liver were collected and bacterial colony forming units (CFUs) per individual organ were determined by plating a series of 10-fold serial dilutions of the organ homogenates on TSA plates. The number of colonies was determined after incubation for 24 h at 37°C. The experimental procedures on mice and the facilities used to hold the experimental animals were in compliance with the rules of the Virginia Tech Institutional Animal Care and Use Committee.

4.4.5 Statistical analysis

All statistical analyses for bacterial clearance from organs were performed using the Student two-tailed *t* test using Microsoft Excel. *P* values ≤ 0.05 were considered significant.

4.5 RESULTS

4.5.1 Characterization of silica xerogels

The synthesized acid base-catalyzed silica xerogel and silica xerogel modified by the addition of low-molecular-weight PEG matrices were transparent, glassy, and crack-free monoliths. The addition of gentamicin to the xerogel did not change the physical characteristics of the particles. This indicates that the gentamicin was homogeneously distributed throughout the xerogel without any macroscopic phase separation. To avoid any damage or loss of activity of the antibiotic, room temperature and low-acidity parameters were used. The particle sizes of the porous silica xerogel and porous silica-PEG were 190 to 395 and 220 to 342 nm, respectively, and the zeta potentials (surface charges) were -1.78 and -6.24, respectively. The EDX analysis was performed on several different areas which clearly showed only two major peaks attributed to Si and O which confirm the absence of any un-reacted reagents from the starting precursor.

4.5.2 Infrared Spectroscopy Analysis

Figure 4.1. shows the IR spectra for the silica xerogel and the silica xerogel/PEG. The presence of two absorption bands at $1200\text{--}1000\text{ cm}^{-1}$ and 800 cm^{-1} is characteristic of symmetric and asymmetric vibrations of the Si O or O Si O groups. The band at 650-cm^{-1} can be assigned to the symmetric Si-O-Si stretching mode for a four-membered siloxane ring and 950 cm^{-1} indicates the presence of the Si O H group. The OH bands observed at $3000\text{--}3700\text{cm}^{-1}$ is due to the presence of absorbed water in silica xerogels. The intensity of the Si-OH band at 950 cm^{-1} present in prepared silica xerogel decreases after the loading of PEG. This can be ascribed to the interaction between the PEG and Si-OH, which may react and undergo cross-linking during the formation of the silica lattice of the matrix. The vibration bands at $1160\text{--}1060\text{ cm}^{-1}$ are attributable to stretching vibrations of the C O and C C groups of PEG. These vibration bands are indicative of

the presence of PEG. In summary, the spectra of all PEG/xerogels were typical of acid-catalyzed, well-hydrolyzed silica xerogels with a high concentration of terminal groups (silanol). Additionally, the silica without PEG but with antibiotics looks similar as the spectrum of pure silica xerogel and did not contain characteristic bands attributed to the pure drug. The possible reason could be shielding of the drug by the microporous structure of the gel which obstructs its identification by IR.

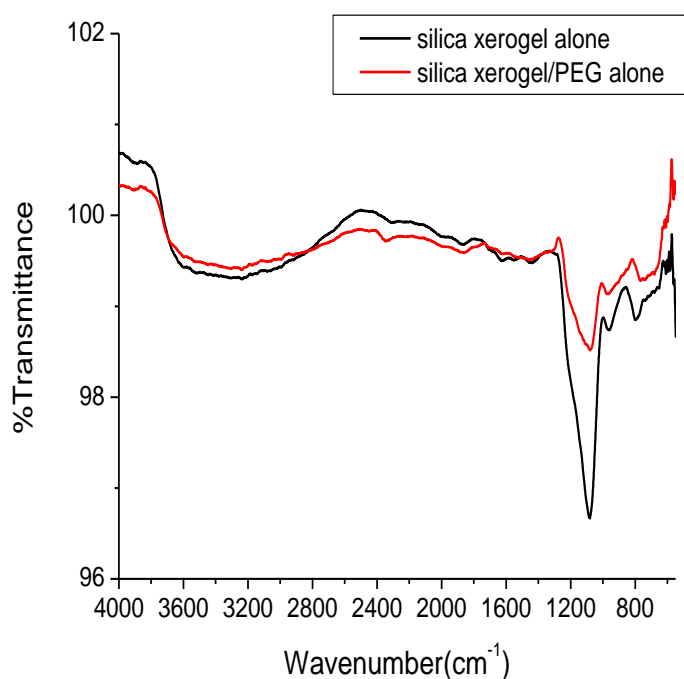


Figure 4.1. FTIR Spectra of silica xerogel and PEG/silica xerogel.

4.5.3 N₂ adsorption-desorption isotherm analysis

N₂ adsorption- desorption isotherms and pore parameters of porous silica xerogel and porous silica xerogel/PEG matrix are shown in Table 4.1. The data were recorded over the relative pressure (P/P₀) from 0 to 1 at -196°C. Based on the IUPAC classification scheme, the isotherm curve observed is of type IV, which has a characteristic loop at around 0.5 and 0.8 of

P/P₀. Accordingly, these isotherms show low adsorption at lower relative pressures and a sudden increase in adsorption at high relative pressure due to capillary condensation in the mesoporous structure. These isotherms describe solids with a well-defined distribution of the mesoporous structure. The pore size of the silica xerogel and silica xerogel/PEG is large enough to allow gentamicin molecules to diffuse through the pore channels. This leads to different levels of decrease in nitrogen adsorption reflecting the different storage amount of the drug in the porous network. The loading of gentamicin molecules leads to a decrease surface area, and pore volume. These results confirms that the drug was introduced inside the channels of silica xerogel, and the porous structure remained as the drug was loaded.

Table 4.1. The structural parameters of the silica xerogel and silica xerogel-PEG ^a

Sample	S_{BET} (m²/g)	V_{pore} (m³/g)	D_{peak} (nm)
Silica xerogel	412.2	1.459	9.60
Silica xerogel-gentamicin	21.14	0.068	3.60
Silica xerogel/PEG	230.5	1.096	1.43
Silica xerogel/PEG-gentamicin	38.89	0.054	1.717

^a S_{BET}, BET surface area; V_{pore}, pore volume; D_{peak}, pore diameter.

4.5.4 Scanning and Transmission Electron Microscopy

Scanning electron microscope (SEM) images of fractured surfaces of the silica xerogel and the silica xerogel/PEG are shown in Figure 4.2. The xerogel particles have a spherical morphology that are joined together to form agglomerates a few hundred nm in diameter. The SEM micrograph indicates a hierarchical morphology with the clusters of agglomerates organized into larger clusters and shows a distribution of large voids (mesopores). These pores are seen lying outside the agglomerates with small openings leading into them. The SEM pictures of the silica/PEG reveal that all the synthesized xerogels have an external protective coating with the wall surfaces appearing smooth and compacted. From the SEM analysis, it is obvious that the textural mesoporosity of the silica xerogel depends greatly on the silica primary particle size and its packing. The structured pore distribution can be obtained only from ordered and uniformly size particles.

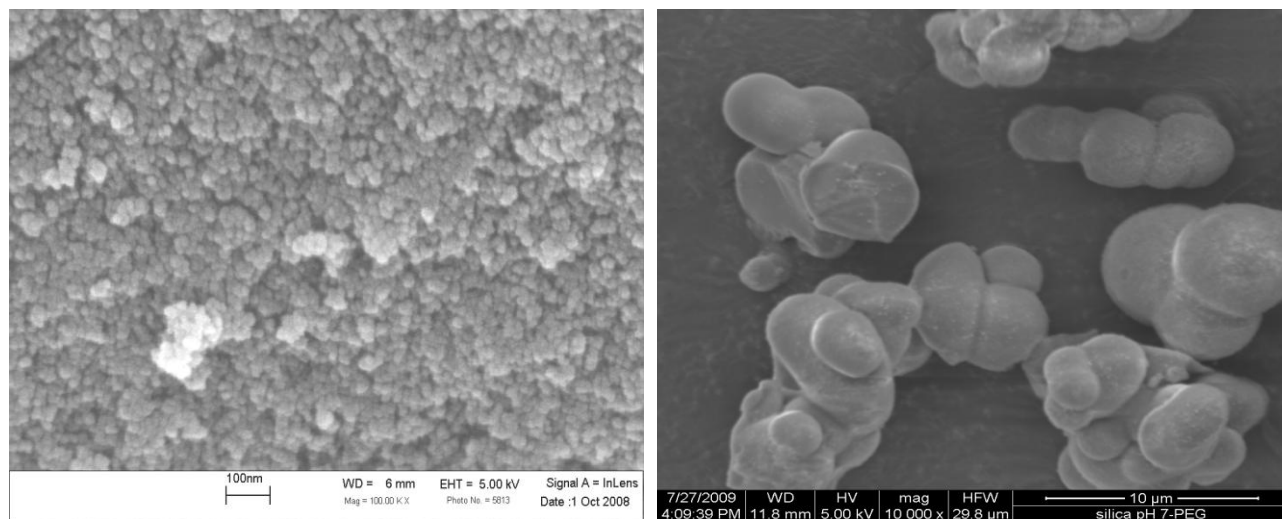


Figure 4.2. SEM images of (A) silica xerogel, (B) PEG/silica xerogel complex.

A transmission electron microscopy (TEM) image of the silica xerogel particle is shown in Figure 4.3. The framework structure and textural porosity associated with silica xerogel sample are evaluated. The porosity originates from the cavities between the particles which are closely packed together. The samples consist of numerous randomly interconnected worm-like porous interconnected channels. The details observed are typical of porous silica prepared via non template method.

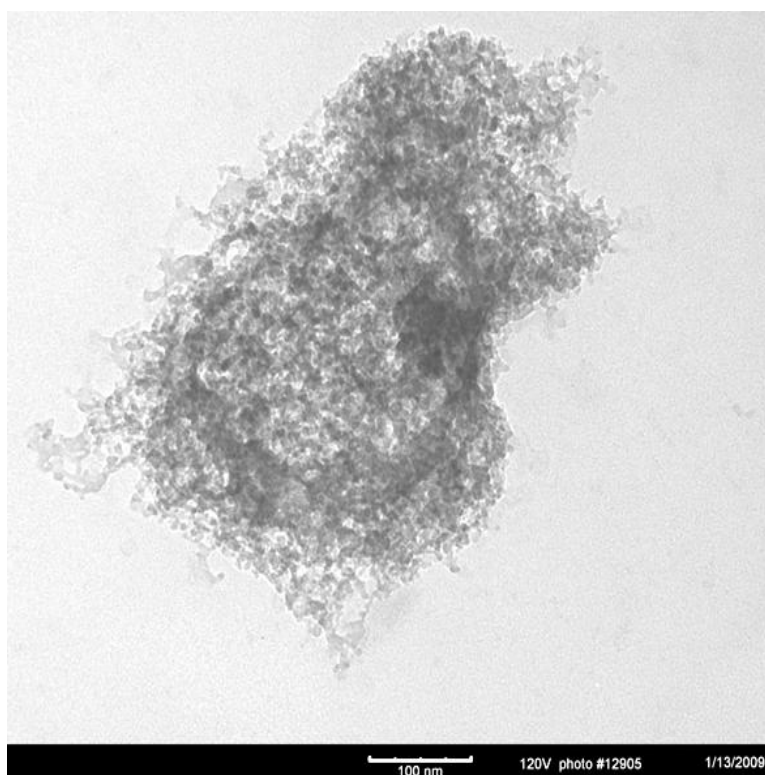


Figure 4.3. TEM image of silica xerogel showing the agglomerations of spherical-like nanoparticle and disordered framework pores.

4.5.5 Thermogravimetry Analysis

Thermogravimetric analysis curves of silica xerogel and silica xerogel/PEG complex with gentamicin are illustrated in Figure 4.4. The sample weight loss below 220°C is attributed to evaporation of water for both systems. The weight loss of about 31.22% observed between 220-

310°C for silica-drug complex is due to the apparent removal of drug molecules stored in the porous network. This indicates the gentamicin storage capacity is 31.22 % (572.20mg drug/g of silica). For silica/PEG-drug complex two weight losses are observed. The weight loss between 220-310°C is due to the removal of drug molecules and the other weight loss of 16.95% is due to removal of PEG molecules in the network. In comparison to silica xerogel/drug complex the storage capacity of silica/PEG drug complex was less possibly due to entrapment of PEG molecules.

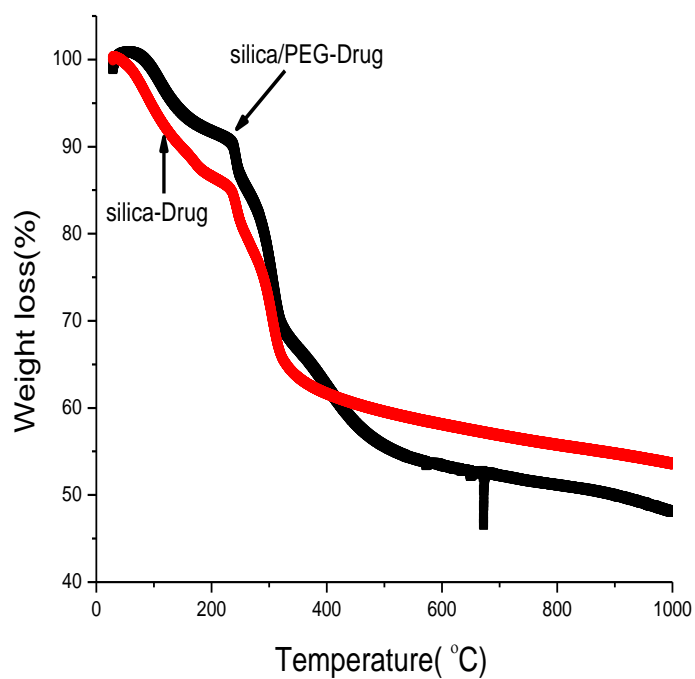


Figure 4.4. TGA curves of the silica xerogel/drug and PEG/silica xerogel/drug systems.

4.5.6 *In-vitro* release studies of entrapped gentamicin from xerogel and xerogel/PEG matrix

In-vitro release profiles of gentamicin immobilized in the silica xerogel and silica xerogel/PEG matrix are presented in Figure 4.5. All samples showed a higher release rate followed by a slower, steady release. Silica xerogel/PEG was used to investigate how the polymer (PEG) concentration influences the release of gentamicin. Incorporation of 2% PEG in the fabrication process increased the release of gentamicin from the xerogel. There was a sustained release of gentamicin (57% in 33 h) from the silica xerogel network, while with the addition of 2% PEG the gentamicin release rate reached 90% in 33 h.

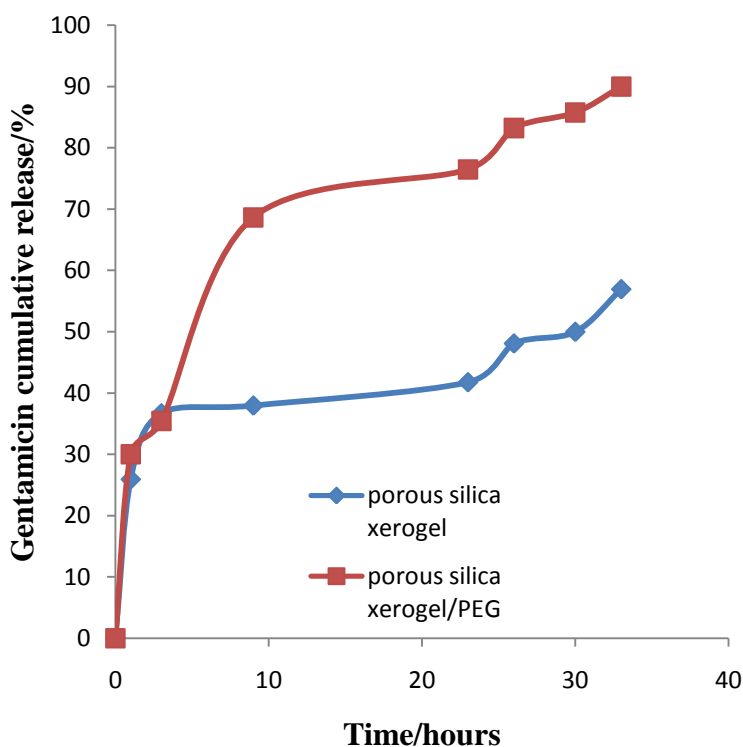
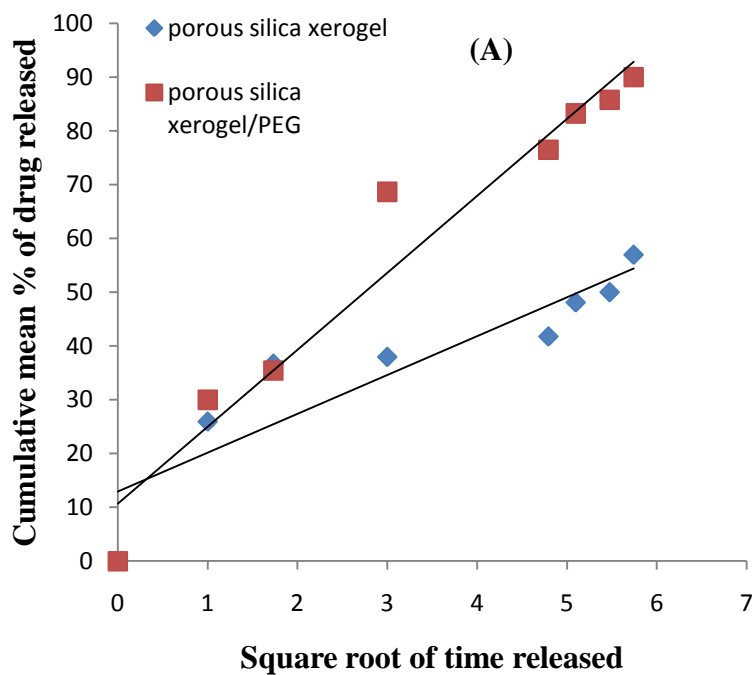


Figure 4.5. Cumulative release of gentamicin from silica xerogel and silica xerogel-PEG complex. *In-vitro* release profiles of gentamicin immobilized in the silica xerogel and that in the xerogel/PEG matrix showed a higher release rate followed by a slower, steady release. There was

a sustained release of gentamicin (57% in 33 h) from the silica xerogel network, while with the addition of 2% PEG the gentamicin release rate reached 90% in 33 h.

Additionally, to evaluate the release mechanism of the gentamicin, the results were analyzed according to the first order equation and Higuchi model[24, 25]. As per this model a straight line is expected if drug release from the carriers is based on a diffusion mechanism. The Higuchi equation model best describes the gentamicin release from the porous silica xerogel carriers and is consistent with a Fickian diffusion mechanism. The plot for the Higuchi model shows linear behavior with correlation coefficients $r > 0.93$. For the first order equation (cumulative percentage of drug release versus square root of time) the correlation coefficients exhibited a linear relationship ($r > 0.90$). The two mathematic models of first-order and Higuchi are reported in Figure 4.6. (A and B) and the correlation coefficients of the models obtained for all of the gentamicin-loaded silica xerogel and silica xerogel/PEG are compared in Table 4.2.



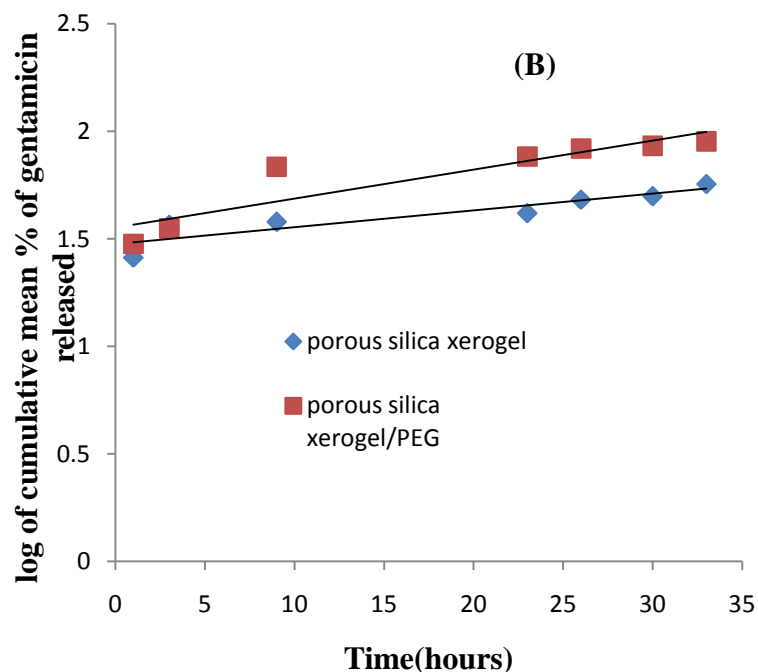


Figure 4.6. (A) Cumulative release of gentamicin (Q) versus square root time profile (Higuchi model), (B) First-order plot of gentamicin released versus time.

Confocal Analysis

The silica xerogel and silica xerogel/PEG particles were successfully loaded with FITC. Confocal fluorescence images of macrophage cells (Figure 4.7.) clearly show the efficient uptake of the silica xerogel-FITC and silica xerogel/PEG-FITC silica particles after 1 hour incubation.

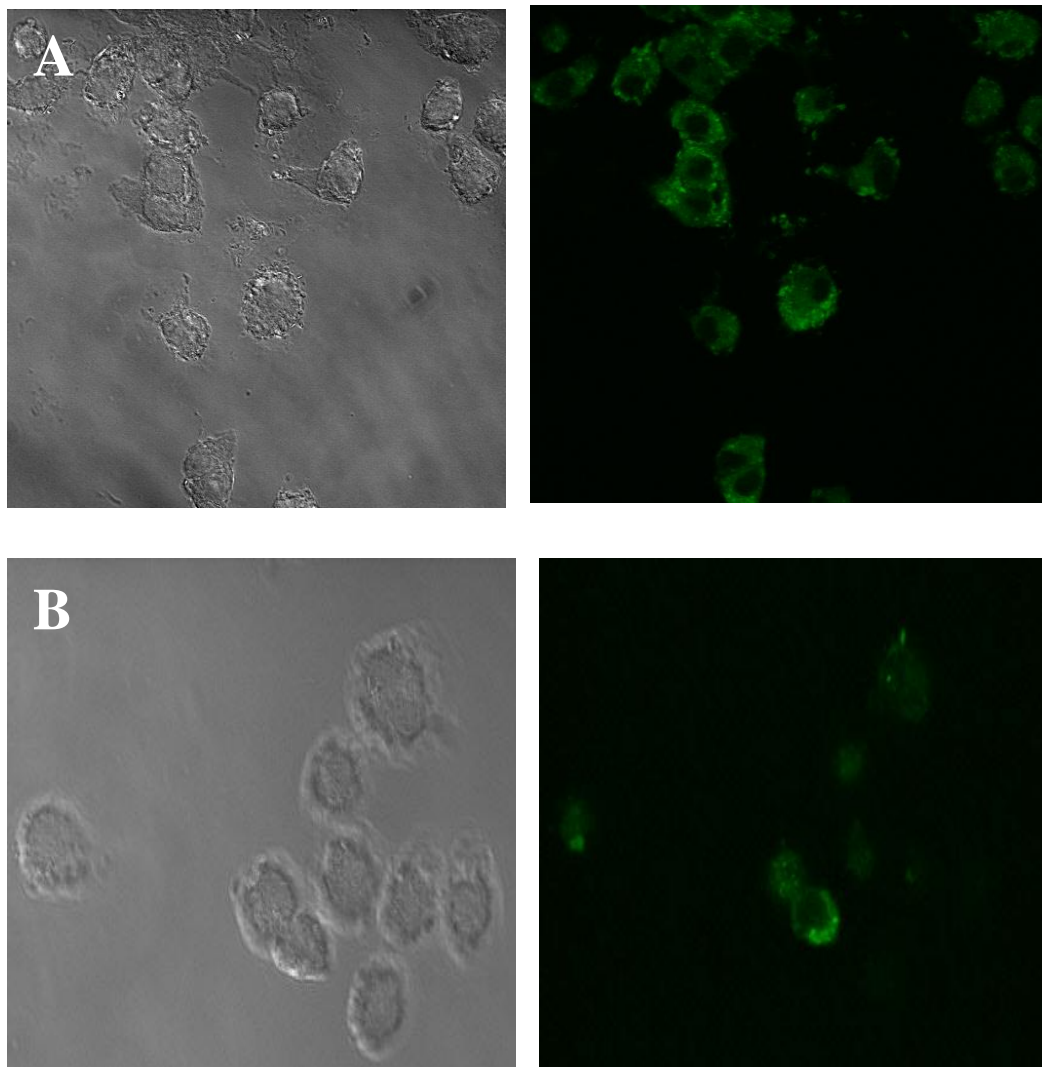


Figure 4.7. Confocal microscopy images of macrophage cells loaded with the (A) silica xerogel-FITC, (B) PEG/silica xerogel/FITC. (Left) transmitted image of cell lines, (Right) endocytosed green fluorescent image of silica xerogel particles.

Table 4.2. Correlation coefficients of different mathematical models for gentamicin-loaded silica and PEG/silica xerogels.

Material	First-order	Higuchi
Gentamicin-loaded silica xerogel	0.9163	0.9306
Gentamicin-loaded silica xerogel/PEG	0.9109	0.9737

4.5.7 *In-vivo* infection assay

The efficacy of the antibiotic loaded silica versus the free form of the same concentration of gentamicin was tested in AJ 646 mice. The treatment of mice started three days after infection with *S. typhimurium*. The mice received two doses of free gentamicin, antibiotic-loaded silica xerogel with PEG or control silica. At 2 days after administration of the last dose, the animals were euthanized, and the CFUs in the liver and spleen were assayed. The results are summarized in Table 4.3. The xerogel/PEG gentamicin therapies induced a significant ($P < 0.05$) reduction in the log CFUs of *S. typhimurium* in the spleen and liver of infected mice. The empty xerogel and the free gentamicin did not produce a significant reduction of *S. typhimurium*.

Table 4.3. Efficacy of two doses of Silica-antibiotic hybrid against infection with *S.typhimurium*^a.

Treatment	Log CFU±SD/ spleen	Reduction (log)	Log CFU±SD/ liver	Reduction (log)
No treatment	3.16 ±0.06	0.00	2.80 ±0.09	0.00
Silica control	3.34 ±0.14	+0.18	2.65±0.03	0.15
Free gentamicin	3.38 ±0.15	+0.22	2.73 ±0.11	0.07
Silica gentamicin	2.71 ±0.07	0.45*	1.67 ±0.22	1.13*
Silica –PEG – gentamicin	2.75 ±0.11	0.41*	1.65 ±0.43	1.15*

^a Groups of five mice each were infected intraperitoneally with *Salmonella* serovar Typhimurium (4×10^3 CFU/mouse). After 72 h, the animals received two doses of free or silica-loaded antibiotics (150 µg/mouse). At 48 h after administration of the last dose, the animals were euthanized; liver and spleen were assayed for CFU. Values represent the mean ± standard error numbers of CFU. Statistical significance levels were defined as $P < 0.05$ (shown by asterisks).

4.6 DISCUSSION

The development of a new drug carrier capable of intracellular delivery of sustained released therapeutics to where the intracellular pathogen resides will allow intracellular accumulation of the antibiotic after particle degradation and will improve drug targeting. Moreover, sustained drug delivery could reduce long-term treatment, reduce dosing frequency, and eliminate some of the toxic side effects associated with the free drug. In the present study, we investigated the effect of sol-gel processing parameters on the delivery of gentamicin and the efficacy of treatment compared to that of free drug against murine salmonellosis. By varying the sol-gel synthesis conditions, specifically the pH of the sol, the final microstructure of the silica xerogel and release rate of gentamicin was varied. In silica xerogel synthesis, the pH of the initial hydrolyzed sol was raised from pH 2 to 6-6.5 with NH_4OH . With increase in pH, the rate of gel formation or condensation reaction is affected, which influences the final silica xerogel network structure. During the pH 2 condition, which is near the isoelectric point (IEP), the gel formation occurs slowly and this reaction time increases with increase in pH towards basic [26]. Hence, with the addition of NH_4OH base catalyst, the pH of the sol increases and gel formation rate increases which leads to formation of a more porous network. The drug molecules entrapped in the sol-gel matrix remained in a biologically active form, and the bactericidal effect was retained upon its release. The fabrication method using a room-temperature synthetic route and low acid was essential to preserve the antibiotic activity. The pore size of the silica xerogel and silica xerogel/PEG matrix is large enough to allow gentamicin molecules to diffuse through the pore channels, which leads to different levels of decrease in nitrogen adsorption, reflecting the different storage amounts of the drug in the porous network. The incorporation of gentamicin

molecules into the silica xerogel leads to a decrease in pore diameter, surface area, and pore volume (Table 4.1.).

PEG in high concentration has been widely used as a successful strategy to incorporate hydrophilic chains or to change the surface charges of the therapeutic nanoparticles, resulting in increased blood circulation time and decreased phagocytosis possibly due to decreased nonspecific interaction of the complex with serum components [14]. In this study, PEG was used at a low concentration to control the pore properties and enhance the release of the cargo. By incorporation of 2% PEG during hydrolysis, the channels were better connected with increased pore volume (Table 4.1.). Thus, it is obvious that the pore structure of silica xerogel can be modified by addition of PEG and that the silica xerogel/PEG with various pore structures can be prepared by changing the PEG ratio. The larger pore volume and hydrophilic factors facilitate more penetration of the immersion solution inside the silica lattice and accelerate the diffusion of the gentamicin molecules in a given period of time. The *in-vitro* drug release profiles of the gentamicin from the xerogel and that from the silica xerogel/ PEG were distinctly different at pH 7.4. Experimental results suggest that the release of gentamicin from the silica xerogel matrices is a combination of diffusion and swelling of the matrix. For silica alone, due to limited interconnection of the channels, the immersion solution penetrates slowly through the silica matrix to the interior, and therefore, the release of gentamicin from the silica matrix was delayed. For the PEG-silica xerogel complex, during the immersion time, a partial physical erosion of the material surface could have taken place followed by penetration of solution inside the PEG-silica complex. Incorporation of PEG in the silica matrix allows formation of a more interconnected and hydrophilic porous network. This allows the immersion solution to freely penetrate the pores of

the matrices, causing swelling. This allows the gentamicin to be more easily leached out through the interconnected channels.

Both release rates were sufficiently low to signify that the silica xerogel remained intact under physiological conditions at pH 7.4, and this could enhance phagocytosis by the reticuloendothelial system [20] and reduce ototoxic and nephrotoxic effects associated with free gentamicin [4, 15]. Although the faster release of the drug after addition of 2% PEG did not alter the efficacy of treatment (Table 4.2.), it should be useful for other applications that require faster release of therapeutics without interfering with the phagocytosis process.

Determination of the efficiency of the silica xerogel and silica xerogel/PEG for elimination of *Salmonella* from the spleen and liver of infected mice was assessed after treatment with two doses. The results indicated that both silica xerogel and xerogel-PEG were more effective in clearing the infection in the spleen and liver than was the same dose of free drug. The silica xerogel and silica xerogel/PEG achieved a 0.45- log and a 0.41-log reduction in the spleen, respectively, while for the free drug there was no reduction. Both of these values were statistically significant ($P<0.05$) in comparison with the results achieved for the negative control. On the other hand, silica xerogel and xerogel-PEG achieved statistically significant 1.13-log and 1.15-log reduction in the liver ($P<0.05$), respectively, while for the free drug, the reduction was a non-significant value of 0.07 log from the results achieved for the control. To achieve intracellular delivery of aminoglycosides, several drug delivery strategies have been utilized using liposome and polymeric carriers [3, 9]. Although these drug delivery systems have improved the intracellular delivery of aminoglycosides, they still suffer from low drug incorporation. Silica xerogel obtained by the techniques used in this study contained 31% of its weight in antibiotic, 31-fold higher than the values reported earlier using liposome [5].

The higher loading capacity of the silica xerogel is attributed to the significant clearance of the infection from the mice. Our previous experiment used only 17% loading of gentamicin, and in these studies, the clearance was not statistically significant [13]. This clearly indicates that we could achieve a higher rate of clearance of infection by changing the porosity and increasing the drug loading capacity of the silica xerogel. It is possible that, by proper engineering of the sol-gel process, even higher drug loading capacities could be achieved, but the data show that at the current drug loading levels used in this study, a sufficient amount of drug is delivered. One variation of the process, which could achieve much higher drug loading amounts, would be using aerogel particles as drug delivery carriers. Aerogels have an open mesoporous structure with porosity up to 98% by volume and a high surface area of 400 to 1,000 m²/g, which would be suited for high loading of the drugs [17].

The present study demonstrates the feasibility and efficacy of targeting *Salmonella* by using gentamicin incorporated into bioactive porous silica made by a xerogel processing technique and a room-temperature synthesis route. The gentamicin-hybrid silica xerogel showed a significantly higher rate of bacterial clearance from organs than did the same dose of free drug. Although the mouse model did not provide direct evidence that the hybrid xerogel was taken up intracellular, these results indicate that the porous silica xerogel could be used as a drug delivery system to control salmonellosis.

4.7 REFERENCES

- [1] M. Ahola, P. Korteso, I. Kangasniemi, J. Kiesvaara, A. Yli-Urpo. 2000. Silica xerogel carrier material for controlled release of toremifene citrate. *Int. J. Pharm.* **195**: 219–227.
- [2] J.F.T. Conroy, M. E. Power, J. Martin, B. Earp, B. Hosticka, C.E. Daitch, P.M. Norris. 2000. Cells in sol-gels I: a cytocompatible route for the production of macroporous silica gels. *J. Sol Gel Sci. Technol.* **18**: 269–283.
- [3] E. Fattal, J. Rojas, L. Roblot-Treupel, A. Andremont, P. Couvreur. 1991. Ampicillin-loaded liposomes and nanoparticles: comparison of drug loading, drug release and in vitro antimicrobial activity. *J. Microencapsul.* **8**: 29–36.
- [4] A. Forge, J. Schacht. 2000. Aminoglycoside antibiotics. *Audiol. Neurootol.* **5**: 3–22.
- [5] R.M. Khalil, F.E. Murad, S.A. Yehia, M.S. El-Ridy, H.A. Salama. 1996. Free versus liposome-entrapped streptomycin sulfate in treatment of infections caused by *Salmonella enteritidis*. *Pharmazie* **51**: 182–184.
- [6] P. Korteso, M. Ahola, S. Karlsson, I. Kangasniemi, A. Yli-Urpo, J. Kiesvaara. 2000. Silica xerogel as an implantable carrier for controlled drug delivery-evaluation of drug distribution and tissue effects after implantation. *Biomaterials* **21**: 193–198.
- [7] P. Korteso, M. Ahola, S. Karlsson, I. Kangasniemi, J. Kiesvaara, A. Yli-Urpo. 1999. Sol-gel-processed sintered silica xerogel as a carrier in controlled drug delivery. *J. Biomed. Mater. Res.* **44**: 162–167.
- [8] E.J. Lee, D.S. Shin, H.E. Kim, H.W. Kim, Y.H. Koh, J.H. Jang. 2009. Membrane of hybrid chitosan-silica xerogel for guided bone regeneration. *Biomaterials* **30**: 743–750.

- [9] P. Lutwyche, C. Cordeiro, D.J. Wiseman, M. St.-Louis, M. Uh, M. J. Hope, M.S. Webb, B.B. Finlay. 1998. Intracellular delivery and antibacterial activity of gentamicin encapsulated in Ph-sensitive liposomes. *Antimicrob. Agents Chemother.* **42**: 2511–2520.
- [10] M. McClelland, K.E. Sanderson, J. Spieth, S.W. Clifton, P. Latreille, L. Courtney, S. Porwollik, J. Ali, M. Dante, F. Du, S. Hou, D. Layman, S. Leonard, C. Nguyen, K. Scott, A. Holmes, N. Grewal, E. Mulvaney, E. Ryan, H. Sun, L. Florea, W. Miller, T. Stoneking, M. Nhan, R. Waterston, R. K. Wilson. 2001. Complete genome sequence of *Salmonella* Typhimurium LT2. *Nature* **413**: 852–856.
- [11] D.M. Monack, D.M. Bouley, S. Falkow. 2004. *Salmonella typhimurium* persists within macrophages in the mesenteric lymph nodes of chronically infected Nramp1^{+/+} mice and can be reactivated by IFN gamma neutralization. *J. Exp. Med.* **199**: 231–241.
- [12] D.M. Monack, A. Mueller, S. Falkow. 2004. Persistent bacterial infections: the interface of the pathogen and the host immune system. *Nat. Rev. Microbiol.* **2**: 747–765.
13. P. Munusamy, M.N. Seleem, H. Alqublan, R. Tyler, Jr., N. Sriranganathan, G. Pickrell. 2009. Targeted drug delivery using silica xerogel systems to treat diseases due to intracellular pathogens. *Mater. Sci. Eng. C* doi:10.1016/j.msec.2009.05.020.
- [14] A. Sato, S.W. Choi, M. Hirai, A. Yamayoshi, R. Moriyama, T. Yamano, M. Takagi, A. Kano, A. Shimamoto, A. Maruyama. 2007. Polymer brush stabilized polyplex for a siRNA carrier with long circulatory half-life. *J. Control. Release.* **122**: 209–216.
- [15] M.N. Seleem, N. Jain, N. Pothayee, A. Ranjan, J. S. Riffle, N. Sriranganathan. 2009. Targeting *Brucella melitensis* with polymeric nanoparticles containing streptomycin and doxycycline. *FEMS Microbiol. Lett.* **294**: 24–31.

- [16] I.I. Slowing, J.L. Vivero-Escoto, C.W. Wu, V.S. Lin. 2008. Meso-porous silica nanoparticles as controlled release drug delivery and gene transfection carriers. *Adv. Drug Deliv. Rev.* **60**: 1278–1288.
- [17] I. Smirnova, J. Mamic, W. Arlt. 2003. Adsorption of drugs on silica aerogels. *Langmuir* **19**: 8521–8525.
- [18] B.G. Trewyn, S. Giri, I. I. Slowing, V. S.-Y. Lin. 2007. Mesoporous silica nanoparticle based controlled release, drug delivery, and biosensor systems. *Chem. Commun.* **31**: 3236–3245.
- [19] B.G. Trewyn, I.I. Slowing, S. Giri, H.-T. Chen, V.S.-Y. Lin. 2007. Synthesis and functionalization of a mesoporous silica nanoparticle based on the sol-gel process and applications in controlled release. *Acc. Chem. Res.* **40**: 846–853.
- [20] A. Vazquez-Torres, J. Jones-Carson, A.J. Baumler, S. Falkow, R. Valdivia, W. Brown, M. Le, R. Berggren, W.T. Parks, F.C. Fang. 1999. Extraintestinal dissemination of *Salmonella* by CD18-expressing phagocytes. *Nature* **401**: 804–808.
- [21] L. X. Wen, D. Hao-Min, J.X. Wang, J.F. Chen. 2006. Porous hollow silica nanoparticles as carriers for controlled delivery of ibuprofen to small intestine. *J. Nanosci. Nanotechnol.* **6**: 3139–3144.
- [22] Y. Zhu, J. Shi. 2007. A mesoporous core-shell structure for Ph-controlled storage and release of water-soluble drug. *Microporous Mesoporous Mater.* **103**: 243–249.
- [23] Y. Zhu, J. Shi, Y. Li, H. Chen, W. Shen, X. Dong. 2005. Hollow mesoporous spheres with cubic pore network as a potential carrier for drug storage and its in vitro release kinetics. *J. Mater. Res.* **20**: 54–61.

- [24] T. R. Bryans, V.L. Brawner, E. L. Quitevis. 2000. Microstructure and Porosity of Silica Xerogel Monoliths Prepared by the Fast Sol-Gel Method. *Journal of Sol-Gel Science and Technology*. **17**: 211–217.
- [25] A. Fidalgo, L.M. Ilharco. 2004. Chemical Tailoring of Porous Silica Xerogels: Local Structure by Vibrational Spectroscopy. *Chem. Eur. J.***10**: 392-398.
- [26] P. Korteso, M. Ahola, M. Kangas, A. Yli-Urpo, J. Kiesvaara, M. Marvola. 2001. In vitro release of dexmedetomidine from silica xerogel monoliths: effect of sol-gel synthesis parameters. *International Journal of Pharmaceutics*. **221**: 107–114.
- [27] M. Prokopowicz. 2007. Silica-Polyethylene Glycol Matrix Synthesis by Sol-Gel Method and Evaluation for Diclofenac Diethylammonium Release. *14*: 129-136.

CHAPTER 5

SYNTHESIS AND CHARACTERIZATION OF MAGNETIC SILICA XEROGELS CONTAINING ANTIMICROBIALS FOR TARGETING INTRACELLULAR PATHOGENS

Journal of Bionanoscience 2009, 3, 1-6

**Authors: Prabhakaran Munusamy, Mohamed N. Seleem, Nammalwar Sriranganathan, and
Gary Pickrell**

5.1 ABSTRACT

Nanotechnology has contributed significantly to pharmacology and antimicrobial therapy through drug delivery systems targeting phagocytic cells that are infected by intracellular pathogens. Magnetically controlled drug release may facilitate the entrance of the drug into the intracellular replicative niche of these pathogens. Furthermore, sustained drug delivery could reduce long-term treatment, improve drug bioavailability, reduce dosing frequency, encourage patient compliance and eliminate some of the toxic side effects associated with the free drug. Porous magnetic silica xerogel (Fe/silica) particles were fabricated using the sol-gel technique. The formation and loading of iron was confirmed by Fourier transform infrared spectroscopy and N₂ adsorption measurements. The *in-vitro* drug release studies confirm that the release rate can be adjusted by magnetic field ON-OFF mechanism. In presence of magnetic field, the iron particles loaded in the silica xerogel matrix undergoes orientation changes, which lead to enlargement of

pore channels. This creates the possibility of easy and effective drug release in comparison to slow release of xerogel without iron oxide embedded in it. The uptake of FITC-loaded magnetic silica xerogel complexes by macrophage cells observed by confocal microscopy indicates that the prepared magnetic silica xerogel particles can readily be taken up by macrophage cells in a relatively short period of time. Administration of 2 doses of Fe/silica xerogel complex significantly reduced *Salmonella* infection compared to free drug in a mouse model. The reduction for Fe/silica xerogel in the spleen of infected mice were 0.47 while, in the livers were 0.79 respectively. These results imply that this novel ON-OFF process of drug release methodology using magnetic xerogel system offers numerous possibilities in treating chronic diseases by intracellular pathogens. The particles could be designed for uncontrolled slow diffusion to a regulated release of (therapeutically effective) curative dosage after reaching the intracellular location where the bacteria reside.

5.2 INTRODUCTION

Treatment and control of diseases caused by intracellular pathogens like *Brucella*, *Salmonella* and *Mycobacterium* are difficult, since, these agents localize in intracellular compartments within phagocytic cells and most antimicrobials, although highly active *in-vitro*, do not actively pass through cellular membranes [1,2]. Thus, an optimum strategy to treat these infections should include targeting of a highly active drug to the intracellular compartment where bacteria replicate, as well as prolong the release of that antimicrobial, reduce the number of doses and associated toxicity. If antimicrobials could be targeted and delivered specifically into the replicative niche of the intracellular pathogens, clearance of organisms and the abilities to improve innate and adaptive immune responses could be enhanced considerably.

Our strategy is to develop a stimuli-responsive, controlled release system which can effectively deliver the required dosage of the appropriate drug into the replicative niche of the intracellular pathogens. This strategy can improve patient compliance, reduce the number of doses and decrease drug toxicity. One of the prominent and most studied controlled release materials for drug delivery applications are sol-gel derived porous silica [3]. It is of special interest in controlled release applications as it has already been used for different kinds of antibiotics where drug molecules are simply entrapped within the silica matrix without any chemical bonding [4]. The drug molecules entrapped in the sol-gel matrix remain in a biologically active form and the bactericidal effect is retained upon its release. They are biocompatible in nature and have been proved so *in vivo* [5-8]. Magnetic materials have been widely used in various types of medical applications and recently in the field of drug delivery [9]. For magnetic drug targeting, the drug has to be immobilized on a magnetic xerogel carrier possessing magnetic properties. The magnetic xerogel carriers can be driven to release at a specific site by a magnetic field [9-11].

Another major area of practical interest is to trigger the drug release once it arrives at therapeutic sites [12-14]. A real-time burst control of drug release needs a quickly responsive drug release mechanism to release a precise amount of the drug when the body needs it. Hence, it may be possible to use a combination of silica xerogel and iron particle composites as a magnetically-controlled potential drug carrier system for treating intracellular pathogens, and development of such a system is the focus of this paper.

5.3 EXPERIMENTAL DETAILS

5.3.1 Preparation of sol-gel processed Fe/Silica particles

Fe/silica xerogel particles were prepared at room temperature by two phase acid-base hydrolysis and polycondensation of tetraethoxysilane (TEOS, Aldrich) [15]. The hydrochloric acid was used as the acid catalyst and NH_3 as the base catalyst. The molar ratio of water to TEOS was fixed at 1:8. The weight ratio of antibiotics (gentamicin) to silica was 10-15%. Briefly, 10.4g of TEOS were slowly added to 7.2 g of a solution of distilled water and HCl with a pH value of 2.0. The resulting solution was magnetically stirred at 300 rpm for 30 min at room temperature. After the completion of the hydrolysis reaction, the nitric acid in the resultant homogenous solution was neutralized with an NH_3 base. The pH was adjusted to a range of 7-7.3 by drop wise addition of 1M NH_4OH . The sol obtained was kept stirred constantly for another 30min. For preparation of Fe/silica particles, 2 g of $\text{Fe}(\text{NO}_3)_3 \cdot 9 \text{H}_2\text{O}$ was dissolved in water and added to the above silica xerogel solution to form a clear hydrolyzed sol and kept stirred constantly for 1h at room temperature. Gentamicin sulfate was added to this solution to form a clear hydrolyzed sol. The resulting drug loaded sol was allowed to gel and was subsequently dried at room temperature for 3 days. The dried gentamicin loaded xerogel was then crushed and refined into powders with an average particle size of approximately $<1 \mu\text{m}$.

5.3.2 Synthesis of fluorescein isothiocyanate(FITC)-labeled porous Fe/silica particles

For loading FITC to Fe/silica xerogel samples, 3 ml of FITC solution 5 mg/ml in ethanol was stirred in the presence of 50mg of Fe/silica xerogel samples. The reaction mixture was vigorously stirred for 3 h at room temperature. The resulting solid was filtered, washed thoroughly with ethanol and dried in air for 24 h.

5.3.3 Cell culture and localization of Fe/silica - FITC

To study the ability of the FITC tagged magnetic silica xerogel particles to enter cells, macrophage cell line J774. A1 was used for this study. The J774A.1 cells were routinely grown as monolayers in 75 cm² tissue culture Flask (Corning Corporation Inc.) in a humidified 5% CO₂ atmosphere at 37°C. The cells were cultured and maintained in Dulbecco's modified Eagle's medium (DMEM) supplemented with 10% fetal bovine serum (FBS). At 90% confluency the cells were gently scrapped, seeded in six-well plates at density of 0.5x10⁶ cells/well and incubated for 24 h in a humidified 5% CO₂ atmosphere at 37°C to allow for attachment. Before the experiment, the culture media was discarded from each well, 200 µl (1.5mg/ml) Fe/silica-FITC in DMEM supplemented with 10 % FBS were added to each well. After 1 h of incubation, cells on cover slips were washed three times with phosphate buffered saline (PBS) and fixed in 4% paraformaldehyde for 1 h, washed twice with PBS before mounting with Flouromount-G fluid (Southern Biotechnology Associates Inc.). Intracellular localization of silica was visualized using a Zeiss LSM 510 laser scanning microscope.

5.4 CHARACTERIZATIONS

The powder X-ray diffraction (XRD) patterns of porous Fe/silica were collected with a Siemens D-4000 powder diffractometer using Cu K α irradiation. The particle size and zeta potential of the Fe/silica xerogels were carried out in Malvern Zetasizer Nano Series. The Infra-Red (IR) spectra for powder samples were measured using a Fourier transform infrared spectrophotometer (FTIR) (PerkinElmer). The N₂ adsorption analysis was measured using nitrogen gas adsorption isotherms at 77 K in Autosorb-1 MP (Quantachrome Co.). The specific surface area and porosity parameter were calculated using the Barrett-Joyner-Halenda (BJH) technique [21]. Before the N₂ adsorption-desorption isotherm analysis, the samples were crushed and degassed at 200°C for 2h. The morphologies of the synthesized magnetic silica xerogels were examined using field emission scanning electron microscopy (FE-SEM, JEOL-6500). Prior to SEM analysis, the particles were sputter coated with gold. For drug release testing, the magnetic silica xerogels containing gentamicin were first immersed in 20 ml of PBS, pH 7.4 and then UV-visible spectroscopy(UV-Vis) was used for the characterization of the absorbance peaks at 246 nm to determine the release concentration of gentamicin. The magnetization of Fe/silica xerogel samples were measured with a Helmholtz coil setup in the range of 0.3-1KA/m. All measurements were conducted at room temperature.

5.4.1 Bacterial strain

Salmonella typhimurium strain LT2 [11] was routinely grown at 37°C in tryptic soy broth (TSB) or on tryptic soy agar (TSA, Difco).

5.4.2 Animal experiment (*in-vivo* infection assay)

To study efficacy of the Fe/silica xerogel loaded antibiotic *in vivo*, female 6 weeks old AJ 646 mice (Charles River Laboratories, MA) 6 weeks old were used. Groups of five mice each were infected intraperitoneally with *S. typhimurium* (4×10^3 CFU/mouse). The animals received two doses of (1) Fe/silica control, (2) free gentamicin 150 μ g, (3) Fe/silica xerogel/gentamicin 150 μ g, and (5) PBS at days 3 and 5 post-infection. The animals were euthanized 48 h after administration of the last dose. The spleen and liver were collected and bacterial colony forming units (CFUs) per individual organ were determined by plating a series of 10-fold serial dilutions of the organ homogenates on TSA plates. The number of colonies was determined after incubation for 24 h at 37°C.

The experimental procedures on mice and the facilities used to hold the experimental animals were in compliance with the rules of the Virginia Tech Institutional Animal Care and Use Committee.

5.4.3 Statistical analysis

All statistical analyses for bacterial clearance from organs were performed using the Student two-tailed *t* test using Microsoft Excel. *P* values ≤ 0.05 were considered significant.

5.5 RESULTS AND DISCUSSION

The synthesized acid-base catalyzed Fe/silica xerogel after addition of gentamicin drug is transparent, glassy and crack-free monoliths (Figure 5.1.). This indicates that the gentamicin was homogeneously distributed throughout the xerogel without any macroscopic phase separation. To prevent denaturation and damage of the antibiotic activity, room temperature and low acidity parameters were selected for synthesis of the magnetic silica xerogel-antibiotic composites.



Figure 5.1. Acid-base catalyzed Fe/silica xerogel monolith.

X-Ray Diffraction analysis

The structural information of Fe/silica xerogel particles was confirmed by XRD patterns. Figure 5.2. shows the X-ray powder diffraction patterns of Fe/silica xerogel particles. The diffraction patterns for xerogel only show a line broadening centered at $\sim 22^\circ$ indicating the presence of amorphous silica particles [16]. The broad nature of the XRD pattern observed all the way from 10° to 80° represent the amorphous nature of small sized iron particles. Alternatively it is also possible that Fe particles gets highly dispersed onto the large internal pore surface or embedded in to the amorphous pore wall without formation of crystalline Fe particles [17].

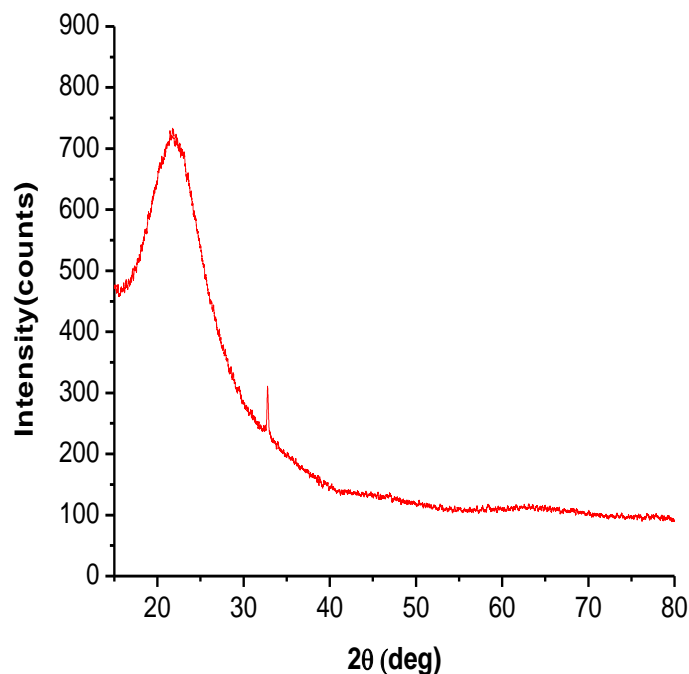


Figure 5.2. X-ray diffraction patterns of porous Fe/silica xerogels. No diffraction peaks except for the broad band assigned to the characteristic reflection of amorphous SiO₂ can be found ($2\theta = 22^\circ$).

Figure 5.3. (A and B) shows FTIR spectra xerogel alone and for Fe/silica xerogel. The group of bands observed corresponds well with the band positions for silica xerogel. The spectrum for silica xerogel consists of bands at $\sim 3400\text{cm}^{-1}$ attributed to the OH group and vibrational stretching mode of the water molecules [16]. The other bands observed for silica xerogel alone are Si-O-Si asymmetric stretching modes of siloxane at 1100cm^{-1} and Si-OH bending mode at 805cm^{-1} . Other than above observed bands few more new bands are observed for iron and silica xerogels. The bending band at 1630cm^{-1} corresponds to the -OH vibration mode and to Si-OH and Fe-OH bonds [17, 18]. The stretching bands at 1100 and the deformation band at 805cm^{-1} correspond to symmetric and asymmetric stretching modes of Si-O-Si and to the Si-

OH and Fe-O bonds. The smaller shoulder bands observed around 550 to 650 cm^{-1} are assignable to Fe-O bonds in Fe-O-Fe systems [18, 19].

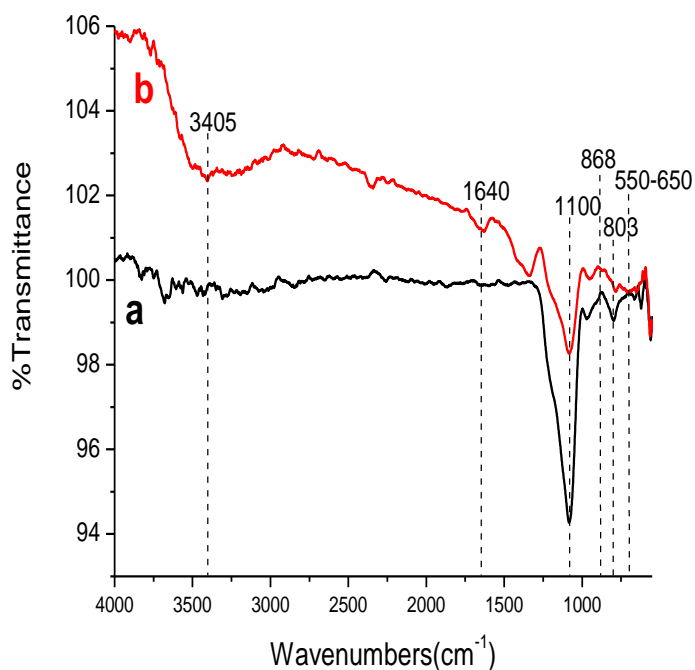


Figure 5.3. FTIR spectra for the (a) silica xerogel and (b) Fe/silica xerogel /iron oxide complex. The group of bands observed corresponds well with the band positions for silica xerogel. The smaller shoulder bands observed around 550 to 650 cm^{-1} are assignable to Fe-O bonds in Fe-O-Fe systems.

As additional structural information, energy dispersive X-ray analysis (EDX) analysis were performed for Fe/Silica xerogel particles.

Typical EDX spectra of all the samples are shown in Figure 5.4. The major EDX peaks correspond to the elements Si, O, and Fe are observed which confirms the absence of any unreacted original reagents.

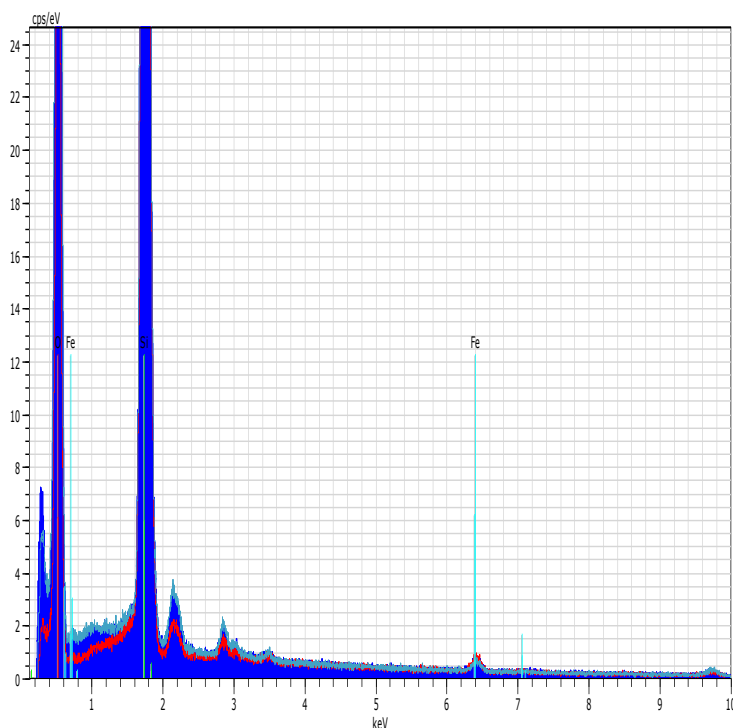


Figure 5.4. EDX pattern of Fe/silica xerogel particles prepared by acid-base catalyzed process.

The particle size measurements were carried out by suspending porous silica xerogel particles in a PBS solution pH 7.4. The particle size distribution was in a broad range from ~1.5 to 2 μm . The ζ -potential of -9.81 was measured for the silica xerogel particles, due to the presence of the hydroxyl group on the surface of silica, producing a negative surface charge [20].

The SEM image of the fracture surfaces of a Fe/silica xerogel are shown in Figure 5.5. The micrograph shows that the solid skeletal phase has a globular morphology with primary particles, 20–40 nm in diameter, that are joined together to form agglomerates a few hundred nm in diameter. The agglomerates are smaller and more closely packed with iron particles distributed in the silica matrix.

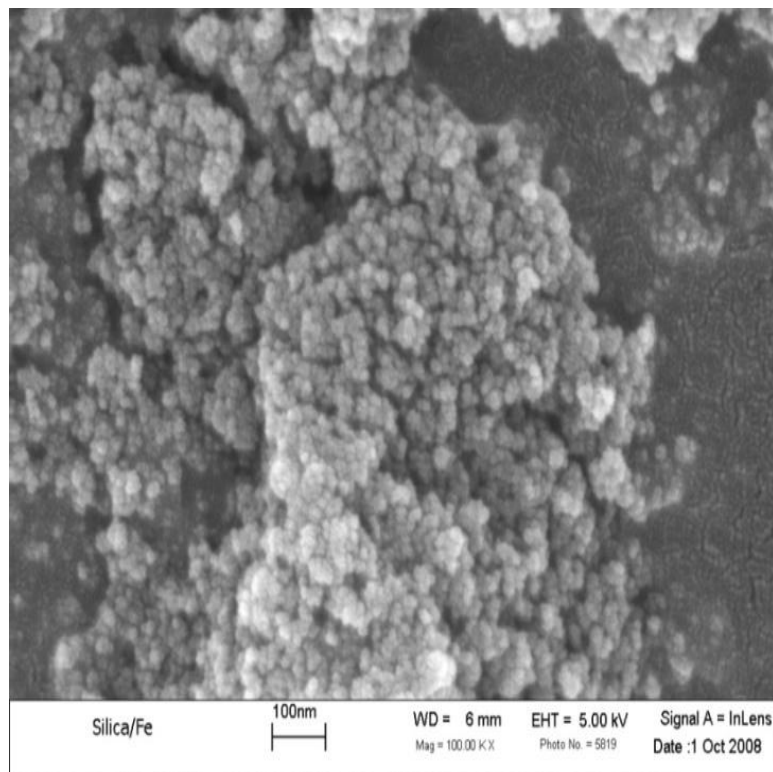


Figure 5.5. High-magnification scanning electron micrographs for acid-base catalyzed porous Fe/silica xerogel complex. The globular morphology with the clusters of agglomerates is seen. The mesoporous result from organized packing of globules in to large clusters.

The N_2 adsorption-desorption data for Fe/silica xerogels are shown in Figure 5.6. The mesoporous which result from compacted packing of globules as revealed in the SEM micrographs correlated well with the N_2 adsorption desorption isotherm data. According to Brunauer, Deming, Deming and Teller (BDDT) classification, the isotherm observed was of type IV, which is characteristic for acid-base catalyzed xerogels. The lower adsorption pressure and gradual increase in adsorption with increasing relative pressure which are characteristic for type IV isotherm indicates less microporosity and broader distribution of larger pores which are in the range of ~ 1 to 50nm. Also observed were hysteresis and large pore cavities which are

characteristics of type-IV isotherm[21]. The SEM analysis showed openings which are uniform in diameter formed by the voids between the agglomerates which are consistent to the steepness observed in the desorption branch. The steepness observed in the desorption branch provides the evidence for uniformity in the diameter of the openings. The SEM analysis of the microstructure, and well correlated with the interpretation from the N₂ adsorption-desorption isotherm.

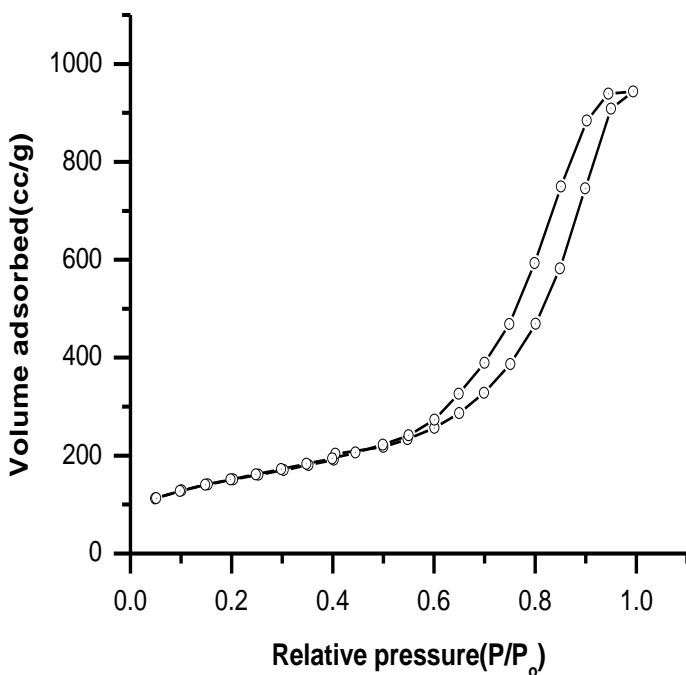


Figure 5.6. N₂ adsorption-desorption isotherms for acid-base catalyzed Fe/silica xerogels. The lower adsorption pressure and gradual increase in adsorption with increasing relative pressure which are characteristic for type IV isotherm indicates less microporosity and broader distribution of larger pores which are in the range of ~ 1 to 50nm.

The Barrett-Joyner-Halenda (BJH) method was used for determining the pore distributions for the prepared Fe/silica xerogel particles [21]. Figure 5.7. shows the pore size distribution with average pore diameter of ~173Å (17.3nm) as determined by the BJH method. In the pore diameter

distribution, a narrow peak was observed which decreases with increasing pore diameter. The observed shape of the distribution was consistent with micro and mesopore structures[21]. The Brunauer-Emmett-Teller (BET) surface area, pore size and pore volumes were decreased after the impregnation of iron in to the porous network. The values are shown in Table 5.1. The pore size greatly reduced from 88 Å to 38Å after impregnation of iron. The formation of iron particles within the silica xerogel network was confirmed by reductions in the Brunauer-Emmett-Teller (BET) surface area, pore size and pore volume [22-24].

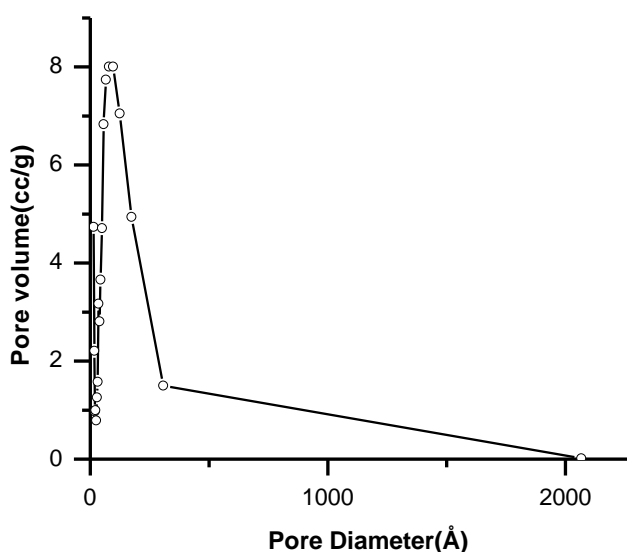


Figure 5.7. Pore distributions determined from the desorption isotherms for acid- base-catalyzed Fe/silica xerogel. Pore size distribution with average pore diameter of ~ 173 Å (17.3nm). The shape of this distribution is consistent with a microstructure composed of micropores and mesopores.

Table 5.1. Physical properties of porous silica xerogel and Fe/Silica xerogel from N₂ adsorption-desorption isotherms, ^a Calculated by the BJH method

Sample	Surface area/m²/g	Pore Diameter/Å^a	Pore Volume/cm³/g^a
Porous silica Xerogel	173.20	61	0.370
Porous Fe/silica xerogel	11.39	16	0.05

Confocal analysis:

The cellular uptake of Fe/silica xerogel particles was investigated by confocal microscopy analysis. Figure 5.8. shows the confocal image of magnetic silica xerogel particles internalized into macrophage cells. The image was taken after 1 h incubation of magnetic silica xerogel particles at 37°C. This allows potential use of Fe/silica xerogel particles as biomarker for multi-modal imaging applications.

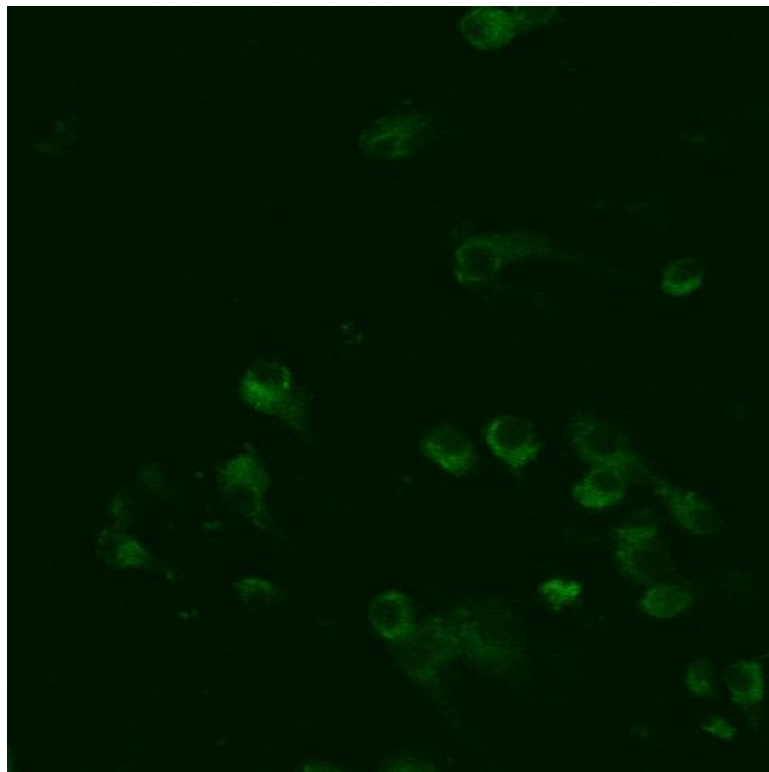


Figure 5.8. Confocal image of Fe/silica xerogel particles in macrophage cells after 1 h of uptake time; particles are tagged with FITC (green).

5.5.1 Magnetic field controlled drug release

For drug release experiments, gentamicin-containing Fe/silica xerogels were dispersed in PBS solution. The silica xerogels show drug release profile similar to one observed under the condition of a magnetic field, but with different amounts of drug release. Figure 5.9. shows the cumulative gentamicin drug release profile for Fe/silica xerogel with and without the application of the magnetic stimulation. During the first hour of exposure to the magnetic field, a sharp burst release pattern was displayed. Then, the release profile was restored to a steady state, and slow release. The burst release observed was due to the magnetic field associated perturbation with

silica xerogel magnetic particles. The Fe/silica xerogel particles are shown for comparison without applying any magnetic field.

The results suggest that the burst release under magnetic field may be related with the silica xerogels magnetic properties. By this means, the drug release behavior of these particles can be precisely controlled from a steady state, slow profile to a burst profile by means of exposure to the magnetic field stimuli. This observation suggests that the variation in the structure of the Fe/Si particles is physically reversible, and it is believed that the magnetically induced deformation of the xerogels as a result of the oscillation or vibration of the embedded magnetic particles can be elastic. This elastic deformation ensures a long-term, reliable controlled release of the drug. In addition, the fast response of the xerogels with respect to burst release of the drug right after subjecting it to the magnetic field stimulus provides greater potential for an on-time drug release for medical applications. The results imply that the drug molecules in the xerogels exactly followed the signals switching from burst to slow release for each operation.

This mechanism clearly explains that the drug release behavior of porous Fe/silica particles can be changed from burst release to a slow release profile, steady state or vice versa by means of an “ON/OFF” mechanism switch. This principle provides potential advantages over other drug delivery methods, because the amount of drug delivered can be precisely controlled by the application of an external magnetic field. That is by applying a magnetic field, the drug release concentration can be instantly increased and under suitable control, the drug concentration can be monitored in such a way that it reaches the bactericidal concentration for the desired period of time inside the phagocytes for a cure.

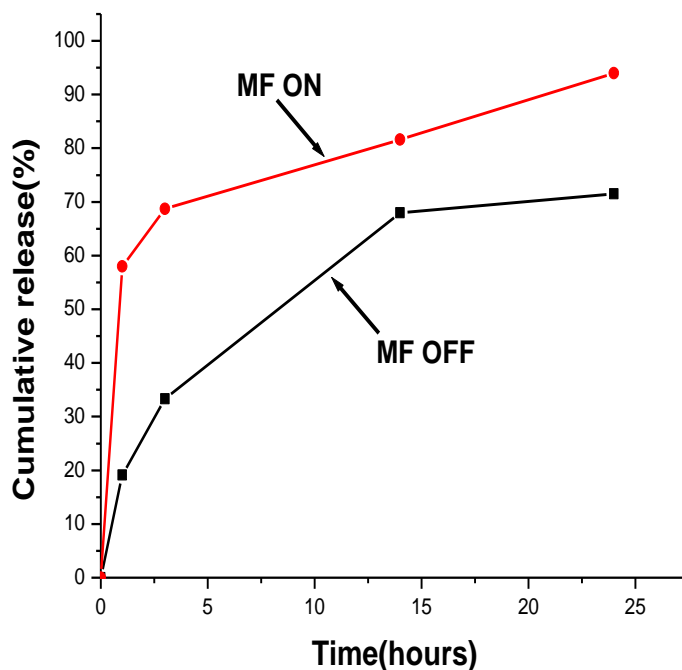


Figure 5.9. Cumulative drug release profiles from magnetically controlled porous Fe/silica xerogel particles and the control group of silica xerogel particles without magnetic simulation. (Red line- Drug release profile from Fe/silica xerogel complex with magnetic simulation, Black line- Control group of Fe/silica xerogel complex without magnetic simulation). Drug loaded silica xerogel/Fe were actuated by applying magnetic field. Increase in the amount of drug release was observed in presence of magnetic excitation.

5.5.2 Mechanism of Magnetic-Sensitive Drug Release Behavior

Figure 5.9. shows the hypothesized drug release mechanism from the Fe/silica xerogel particles. During initial stages of the experiment in the absence of magnetic force, the magnetic field which exists in the silica xerogel will be disoriented. During this period, the drug release profile follows a diffusion release mode where no magnetic force is applied. When the magnetic force is applied to the xerogel particles, a bulk magnetic moment is produced due to the alignment

of magnetic moments present in the xerogel particles. This possibly leads to a rearrangement of the iron particles inside the silica xerogel matrix which also provides a change in the porous network. Hence, the drug molecules which are entrapped inside the confined network experience additional forces in addition to the free energy gradient produced by the chemical potential difference; this causes a rapid and significant release, when the xerogel particles are subjected to magnetic field. In the absence of magnetic field, the random orientation of iron particles is limited. This leads back to normal slow and steady diffusion profile release.

In summary, targeting intracellular pathogens using magnetic silica xerogels can have the potential to treat chronic infections. Though the exact release mechanism is not confirmed, our preliminary investigations have shown a remotely controlled drug release model where we can precisely control the amount of drug release by alternating magnetically triggered operations. By the ON-OFF magnetic field operation method we can effectively deliver the required dosage of drug to specific disease causing bacteria within the cells. This will allow a reduction in the amount of drug used and the duration required to kill the intracellular pathogens. This method can provide significant advantages over other drug release methods in a way that the overall amount of antibiotic dose and duration of treatment required for the control of intracellular bacteria can be greatly reduced. Other than antimicrobials, porous silica magnetic xerogels are versatile and bind any proteins, antimicrobial peptides and antibodies, since they can be easily functionalized. This may allow for easy recognition of the bacteria to enhance the targeting and our ability to generate xerogel particles that allow rapid internalization by the phagocytic cells that host the bacteria.

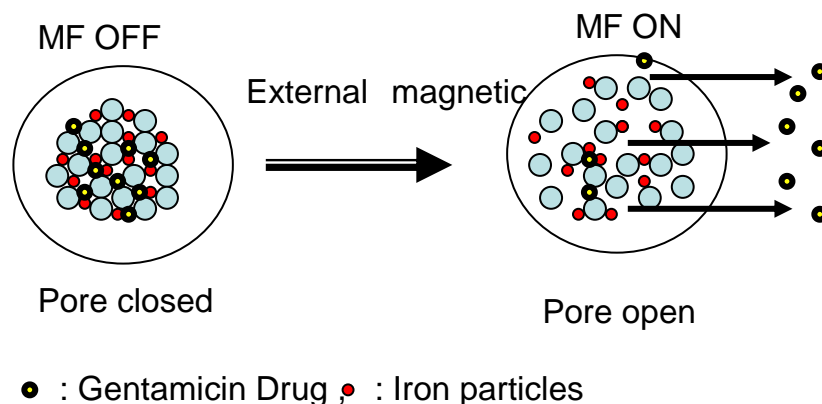


Figure 5.10. Mechanism for drug release from porous Fe/silica xerogel. During the application of the magnetic field, the silica matrix may undergo a structural change. The structural change (rearrangement of the particles in confined space) allows for open configuration of the silica xerogel/Fe complex which allows higher drug release.

5.5.3 In-vivo infection assay

The efficacy of the Fe/silica xerogel versus the free form of the same concentration of gentamicin was tested in AJ 646 mice. The treatment of mice started three days after infection with *S. typhimurium*. The mice received two doses of free gentamicin, antibiotic-loaded Fe/ silica xerogel and empty silica xerogel. At 2 days after administration of the last dose, the animals were euthanized, and the CFUs in the liver and spleen were assayed. The results are summarized in Table 5.2. The Fe/silica xerogel/gentamicin therapy induced a significant ($P < 0.05$) reduction in the log CFUs of *S. typhimurium* in the spleens and livers of infected mice. The empty xerogel and the free gentamicin did not produce a significant reduction of *S. typhimurium*. The *in vitro* drug release rate in PBS was 72% in 25 h duration. The slow release rate for Fe/silica xerogel complex at pH 7.4 makes it efficient for intracellular pathogen as this allows for sufficient time for the particles to undergo phagocytosis without cargo release.

Table 5.2. Efficacy of two doses of Silica-antibiotic hybrid against infection with *S.typhimurium*

a.

Treatment	Log CFU/ spleen	Reduction (log)	Log CFU/ liver	Reduction (log)
No treatment	3.16 ±0.06	0.00	2.80 ±0.09	0.00
Free gentamicin	3.38 ±0.15	+0.22	2.73 ±0.11	0.07
Fe/Silica/genta micin	2.75 ±0.11	0.47*	2.01 ±0.29	0.79*

a Groups of five mice each were infected intraperitoneally with *Salmonella* serovar Typhimurium (4×10^3 CFU/mouse). After 72 h, the animals received two doses of free or Fe/silica-loaded antibiotics (150 µg/mouse). At 48 h after administration of the last dose, the animals were euthanized; liver and spleen were assayed for CFU. Values represent the mean ± standard error of CFU. Statistical significance levels were defined as $P < 0.05$ (shown by asterisks).

5.6 CONCLUSION

In these studies, we have shown the potential possibility of using Fe/silica xerogel particles in controlled release of drug molecules for the targeting of intracellular pathogens. A main requirement in treating intracellular pathogens currently is the need for appropriate drug to be delivered in a precise manner inside the phagocytic cells. Using our proposed magnetic drug release method, delivering Fe/silica complexes can achieve effective drug delivery, which can be adjusted by controlling the magnetic field remotely. The magnetic silica particles due to their size and zeta potential will be recognized by phagocytic cells as foreign bodies and will be phagocytosed out of circulation. Having an ON/OFF switch will ensure that the magnetic particles will not release the cargo in the circulation. Once the magnetic particles enter phagocytic cells, the cargo then can be released by turning on the magnetic field. A further detailed investigation of the effect of the silica xerogel/Fe particles in targeting intracellular pathogens (*Salmonella*) *in-vivo* proves the efficiency of these particles.

5.7 REFERENCES AND NOTES

- [1] M.N. Seleem, S. M. Boyle, N. Sriranganathan. 2008. *Vet Microbiol.* **129**: 1-14
- [2] W.H. Hall. 1990. *Rev Infect Dis.* **12**: 1060-99.
- [3] B. G. Trewyn, I.I. Slowing, V.S.-Y. Lin. 2006. *Chem.Communications.* **31**: 3236-3245.
- [4] J.F. Chen, J.X. Wang, L. Shao. 2004. *Biomaterials.* **25**:723-727.
- [5] J.E. Fuller, L.S. Ferreira, H.S. Ow, N.N. Nguyen, U.B. Wiesner, R.S. Langer. 2008. *Biomaterials.* **29**: 1526-1532.
- [6] C.C. Briones, J.M. Lanao. 2008. *J.controlled release.* **125**: 210-227.
- [7] L. Meseguer-Olmo, M.J. Ros-Nicolas, M. Clavel-Sainz, V. Vicente-Ortega, M. Alcaraz-Banos, A. Lax-Perez, D. Arcos, C.V. Ragel, M. Vallet-Regi. 2002. *Journal of Biomedical Materials Research.* **61**: 458-465.
- [8] H.M. Yiyao Liu, M. Nakamura. 2007. *International Journal of Cancer.* **120**: 2527- 2537.
- [9] A.S. Lubbe, C. Bergemann. *Journal of Surgical Research.* **95**: 200–206.
- [10] C.C. Berry. 2005. *Mater. Chem.* **15**: 543-547.
- [11] S. Rudge, C. Vessely, J. Koda, S. Stevens, L. Catterall. 2001. *Journal of Controlled Release.***74**: 335–340.
- [12] D.F. Silvestri. *BioMedical Engineering OnLine*, 3 (2004)
- [13] S. Giri, P. Michael, Stellmaker, V.S.-Y. Lin. 2005. *Angew. Chem. Int. Ed.*, **44**: 5038-5044.
- [14] S.T. Liu, T. Liu, D.M. Liu, S.Y. Chen. 2006. *Langmuir.* **22**: 5974-5978.
- [15] T.R. Bryans, E.L. Quitevis, *Journal of Sol-Gel Science and Technology.* 2000. **17**: 211-217
- [16] M.S. Kamal, H.A.M. Khalil, T.T. Ali. *Langmuir.* 2008. **24**: 1037 – 1043.
- [17] H.J. Kim, S. Haam, Y.G. Shul, S.Y. Song, T. Tatsumid. 2006. *J. Mater. Chem.* **16**: 1617-1621.

- [18] E. Barrado, F. Prieto, J. Medina. 2005. *Journal of Non-Crystalline Solids*. **351**: 906–914.
- [19] G. Ennas, G. Piccaluga, S. Solinas, M.P. Morales, C.J. Serna. 2002. *J. Mater. Res.* **17**: 590 – 596.
- [20] J. Yang, J. Kang, K. Lee, J.S. Suh, H. G. Yoon, Y.M. Huh, S. Haam. 2008. *Langmuir*. **24**: 3417-3421.
- [21] C.J. Brinker and G.W.Scherer, *Sol-gel science. The physics and chemistry of sol-gel processing*, Academic Press, New York (1990)
- [22] P. Korteso, M. Kangas, T. Leino, S. Laakso, L. Vuorilehto , A. Yli-Urpo , J. Kiesvaara , M. Marvola. 2001. *Journal of Controlled Release*. **76**: 227-238
- [23] J. Patarin, R. Zana, 2002. *Current Opinion in Colloid & Interface Science*. **7**:107-115
- [24] S-W Song, S. Kawi. 2005. *Langmuir*. **21**: 9568-75.

CHAPTER 6

SOLUBILITY BEHAVIOR OF MESOPOROUS SILICA/CALCIUM NANOCOMPOSITES

6.1 ABSTRACT

This research study focused on developing water soluble porous silica particles for the treatment of intracellular pathogens. Silica/calcium nano-composites of three different compositions were developed and their water solubility was evaluated with the aim of using it as an intracellular drug delivery carrier. Silica/calcium nano-composites were prepared by a combination of sol-gel and surfactant templating methods. The solubility behavior was evaluated by means of particulate size reduction, weight loss, and N₂ adsorption measurements. The solubility behaviour of the silica/calcium nano-composites was dependent on their calcium content and increasing the calcium content in mesoporous silica increased its degradation rate. Silica/calcium (50/50) had a rapid solubility rate, while silica/calcium (60/40 and 90/10) showed slower solubility behavior. Furthermore, weight loss and N₂ adsorption measurements indicated that the dissolution occurred both from the leaching of calcium and by the degradation of pore channels. The effects of nano-composites on the cells were evaluated by standard cytotoxicity assays. Our results demonstrate a concentration-dependent toxicity for all types of particles tested. Our results demonstrate the potential to use mesoporous silica/calcium nano-composites for drug delivery applications. Specifically, where the degradation property of the drug delivery carrier is important to minimize potential toxic side effects in long-term treatment regimen.

6.2 INTRODUCTION

Over the last few decades, amorphous and crystalline silica has played a significant role in the diverse biomedical applications [34, 24,10]. Porous silica in biological applications, specifically for targeted drug delivery stands out due to its versatile properties [26, 31, 36]. Sol-gel prepared amorphous silica presents many advantageous properties such as ease of preparation, surface functionalization, high drug loading capacity, adjustment of sol-gel parameters for controlled particle size and surface charge [21, 32, 35]. In addition, their biocompatibility and non-toxic nature makes these materials ideal candidates to act as a drug delivery carrier [23]. A principal criterion for any drug delivery carrier is its degree of biocompatibility and biodegradability without toxic side effects. By using a biodegradable drug delivery carrier, accumulation of the carrier can be avoided and eliminate the necessity for removal in the case of long term treatment regimens. The degradability of sol-gel processed silica has been studied under both *in-vitro* and *in-vivo* conditions [25, 1]. Specifically, silica has been shown to dissolve at different rates and be excreted through the kidney [25].

Several different parameters influence the degradation of silica including chemical composition, synthesis process and texture properties. However, it is the structural properties that play a major role in the degradation of silica [38, 15]. The base unit of silicate glasses is defined by the $[\text{SiO}_4]^{4-}$ tetrahedron, which is linked at corners to other $[\text{SiO}_4]^{4-}$ tetrahedral. A common feature observed in these silicates is that each oxygen ion links to two tetrahedrons, which allows for the formation of an open pore arrangement [19, 9]. This open porous structure allows for inclusion of various cations (e.g. Ca^{2+}). The inclusion of cations, referred as network modifiers, allows for a wide range of silicate glasses to be obtained. The addition of modifiers in the silica

network causes a discontinuity in the glassy network through disruption of Si-O-Si bonds. As a consequence, less stable glasses are produced which allow for enhanced solubility [33, 6, 27, 11].

An example of these materials is the series of bioglass compositions such as the triaxial system $\text{SiO}_2\text{-CaO-P}_2\text{O}_5$. Indeed, many compositions in this system have bioactive behaviour i.e., they chemically react with physiological fluids producing hydroxyapatite (HCA), which is equivalent to the mineral component of bone tissue [7, 28, 12, 30]. However, there is a lack of information on the controlled solubility of mesoporous silica particles doped with calcium. Mesoporous silica prepared by doping with Ca and P presents controlled solubility and an enhanced drug releasing capability [18, 8, 37,35, 38]. Furthermore, most of the materials currently under research utilize the texture (pore size, pore volume and surface area) to control the drug release properties [1, 39]. However, most material preparation protocols lead to non-uniform particle morphology and a wider particle size distribution. One of the main criteria for particles to be used as drug carriers includes a carefully controlled particle size distribution. Particles above or below the required size range will not undergo the phagocytic process very efficiently and can get accumulated in the body and be toxic in a long term therapy.

In this study, mesoporous silica/calcium nano-composites were prepared and the influence of calcium on the vitreous mesoporous silica network to break a proportion of Si-O-Si bonds and to have controlled solubility was investigated. The prepared particles were within the nm size range(100-120nm) with a narrow size distribution. With the addition of modifier ions, a disordered network structure was achieved which gave rise to high reactivity in water and solubility rate. It is expected that these experiments will provide an understanding of how the microstructure controls the rate of drug release and if addition of dopant ions to the silica network will eliminate the problem of drug carrier accumulation as it is readily degradable inside the body.

6.3 EXPERIMENTAL PROCEDURE

6.3.1 Synthesis of mesoporous silica/calcium nano-composite

The following chemicals (Aldrich) were used without further purification: Tetraethylorthosilicate (TEOS), cetyltrimethylammoniumbromide (CTAB), calcium nitrate $\text{Ca}(\text{NO}_3)_2$ and sodium hydroxide (NaOH). Deionized water was used for all our experiments. Three different silica/calcium nano-composite concentrations were made. For preparation of silica/calcium particles, a 90/10, 60/40 and 50/50 (weight % ratio) was used. CTAB in the amount of 1g was dissolved in 80 ml distilled water with addition of 2 M NaOH added drop wise with constant stirring at 80° C for 2 h. TEOS was then added drop-wise to this initial solution. After stirring for 5min the calcium nitrate dissolved in 5 ml water was added to this solution. Finally, the whole milky white solution was stirred for another 2 h at 80°C. Then, the prepared sol was centrifuged to separate out the white precipitate obtained and dried at 100° C for 12 h. For removal of the CTAB template, the white precipitate was heated at 700° C for 7 h.

6.3.2 Characterization of mesoporous silica/calcium nano-composite

All the silica/calcium nano-composites were characterized using X-ray diffraction(XRD), scanning electron microscopy (SEM), N_2 adsorption-desorption, dynamic light scattering particle size measurements, and Energy-dispersive X-ray(EDX) and Fourier transform infrared (FTIR) analysis. For the XRD measurements, the samples were crushed to powder and placed on a sample holder. The samples were scanned from 0 to 70 degrees. The morphology of the prepared silica-calcium nanocomposites was observed using SEM analysis. For all of the samples particle size measurements, before and after solubility periods were performed using a dynamic light scattering technique. For these measurements, the samples were immersed in a beaker, which was

filled with distilled water at 3 ml for every mg of the sample. The samples were mixed using a magnetic stirrer at a constant 300 rpm, kept at 37° C. At 7, 24, 32 and 56 h, 1 ml of the stirred sample were collected and the particle size measurements were performed using a polystyrene cuvette. The N₂ adsorption-desorption measurements were run for the silica/calcium compositions before and after soaking in water for 2 days. All the measurements were performed using nitrogen gas adsorption isotherms at 77K. Before the measurements all the samples were degassed under vacuum for 5 h at 300° C in order to remove all of the water from the porous material. The Barrett-Joyner-Halenda (BJH) method was used for calculating the pore volume, pore size and surface area measurements [4]. The Energy-dispersive X-ray (EDX)/mapping analysis was performed to check for chemical composition and distribution of Ca²⁺ in the silica network. FTIR structural analyses were performed for all of the compositions. The samples were crushed and used in powder form for all the measurements.

6.3.3 Solubility test: weight loss and pH measurements

Weight loss and pH measurements were performed to calculate the solubility rate in water. Initially, the dry weight of the sample was measured before immersion in water at 37°C. At predetermined time intervals, the samples were collected and dried completely to remove any residual water. The new dry weight of the samples, after immersion in water was measured. The measurements were done in triplicate and the total measurement time was 6 days

The weight loss was calculated by using the relationship below (Hong et al. 2009):

$$\text{Weight loss}\% = \frac{\text{Initial weight of particles (W1)} - \text{Weight of particles at time "t"(W2)}}{\text{Initial weight of particles (W1)}} \times 100$$

6.3.4 MTS Cell-viability Assay

Cytotoxicity studies were performed using the Cell Titer 96 Aqueous One Solution Assay. The solution reagent contains a tetrazolium compound [3-(4,5-dimethylthiazol-2-yl)-5-(3-carboxymethoxyphenyl)-2-(4-sulfophenyl)-2H-tetrazolium, inner salt; MTS] and an electron coupling reagent (phenazine methosulfate; PES). Twenty hours after seeding the cells, silica/calcium nanocomposites (15 μ g /well) were added to microtiter wells. The cultures were further incubated for 24 h, and then 20 μ l of the Aqueous One Solution reagent was directly added to the culture wells. After 4 h incubation, the absorbance at 490 nm was measured with a standard microplate reader. The quantity of formazan product as measured by the amount of 490 nm absorbance is directly proportional to the number of living cells in culture. The relative cell viability was calculated in relation to control wells containing cell culture medium without nanoparticles or PBS.

6.4 RESULTS

XRD measurements

Figure 6.1. shows the XRD pattern of the samples. For all silica/calcium nano-composites a broad pattern was observed around 20-30° indicating the amorphous nature of samples. With an increase in calcium content, specifically for a silica/calcium ratio of 60/40 and a silica/calcium ratio of 50/50, additional diffraction peaks between 30-55° begin to appear. This observation indicated that with the increase in calcium content, other peaks are observed which are characteristic of the Ca-silicate family of minerals [20, 15].

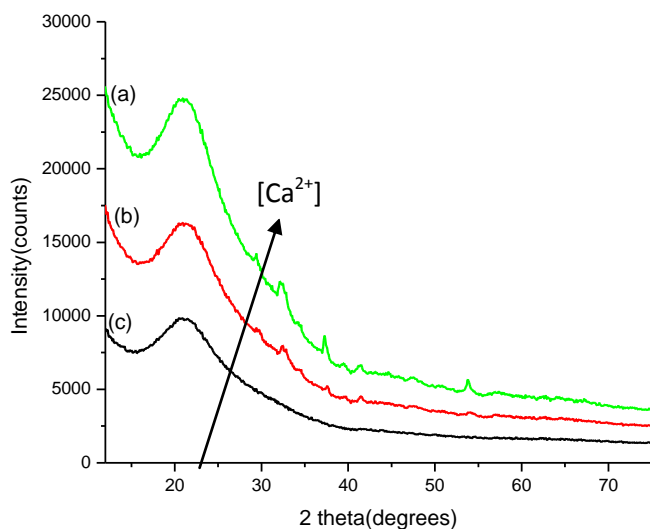


Figure 6.1. XRD pattern of silica/calcium nano-composites of different concentrations (a) silica/calcium-50/50, (b) silica/calcium-60/40 and (c) silica/calcium-90/10.

SEM analysis

Figure 6.2. shows the SEM image of silica/calcium-90/10 nano-composites. The particles sizes are approximately in the range of 100 nm-200 nm. The particles appear to be mostly spherical and the addition of calcium did not change the morphology of the mesoporous silica particles.

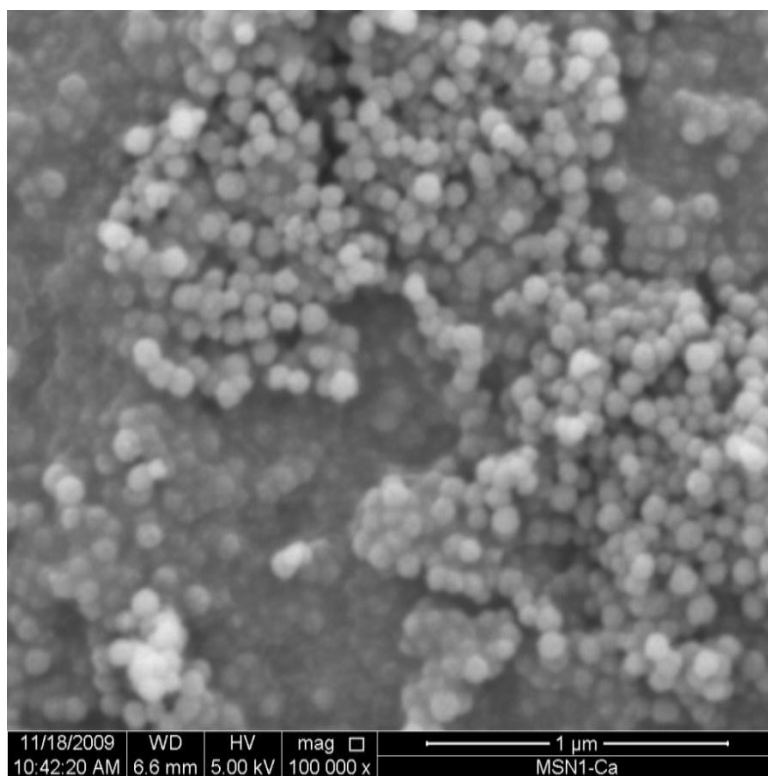
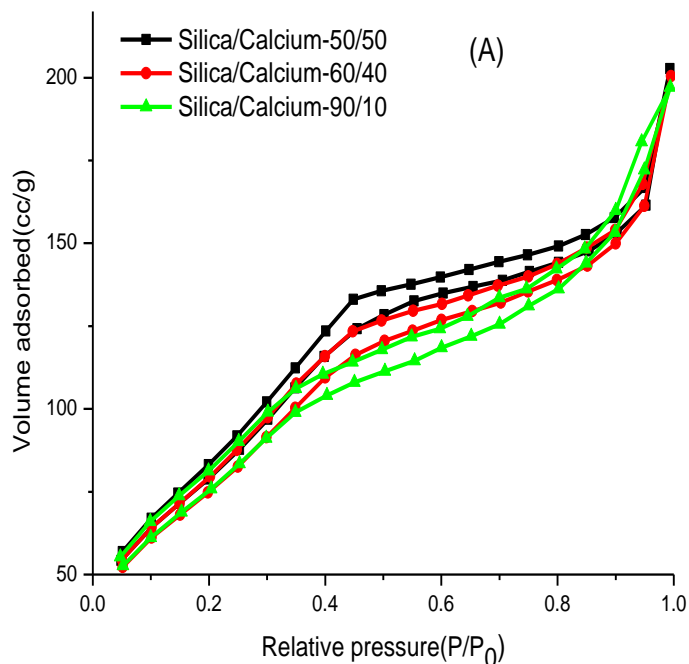


Figure 6.2. SEM image of silica/calcium nanocomposites

N₂ adsorption-desorption measurements

Figure 6.3. and Table 6.1. show the N₂ adsorption-desorption measurement and textural properties for all silica-calcium compositions. Type IV isotherms with H1 type hysteresis loops and a well-defined step between 0.3 and 0.5 of P/P₀ was observed for all the silica-calcium compositions which represented an ordered mesoporous structure. The parallel branches were observed in both adsorption and desorption curves for all the silica-calcium compositions. This indicates that the

pores present were smooth and cylindrical in shape [16]. The surface area and pore volume increased with increase in calcium content or by decreasing the silica content. The pore size distribution was broad and remains the same for all three compositions at ~ 2 nm. As the pore size is determined by the effect of the surfactant used, the addition of calcium did not affect the pore size. Similar results were observed by other authors [38]. The BJH method and adsorption curve were used for calculating the pore volume and pore size. The surface area was calculated using the multipoint BET (Brunauer, Emmett, and Teller) [5] method. The calculated surface area, pore volume and pore size for all compositions were in the range of $\sim 300\text{m}^2/\text{g}$, $\sim 0.3\text{cm}^3/\text{g}$ and $\sim 2\text{nm}$. The increase of the surface area and pore volume with the increase of the calcium content was observed for all three silica/calcium compositions. This implied that the addition of calcium significantly changed the silica network formation by incorporating it in to the Si-O-Si structure, which lead to changes in the surface area and pore volume with the addition of the calcium ions.



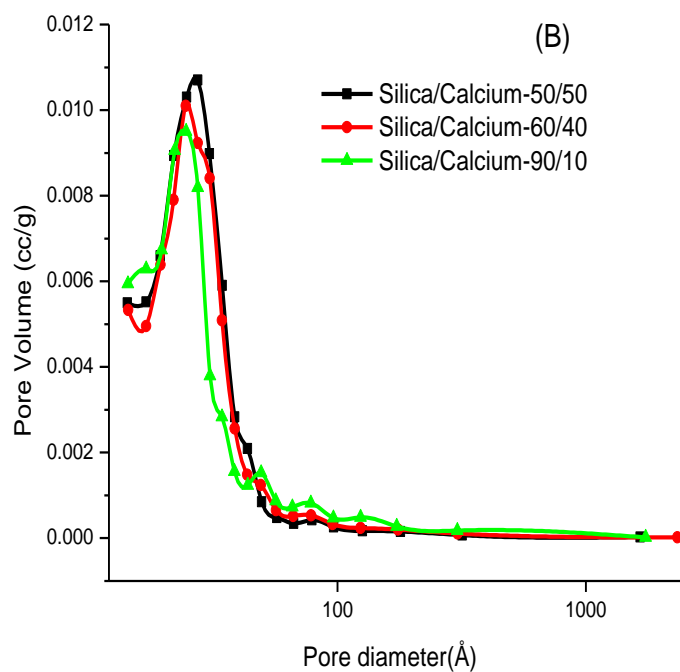


Figure 6.3. N₂ adsorption-desorption isotherm measurements (A) for (a) silica/calcium- 50/50, (b) silica/calcium- 60/40 and silica/calcium- 90/10 compositions and (B) pore size distribution.

Table 6.1. Textural properties of mesoporous silica-calcium compositions

Sample	Surface area(m ² /g)	Pore volume(cm ³ /g)
silica/calcium-50/50	358	0.33
silica/calcium-60/40	333	0.32
Silica/calcium-90/10	320	0.31

Energy Dispersive X-Ray (EDX) Analysis

EDX analyses were performed to determine the chemical composition of all the silica-calcium nano-composites. Figure 6.4(A) shows an EDX spectra representative of all silica-calcium compositions. The major EDX peaks at 4, 0.5, 0.2 and 3.5KeV correspond to the elements Si, O and Ca. Moreover, the EDX analysis of several different areas showed uniform dispersion of calcium in silica and calcium species did not segregate.

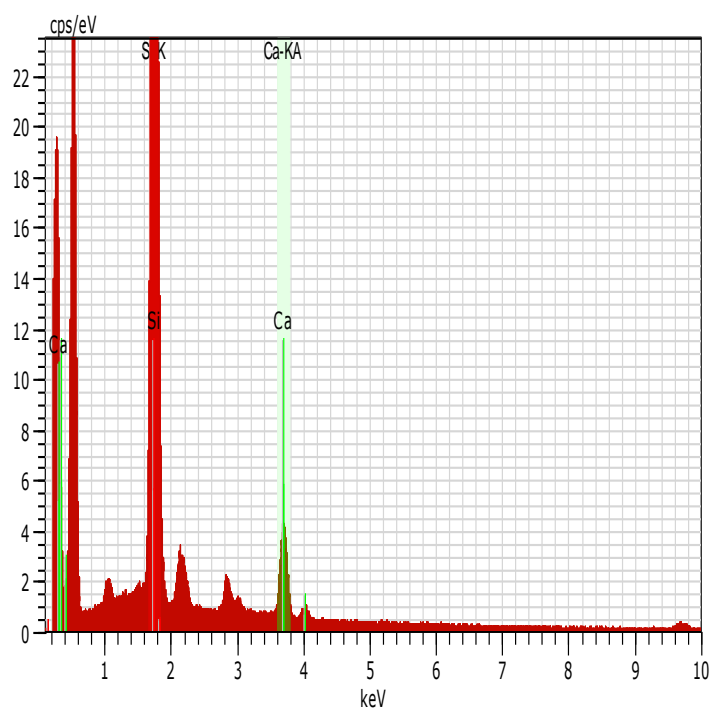


Figure 6.4. EDX analysis for silica /calcium nano-composites, Inset- EDX mapping analysis for silica/calcium-60/40 composition.

FTIR analysis

The FTIR chemical analysis was performed for all the silica/calcium (50/50, 60/40 and 90/10) compositions. These are shown in figure 6.5. For all the silica/calcium compositions the asymmetric stretching vibrations (1105cm^{-1} and 900cm^{-1}), and the Si-O bending vibration around 800 cm^{-1} were observed. With the increase in calcium content (silica/calcium-50/50), the stretching vibration was observed at 1083 cm^{-1} . It is reported that for pure silica the Si-O-Si stretching vibration is observed in the range of $1000\text{-}1300\text{ cm}^{-1}$ with intense absorption band centered around 1120 cm^{-1} and a shoulder around 1220 cm^{-1} . With the increase in calcium content the Si-O-Si adsorption band gets broader with the maximum intensity at 1083cm^{-1} . Similar observations have been reported in the analysis of mesoporous $\text{CaO-MO-SiO}_2\text{-P}_2\text{O}_5$ (M-Mg, Zn, Cu) bioactive/glass composites [15]. The reason behind this process is that with the addition of calcium, the Si-O groups tend to form the network structure $[\text{SiO}_4]$ tetrahedron by involving both bridging and non-bridging oxygen ions [15,13]. With the addition of metallic cations, in this case calcium (Ca^{2+}), the network formation is altered where there will be increases in the number of SiO- groups. This leads to a shift in the Si-O-Si adsorption band to lower wavelength.

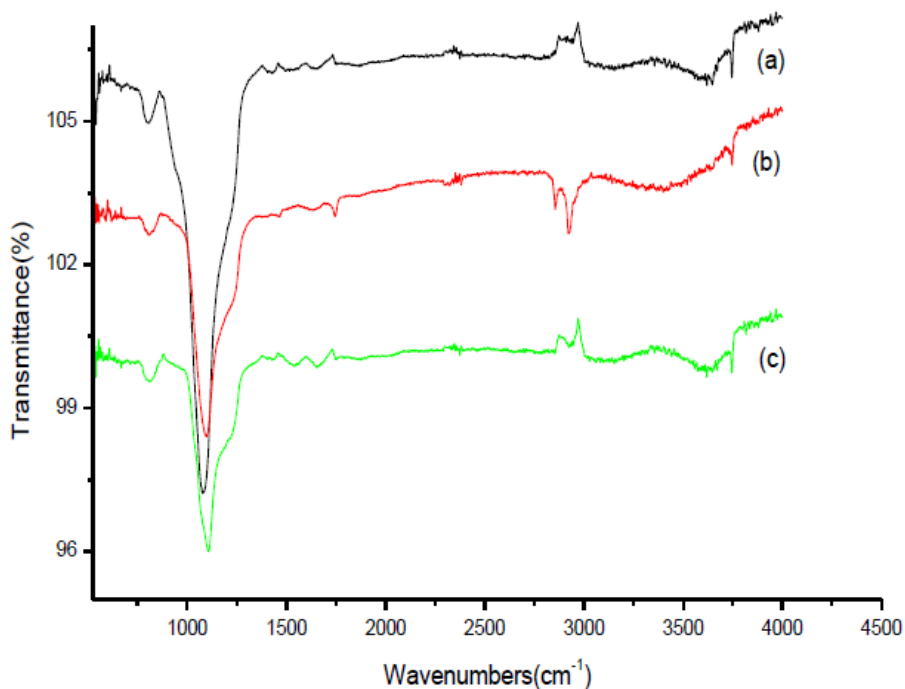


Figure 6.5. FTIR spectra for silica/calcium nano-composites (a) si/ca-50/50, (b) si/ca- 60/40 and (c) si/ca-90/10.

Dissolution behaviour of mesoporous silica/calcium nano-composites

Particle size measurements

Figure 6.6. shows the particle size measurements for as prepared silica-calcium nano-composites of the three different compositions after solubility testing. The drawn posed arrow indicates the increase of the Ca^{2+} concentration in the samples. The average particle size was measured at different solubility time intervals. It was noted that with the increase in calcium content the solubility rate increased and the resulting particle size decreased. Thus for the silica/calcium-50/50 composition the particle size reduced from an average of 160nm to an average of 105 nm in 57h, indicating a faster dissolution rate than for all the other compositions. The silica/calcium-60/40 composition showed an intermediate dissolution rate where the particle size reduced from 160nm to 133nm. The silica-calcium 90-10 however did show a very low dissolution rate.

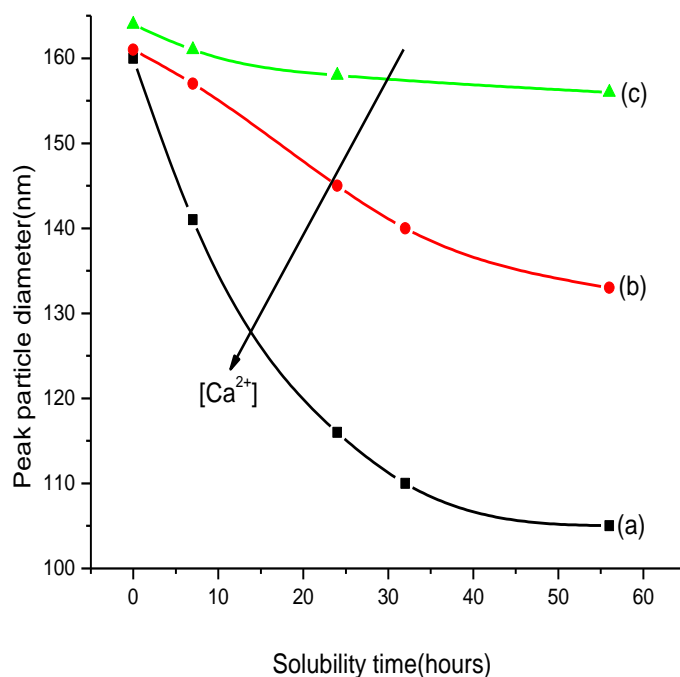


Figure 6.6. Particle size measurements after solubility testing for silica-calcium nano-composites. (a) Silica/Calcium -50/50, (b) Silica/Calcium-60/40, (c) Silica/Calcium- 90/10.

N₂ adsorption –desorption measurements before and after immersion in water

N₂ adsorption measurements were performed for silica-calcium nano-composites before and after immersion in water for 2 days. Figure 6.7. shows the adsorption-desorption isotherms for samples silica/calcium- 50/50, silica/calcium-60/40 and for silica/calcium-90/10. The measured surface area and pore volume data before and after soaking in water is given in Table 6.2. After immersion in water, the surface area decreased and pore volume increased for all three compositions. This was due to the degradation of silica and calcium after soaking in water. In addition, the highest pore volume after soaking in water was observed for the silica/calcium-50/50 particles followed by the silica/calcium-60/40. However, the Si 90-Ca 10 composition shows very

low or no increase in pore volume. This indicated that with an increase in calcium content in the silica matrix, the mesoporous silica particles were very susceptible to attack from water, which leads to changes in its structural properties due to the dissolution of the inorganic walls.

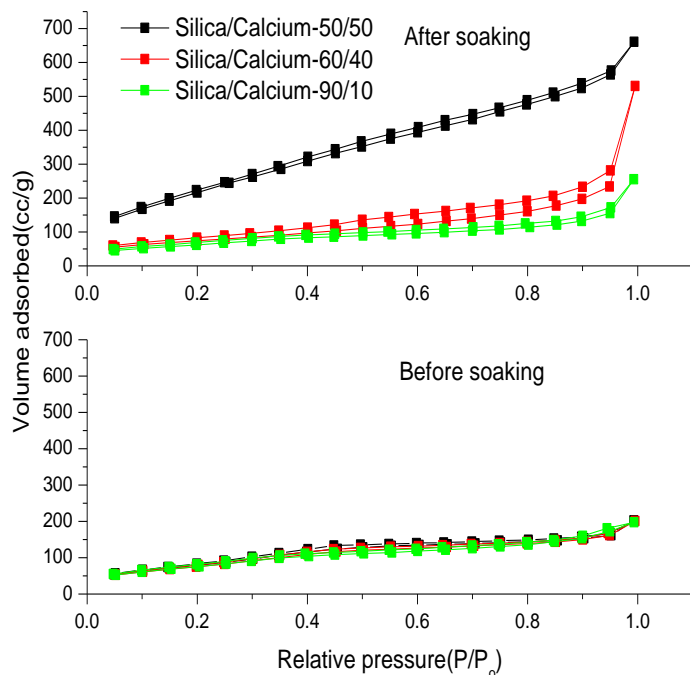


Figure 6.7. N₂ adsorption isotherm measurements for silica-calcium compositions before and after immersion in water.

Figure 6.8. (A), (B) and Table 6.2. shows the change in pore structure before and after immersion in water. For silica/calcium-50/50 and 60/40 there was an increase in pore volume after immersion in water (Table 6.2.). For these compositions, the pore size distribution changed dramatically after immersion in water. For silica/calcium-90/10 there was little change in pore properties where pore volume increased from 0.31 to 0.39 cm³/g. specifically for silica/calcium-50/50 and 60/40 compositions before soaking in water, the pore size distribution was narrow and centered at 24Å and pore volume was ~0.3cm³/g. After water immersion, the number of nano and

mesopores starts to increase with two main pore size ranges occurring between $\sim 20\text{-}30\text{\AA}$ and $\sim 80\text{\AA}$. The release of silica and calcium after immersion in water leads to a change in pore structure morphology by gradually enlarging the interconnected pores.

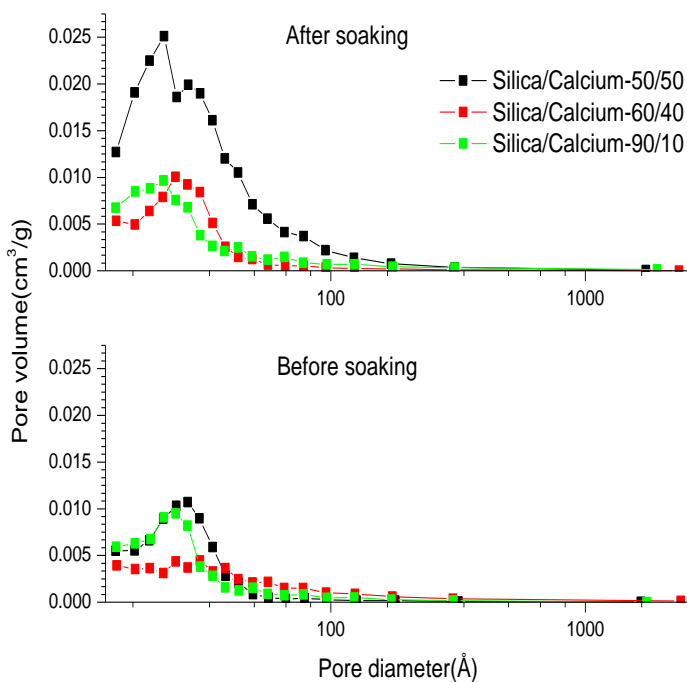


Figure 6.8. Pore size distribution for silica/calcium compositions 90/10, 60/40 and 50/50 before and after immersion in water for two days.

Table 6.2. Textural properties of silica-calcium compositions after immersion in water

Sample	Surface area(m ² /g)	Pore volume(cm ³ /g)
silica/calcium-50/50	233	1.10
silica/calcium-60/40	271	0.81
Silica/calcium-90/10	240	0.39

Solubility Test by weight loss measurements

Figure 6.9. shows the solubility graph for all the silica-calcium compositions tested. As seen in this figure, all the samples started dissolving immediately after immersion in water. However, the silica/calcium-50/50 compositions had the highest dissolution rate in water in comparison to the other two compositions throughout the soaking period. The maximum achieved dissolution was ~55% in 144h for silica/calcium-50/50 compositions. An intermediate dissolution of ~30% was observed for silica/calcium-60/40 compositions after the 144 h soaking time. As was observed with the particle size and porosity measurements, the silica/calcium-90/10 composition possessed a very low dissolution rate, where only 20% was observed at 144 h. From the weight loss measurements, it can be seen that inclusion of calcium had a major effect on the dissolution rate of mesoporous silica particles. With the increase in calcium content, the solubility rate was found to increase accordingly. Therefore, this has shown that the composition of the particles can be used to tailor the dissolution rate of the particles to the desired value.

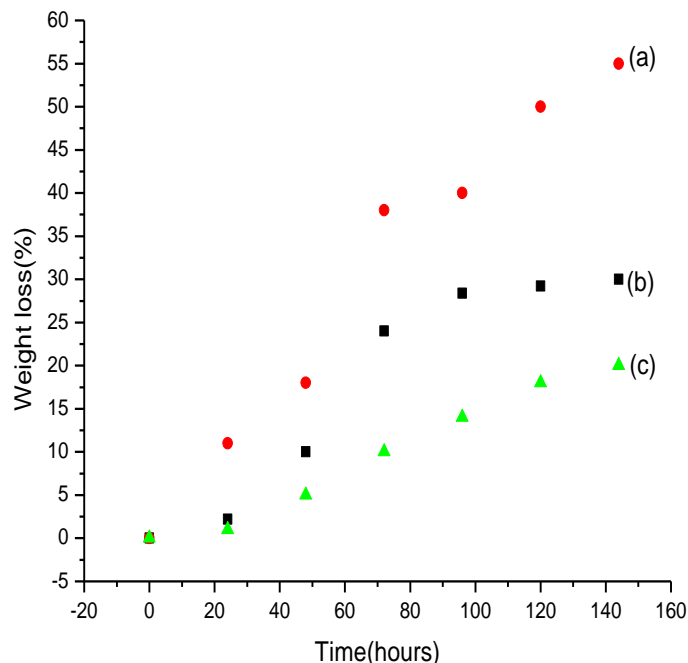


Figure 6.9. Plot for weight loss percentage to dissolution time for silica-calcium compositions. (a) Si/Ca -50/50, (b) Si/Ca-60/40, (c) Si/Ca- 90/10.

6.4.1 Cytotoxicity studies

Figure 6.10 shows that silica/calcium nano-composites had no significant adverse effect on cell activity or not toxic to the cells. Moreover, it is clearly evident that increasing the concentration of calcium, specifically for silica/calcium (50/50), only increases the cell viability and doesn't induce any deleterious effect on cells. This was made in comparison to the untreated macrophages where they are viable even after incubation with a nanocomposite loading as high as 30 $\mu\text{g}/\text{well}$.

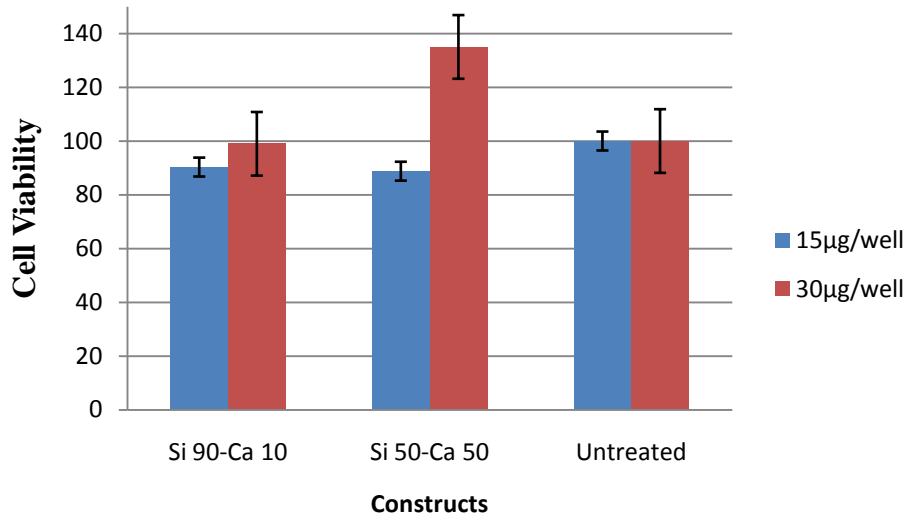


Figure 6.10. MTS assay of the cells incubated with silica/calcium nano-composites (50/50 and 90/10) at a concentration of 15 µg and 30 µg.

6.5 DISCUSSION

Inorganic pure silica has been investigated as a promising drug delivery carrier for treating various bacterial diseases due to their versatile properties which includes high drug loading capacity, sustained drug release etc., [29]. However, in order to avoid the possibility of toxic effects from long term accumulation of the particles, one desired attribute for a drug delivery is for the carrier to degrade and gradually dissolve and eliminated from the body without any toxic residues. There remains a major drawback in using silica for long term treatment, where dissolution of the silica is slow or nonexistent. In the present work, we have investigated the dissolution rate of porous silica-calcium nano-composites, where the amount of calcium played an important role in the dissolution rate of the particles. In both the crystalline and amorphous structures of silica, the network arrangement is such that each oxygen ion can link two silicon tetrahedral which can lead to formation of an open pore arrangement [33]. Specifically, for formation of a range of silica glasses, the open pore arrangement facilitates the inclusion of appropriate dopants into the network [14, 33]. In the present study, calcium was used to control or destabilize the network structure and enhance the degradability of silica. By incorporation of 50% calcium, the siloxane bridging bonds (Si-O-Si) were disrupted which lead to a faster dissolution during immersion in water i.e. higher dissolution. It was rationalized that the larger pore volume and increased surface area for high calcium doped silica facilitated the solvent penetration inside the silica lattice and the nucleophilic attack primarily by the H^+ and OH^- groups of the water. This led to breakdown or degradation of the silica matrix.

Experimental results suggested that the breaking of the silica network takes place by a hydrolysis process with the removal of Ca^{2+} from the network. In the case for pure silica alone, without addition of dopants, the solubility behaviour is inhibited by the stable network of Si-O-Si

bonds. For silica with a higher amount of calcium, calcium silicate (CS) could have formed. CS is a mineral which mainly consists of a network of covalently bonded silica that is interrupted and modified by Ca^{2+} cations. Figure 6.11 show the schematic representation which explains the dissolution mechanism of calcium silicate. This weakly bonded, network-modifying Ca^{2+} containing many local sites which are attached to the network by fewer bridging bonds. This allows for easy exchange of hydrogen ions to Ca^{2+} ions, which gets released to the solution. For instance, the silica/calcium (90-10), the solubility rate was not sufficiently fast due to controlled network hydrolysis by presence of insufficient non-bridging oxygen. This also signifies that the particulates remain reasonably stable under physiological condition. This would be desirable in applications where a slow drug release rate is needed. The silica/calcium-50/50 should be useful for other applications, where faster degradation of material is needed. The degradation property of the silica-calcium compositions were evaluated by particle size measurements, weight loss and N_2 adsorption-desorption.

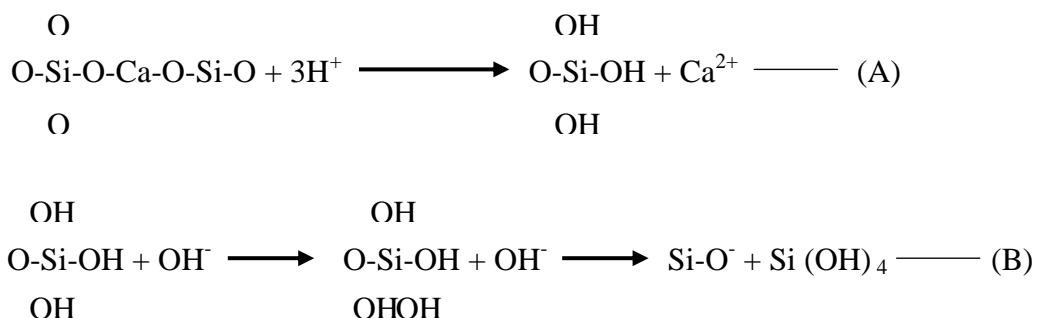


Figure 6.11. Schematic representation of silica dissolution. (A) Silica network modified and interrupted by Ca^{2+} ions which up on immersion in water gets susceptible to nucleophilic attack and exchanges weakly bonded, network-modifying Ca^{2+} for protons. (B) Further nucleophilic

attack primarily by OH⁻ groups in water, structurally deforms [SiO₄]⁴⁻ tetrahedral to five-coordinated intermediates which further breaks down to Si(OH)₄.

Many workers in the field have tried to develop glass compositions for which the rate of dissolution can be controlled [30, 17]. Although, these glass compositions improved/facilitated the bone regeneration applications, they are not useful for intracellular drug delivery applications due to their particle size and shape [3, 22, 2]. The mesoporous silica/calcium compositions obtained by the technique used in this study clearly showed a controllable dissolution rate. The present study demonstrated the feasibility of preparing soluble porous calcium/silica particles using a sol-gel method. The silica particles with high amounts of calcium showed a significantly higher solubility than silica alone or with less content of calcium. Initial biological studies were performed to understand the effects of these particles inside the cellular compartment; the preliminary cytotoxicity results presented here indicated that the porous silica with inclusion of an appropriate amount of calcium had minimal or no toxicity which could be used as a potential drug delivery carrier.

6.6 CONCLUSION

Mesoporous silica/calcium nano-composites were synthesized and characterized for potential drug delivery applications. The FTIR and EDX analysis confirmed the formation of silica/calcium network. All the prepared samples showed a uniform narrow particle size distribution and shape. The dissolution rate of the silica/calcium nano-composites was evaluated by means of particle size distribution measurements. It was found that particles with higher calcium content showed higher dissolution. In addition N₂ adsorption–desorption measurements also showed that higher calcium content particles had significantly higher dissolution rates. For further confirmation, weight loss measurements were carried out where the dissolution rate was measured for each composition. In addition, cellular cytotoxicity studies provide proof of evidence that these particles under *in-vitro* degradation conditions does not induce any harmful effects on cells. All these experiments confirmed that the newly prepared silica/calcium nano-composites showed controllable dissolution rates directly correlated with composition of the particles. This may make these particles useful as drug delivery carriers.

6.7 REFERENCES

- [1] J. Andersson, J. Rosenholm, S. Areva, M. Lindn. 2005. Influences of Material Characteristics on Ibuprofen Drug Loading and Release Profiles from Ordered Micro- and Mesoporous Silica Matrices. *Chem Mater.* **16**: 4160–4167.
- [2] D. Arcos, A. Lopez-Noriega, E. Ruiz-Hernández, O. Terasaki, M. Vallet-Regí'. 2009. Ordered Mesoporous Microspheres for Bone Grafting and Drug Delivery. *Chem. Mater.* **21**: 1000–1009.
- [3] C. Barbé, J. Bartlett, L. Kong, K. Finnie, H.Q. Lin, M. Larkin, S. Calleja, A. Bush, G. Calleja. 2004. Silica Particles: A Novel Drug – Delivery System. *Adv Mat.* **16**: 1959-1966.
- [4] E.P. Barrett, L.G. Joyner, P.P. Halenda. 1951. The determination of pore volume and area distributions in porous substances. I. Computations from nitrogen isotherms. *J. Am. Chem. Soc.* **73**: 373–380.
- [5] S. Brunauer, P.H. Emmett, E.Teller. 1938. Adsorption of gases in multimolecular layers. *J. Am. Chem. Soc.* **60**: 309.
- [6] J. Cle´ment, J.M. Manero, J.A. Planell, G. Avila, S. Marti´nez. 1999. Analysis of the structural changes of a phosphate glass during its dissolution in simulated body fluid. *J Mater Sci Mater Med.* **10**: 729-732.
- [7] L. Dong-Jun, K. Ohsaki, L. Kunio, C. Peng-Cheng, Y. Qing, K. Baba, Q.C. Wang, S. Tenshin, T. Takano-Yamamoto. 1999. Thickness of fibrous capsule after implantation of hydroxyapatite in subcutaneous tissue in rats. *J Biomed Mater Res.* **45**: 322-326.
- [8] K. Franks, I. Abrahams, J.C. Knowles. 2000. Development of soluble glasses for biomedical use Part I: In vitro solubility measurement. *J Mater Sci Mater Med.* **11**: 609-614.

- [9] S.Y. Gadre, P.I. Gouma. 2006. Biodoped Ceramics: Synthesis, Properties, and Applications. *J Am Ceram Soc.* **89**: 2987-3002.
- [10] S. Hudson, J. Cooney, E. Magner. 2008. Proteins in Mesoporous Silicates. *Angew Chem Int Ed.* **47**: 8582 – 8594.
- [11] I. Izquierdo-Barba, A.J. Salinas, M. Vallet-Regí. 1999. *In vitro* calcium phosphate layer formation on sol-gel glasses of the CaO-SiO₂ system. *J Biomed Mater Res.* **47**: 243-250.
- [12] I. Izquierdo-Barba, D. Arcos, Y. Sakamoto, O. Terasaki, A. Lo´pez-Noriega, M. Vallet-Regí. 2008. High-Performance Mesoporous Bioceramics Mimicking Bone Mineralization. *Chem. Mater.* **20**: 3191–3198.
- [13] A.G. Kalampounias, N. Bouropoulos, K. Katerinopoulou, S.N. Yannopoulos. 2008. Textural and structural studies of sol–gel derived CaO- and MgO silica glasses. *Journal of Non-Crystalline Solids.* **354**: 749-754.
- [14] J.C. Knowles. 2003. Phosphate based glasses for biomedical applications. *J Mater Chem.* **13**: 2395 – 2401.
- [15] X. Li, X. Wang, D. Hec, J. Shi. 2008. Synthesis and characterization of mesoporous CaO–MO–SiO₂–P₂O₅ (M= Mg, Zn, Cu) bioactive glasses/composites. *J Mater Chem.* **18**: 4103 – 4109.
- [16] X. Li, L. Zhang, X. Dong, J. Liang, J. Shi. 2007. Preparation of mesoporous calcium doped silica spheres with narrow size dispersion and their drug loading and degradation behavior. *Microporous and Mesoporous Materials.* **102**: 151-158.
- [17] Manupriya, K.S. Thind, G. Sharma, K. Singh, V. Rajendran, S. Aravindan. 2007. Soluble Borate Glasses: In Vitro Analysis. *J Am Ceram Soc.* **90**: 467-471.

- [18] S. Moudgil and J.Y. Ying. 2007. Calcium-Doped Organosilicate Nanoparticles as Gene Delivery Vehicles for Bone Cells. *Adv Mater* **19**: 3130-3135.
- [19] E.A.A. Neel, D.M. Pickup, S.P. Valappil, R.J. Newport, J.C. Knowles. 2009. Bioactive functional materials: a perspective on phosphate-based glasses. *J Mater Chem*. **19**: 690 – 701.
- [20] S. Ni, J. Chang, L.Chou. 2008. In vitro studies of novel CaO–SiO₂–MgO system composite bioceramics. *J Mater Sci: Mater Med*. **19**:359–367.
- [21] R.I. Nooney, D. Thirunavukkarasu, Y. Chen, R. Josephs, A.E. Ostafin. 2002. Synthesis of Nanoscale Mesoporous Silica Spheres with Controlled Particle Size. *Chem. Mater*. **14**: 4721–4728.
- [22] T.A. Ostomel, Q. Shi, C.K. Tsung, H. Liang, G.D. Stucky. 2006. Spherical Bioactive Glass with Enhanced Rates of Hydroxyapatite Deposition and Hemostatic Activity. *Small*. **2**: 1261-1265.
- [23] J.H. Park, L. Gu, G.V. Maltzahn, E. Ruoslahti, S.N. Bhatia, M.J. Sailor (2009) Biodegradable luminescent porous silicon nanoparticles for in vivo applications. *Nat Mater*. **8**: 331-336.
- [24]D.R. Radu, C.Y. Lai, K. Jeftinija, E.W. Rowe, S. Jeftinija, V.S.Y. Lin (2004) A Polyamidoamine Dendrimer-Capped Mesoporous Silica Nanosphere-Based Gene Transfection Reagent. *J. Am. Chem. Soc*. **126**: 13216–13217.
- [25] S. Radin, G. El-Bassyounia, E.J. Vresilovicb, E. Schepersc, P. Ducheyne. 2005. In vivo tissue response to resorbable silica xerogels as controlled-release materials. *Biomaterials* **26**: 1043-1052.
- [26] J.M. Rosenholm, A. Meinander, E. Peuhu, R. Niemi, J.E. Eriksson, C. Sahlgren, M. Linden. 2009. Targeting of Porous Hybrid Silica Nanoparticles to Cancer Cells. *ACS Nano*. **3**: 197–206.

- [27] A.J. Salinas, A.I. Martin, M. Vallet-Regí. 2002. Bioactivity of three CaO–P₂O₅–SiO₂ sol-gel glasses. *J Biomed Mater Res.* **61**: 524-532.
- [28] P. Saravanapavan, J.R. Jones, R.S. Pryce, L.L. Hench. 2003. Bioactivity of gel– glass powders in the CaO–SiO₂ system: A comparison with ternary (CaO–P₂O₅–SiO₂) and quaternary glasses (SiO₂–CaO–P₂O₅–Na₂O). *J Biomed Mater Res.* **66A**: 110-119.
- [29] M.N. Seleem, P. Munusamy, A. Ranjan, H. Alqublan, G. Pickrell, N. Sriranganathan. 2009. Silica-Antibiotic Hybrid Nanoparticles for Targeting Intracellular Pathogens. *Antimicrob Agents Chemother.* **53**: 4270-4274.
- [30] P. Sepulveda, J.R. Jones, L.L. Hench. 2002. In vitro dissolution of melt-derived 45S5 and sol-gel-derived 58S bioactive glasses. *J Biomed Mater Res.* **61**: 301-311.
- [31] F. Torney, B.G. Trewyn, V.S.Y. Lin, K. Wang. 2007. Mesoporous silica nanoparticles deliver DNA and chemicals into plants. *Nature Nanotechnology.* **2**: 295-300.
- [32] B.G. Trewyn, J.A. Nieweg, Y. Zhao, V.S.Y. Lin. 2008. Biocompatible mesoporous silica nanoparticles with different morphologies for animal cell membrane penetration. *Chem Eng J.* **137**: 23-29.
- [33] M. Vallet-Regí, C.V. Ragel, A.J. Salinas. 2003. Glasses with Medical Applications. *Eur J Inorg Chem.* **2003**: 1029-1042.
- [34] S. Wang. 2009. Ordered mesoporous materials for drug delivery. *Microporous and Mesoporous Materials.* **117**: 1-9.
- [35] W. Xu, Q. Gao, Y. Xua, D. Wu, Y. Sun, W. Shen, F. Deng. 2009. Controllable release of ibuprofen from size-adjustable and surface hydrophobic mesoporous silica spheres. *Powder Tech.* **191**: 13-20.

- [36] Z.P Xua, Q.H. Zeng, G.Q. Lu, A.B. Yu. 2006. Inorganic nanoparticles as carriers for efficient cellular delivery. *Chem Eng Sci.* **61**: 1027-1040.
- [37] W. Xue, A. Bandyopadhyay, S. Bose. 2009. Mesoporous calcium silicate for controlled release of bovine serum albumin protein. *Acta Biomaterialia.* **5**: 1686-1696.
- [38] X.X. Yan, H.X. Deng, X.H. Huang, G.Q. Lu, S.Z. Qiao, D.Y. Zhao, C.Y.Yu. 2005. Mesoporous bioactive glasses. I. Synthesis and structural characterization. *Journal of Non-Crystalline Solids.* **351**: 3209-3217.
- [39] L. Zhao, X. Yan, X. Zhou, L. Zhou, H. Wang, J. Tang, Y. Chengzhong. 2008. Mesoporous bioactive glasses for controlled drug release. *Microporous and Mesoporous Materials.* **109**: 210-215.

CHAPTER 7

INFLUENCE OF TEMPLATE CONCENTRATION ON TEXTURE

PROPERTIES AND CONTROLLED DRUG RELEASE

7.1 ABSTRACT

A series of mesoporous silica nanoparticles (MSN's) were prepared by template synthesis method. Influence of surfactant concentration on texture properties of silica nanoparticles was investigated. The Cetyl trimethylammonium bromide (CTAB), a long chain cationic surfactant was used as template. This study revealed that higher the CTAB concentration, larger the surface area and pore volume. The particles with high surface area and pore volumes allowed for high loading of drug molecules. In addition to that mesoporous silica nanoparticles with high pore volume and surface area provides faster drug release rate. For drug release studies, ciprofloxacin hydrochloride was used as a model drug. Furthermore confocal analyses were performed for fluorescein isothiocyanate (FITC) tagged MSN particles which clearly show the uptake of MSN particles within 1 h period of incubation at 37 °C.

7.2 INTRODUCTION

For any material to be used as drug delivery carrier, the most important property would be the ability to load drug molecules and release them at an appropriate rate [1, 2, 3]. Since most of the drugs used are very toxic in nature, the high drug loading and sustained drug release takes the priority in designing a drug delivery system [4, 5]. Many different materials are being investigated for drug delivery applications; however most of these materials are either restricted due to poor drug loading capacity or incomplete drug release properties[6, 7, 8, 9, 10].

The newly developed porous silica nanoparticles provide numerous opportunities for drug delivery applications [11, 12, 13]. Based on the template used and under appropriate sol-gel conditions, the pore structure property can be modified accordingly. In addition to that, the mesoporous particles provide two different surfaces, inner and outer, which can appropriately be surface modified to provide controlled drug release, i.e., the surface of particles can be functionalized based on the drug molecules or targeting moieties to be attached [14, 15, 16]. Based on the above mentioned critical properties, the porosity of the silica particles could be modified for exploring new drug release applications.

The influence of surface modification and influence of different pore sizes (using different chain length surfactant) has been studied previously [17, 18, 19, 20]. Here, we studied the influence of surfactant concentration on the texture properties of silica nanoparticles, specifically, the pore volume and surface area. We, then investigated, how the texture properties affect the drug release profile. For measuring the drug release profile, ciprofloxacin hydrochloride was used as model drug.

7.3 EXPERIMENTAL PROCEDURE

Materials

The following chemicals (Aldrich) were used without further purification: Tetraethylorthosilicate (TEOS), cetyl trimethylammoniumbromide (CTAB), fluorescein isothiocyanate (FITC) and sodium hydroxide (NaOH). Deionized water was used for all our experiments. The molecular structure of ciprofloxacin drug and the CTAB template employed are shown in Figure 7.1(a) and (b) respectively.

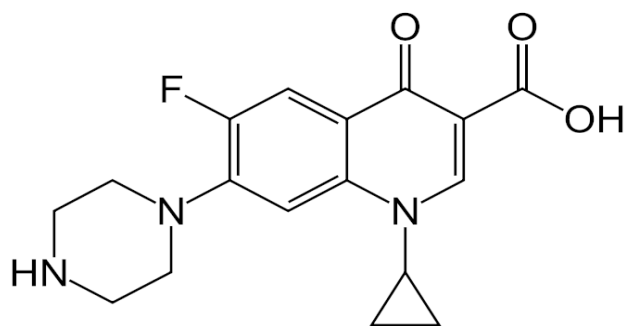


Figure 7.1. (a) Molecular structure of ciprofloxacin.

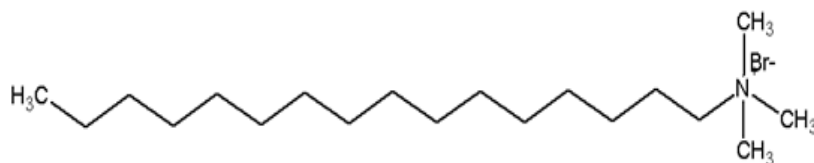


Figure 7.1. (b) Molecular structure of Cetyl trimethylammonium bromide (CTAB) (16 carbon chain).

7.3.1 Synthesis of mesoporous silica nanoparticles

Two reactant compositions were chosen to synthesize the mesoporous silica nanoparticles (MSN1 and MSN2). Water was used as the solvent and cetyl trimethylammonium bromide (CTAB) as the structure directing agent. In a typical synthesis, 1.0 g CTAB was dissolved in a mixture of 450 ml deionized water, followed by the addition of 3.5 ml of 2 M NaOH. The resultant solution was kept at constant stirring at 80°C for 2h. After the solution became homogeneous, 10.0 ml tetraethylorthosilicate (TEOS) was dropped slowly into solution under vigorous stirring. After 2 h, the obtained precipitation was filtered, washed with deionized water and ethanol, dried at 70° C, and finally calcined in air at 600° C for 6 h to remove the CTAB template. According to the concentration of CTAB employed, the synthesized mesoporous silica spheres were assigned as MSN1 (1g CTAB) and MSN2 (2g CTAB). These calcined mesoporous silica nanoparticles were used directly in the following drug loading and release experiments.

Synthesis of fluorescein isothiocyanate-labeled porous silica materials

For loading FITC to mesoporous silica particles, 3 ml of FITC solution 5mg/ml in ethanol was stirred in the presence of 50 mg of MSN1 samples. The reaction mixture was vigorously stirred for 3 h at room temperature. The resulting solid was filtered, washed thoroughly with ethanol and dried in air for 24 h.

7.3.2 Characterization of mesoporous silica nanoparticles

The morphology of the prepared MSN particles was investigated by scanning electron microscopy. The thermogravimetric analysis (TGA) was performed to determine the drug loading amount. The samples were heated between 30° C to 1200° C in air with a flow rate of 30 ml/min

and with a heating rate of 10° C/min. The texture properties (surface area, pore volume and pore size) of the samples were characterized using N₂ adsorption-desorption isotherm measurements. Before each measurement the samples were degassed in vacuum at 200° C for 7 h and the measurements were carried out at 77K. The BJH and BET methods were used for calculating the pore surface area and size distribution, respectively. To determine the morphology, the particles were deposited on a sample grid with an adhesive carbon foil and sputter coated with gold. The morphologies of the synthesized MSN particles were examined using field emission scanning electron microscopy (FE-SEM, JEOL-6500).

7.3.3 Drug loading and drug release studies

To load ciprofloxacin into the mesoporous silica particles, the template removed mesoporous spheres were added into ciprofloxacin drug solution dispersed in water. After soaking for 48 h, the drug-loaded MSN spheres were removed from the solution and were dried in air for 24 h.

In-vitro release of ciprofloxacin was performed by immersing drug loaded MSN particles in water, which was stirred at 300 rpm and maintained at 25°C. The stirring was continued during the whole period of drug release studies to prevent the isolation and to provide uniform distribution of the drug molecules released into the solution. The release ratio of ciprofloxacin from MSN was calculated by examining the concentrations of ciprofloxacin in water at different time intervals.

7.3.4 Cell culture and localization of MSN- FITC

To study the ability of the FITC tagged MSN1 particles to enter cells, macrophage cell line J774. A1 was used for this study. The J774A.1 cells were routinely grown as monolayers in 75 cm² tissue culture Flask (Corning Corporation Inc.) in a humidified 5% CO₂ atmosphere at 37°C. The cells were cultured and maintained in Dulbecco's modified Eagle's medium (DMEM) supplemented with 10% fetal bovine serum (FBS). At 90% confluency the cells were gently scrapped, seeded in six-well plates at density of 0.5x10⁶ cells/well and incubated for 24 h in a humidified 5% CO₂ atmosphere at 37°C to allow for attachment. Before the experiment, the culture media was discarded from each well, 200 µl (1.5mg/ml) MSN1-FITC in DMEM supplemented with 10 % FBS were added to each well. After 1 h of incubation, cells on cover slips were washed three times with PBS and fixed in 4% paraformaldehyde for 1 h, washed twice with PBS before mounting with Flouromount-G fluid (Southern Biotechnology Associates Inc.). Intracellular localization of silica was visualized using a Zeiss LSM 510 laser scanning microscope.

7.4 RESULTS AND DISCUSSION

SEM was used to determine the particle size, particle morphology and the size distribution of the samples. Figure 7.2. shows morphologies of the sample MSN-1. It could be seen that sample MSN1 were regular spheres with smooth surface. The diameters of these materials were about 150-200nm.

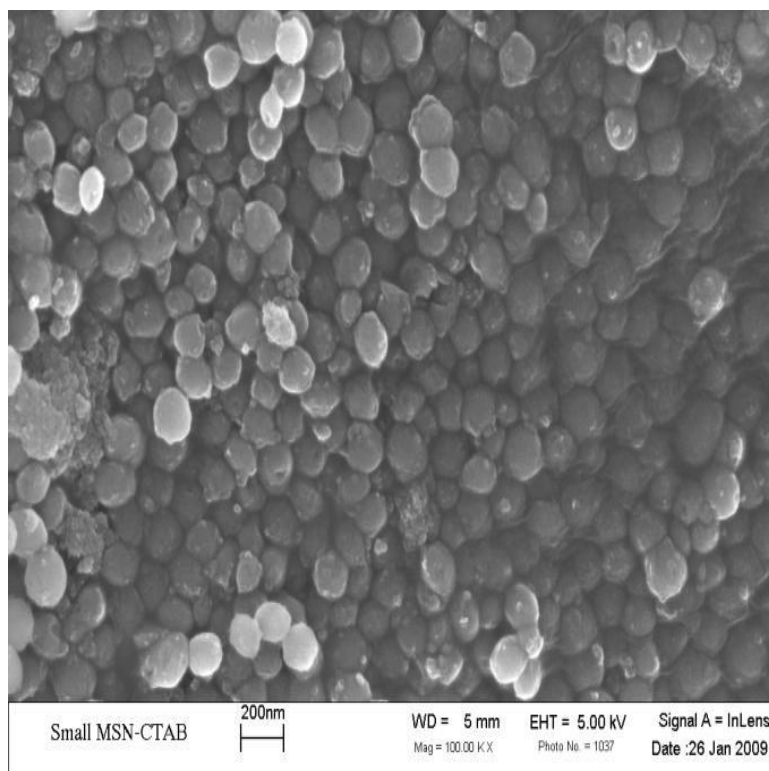


Figure 7.2. SEM image of mesoporous silica particles (MSN1).

TEM study (Figure 7.3.) was performed to further determine pore geometry structure, showing that MSN-1 possess ordered pore system. Furthermore the particles appear roughly spherical in shape.

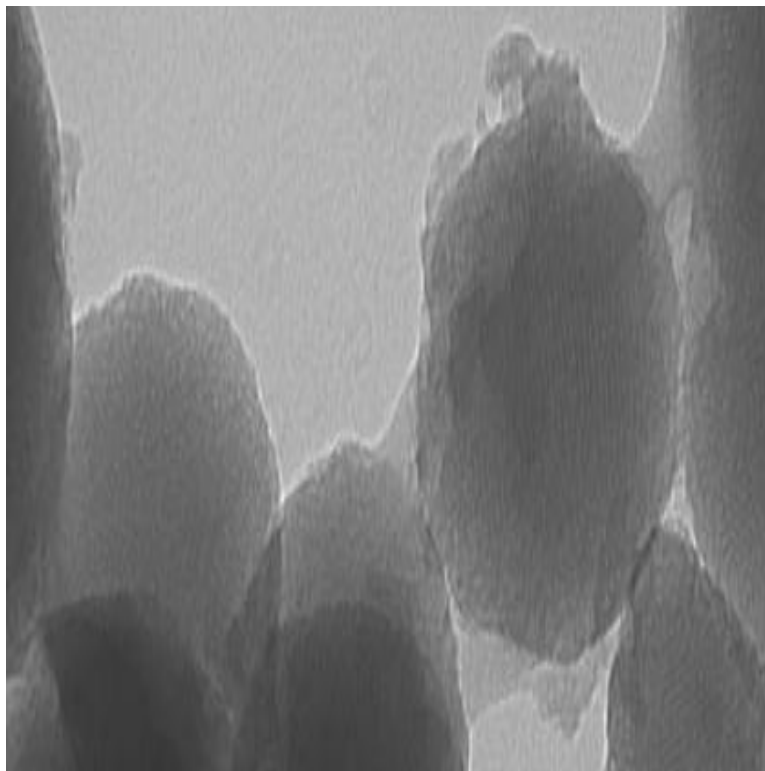


Figure 7.3. TEM image of mesoporous silica nanoparticles (MSN1)

Figure 7.4. show the FTIR spectra for undiluted ciprofloxacin, MSN1 and MSN2 samples after drug loading. For MSN1 and MSN2, the characteristic absorption bands for silica such as Si-O-Si asymmetric stretching vibration ($1000-1250\text{cm}^{-1}$), Si-O bending vibration around 800cm^{-1} , and Si-OH vibration at 950cm^{-1} all well corresponds to formation of silica. Furthermore, the peaks between 1275 and 1655cm^{-1} found in the spectrum of neat ciprofloxacin can be found in same wave number in the spectrum of MSN1 and MSN2. The above observations strongly indicate that the immobilized ciprofloxacin in the mesoporous may chemically bond with silanol groups on the surface of silica

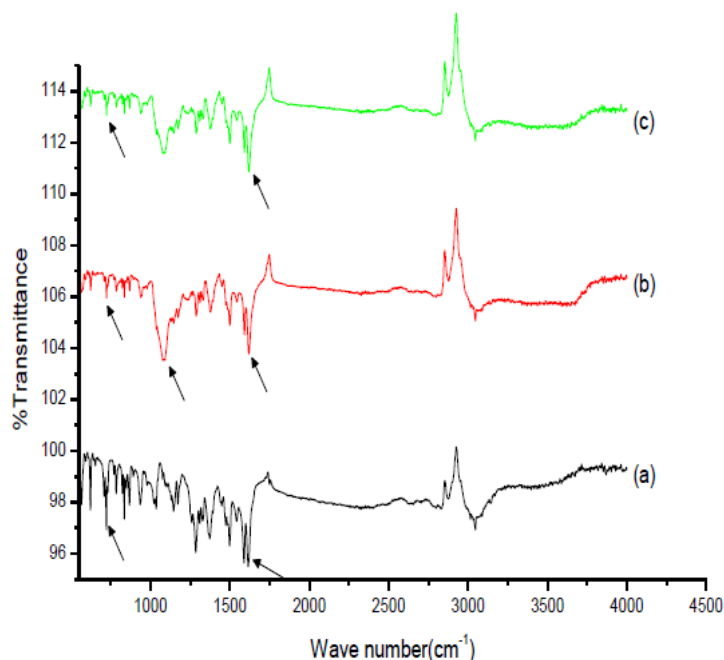


Figure 7.4. FTIR spectra of ciprofloxacin drug (a), MSN1-ciprofloxacin (b), MSN2-ciprofloxacin (c).

Figure 7.5. shows the TGA curves for mesoporous silica nanoparticles, MSN1 and MSN2. For comparison the MSN1 and MSN2 particles loaded with ciprofloxacin drug was also shown. The weight loss observed before 120°C, was due to removal of residual water. By comparison of empty mesoporous silica particles and mesoporous silica/ciprofloxacin, the encapsulation of the drug amount was calculated to be MSN1-5.26 wt% and MSN2- 11.8 wt%. This weight % corresponds to the weight loss between 0 to 1200° C and calculated after deducting the weight loss of empty MSN1 and MSN2 in the same temperature range. Finally the calculated amount(weight%) of drug loading for MSN1-8.4% and MSN2-(14%).

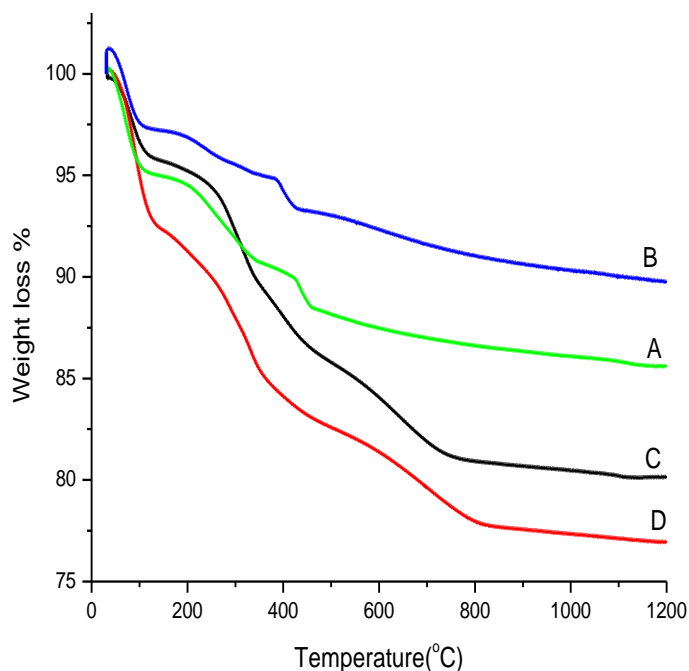


Figure 7.5. TG curves of (A and B) Empty MSN1 and MSN2, (C and D) mesoporous silica nanoparticles MSN1 and MSN2 encapsulating ciprofloxacin drug.

Figure 7.6. shows the N_2 adsorption-desorption isotherms and the corresponding BJH pore size distribution for MSN1 and MSN2. According to the IUPAC nomenclature shape of isotherms observed for MSN1 and MSN2, it can be classified as type IV isotherms [19]. Both the samples show a linear increase in the adsorbed value at low pressures followed by a capillary condensation within the relative pressure range between $0.4 < P/P_0 < 0.5$. This indicates the presence of mesopores [19, 20]. In between the pressure range of $0.5 < P/P_0 < 0.9$, the two samples show different behaviour,

- (i) The isotherm for MSN-1 is relatively linear up to $P/P_0=0.9$, indicating that the pore size distribution is narrow and unimodal. Above $P/P_0=0.9$, a secondary capillary condensation occurs due to interparticulate pores i.e., empty voids between the formed particles [21].
- (ii) For MSN-2 particles, an increase of N_2 uptake is observed after first capillary condensation. This followed by a small loop for $0.4 < P/P_0 < 0.6$, indicates a bimodal pore distribution [21].

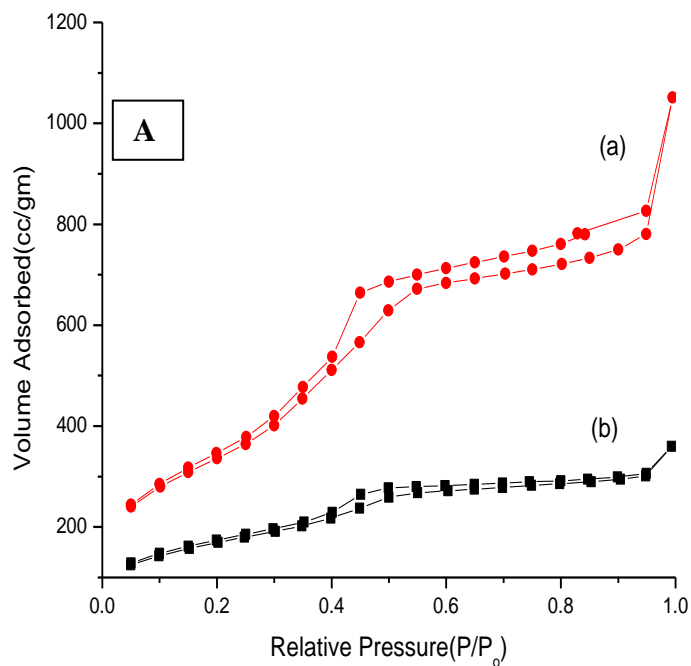


Figure 7.6. (A) Nitrogen adsorption/desorption isotherms of MSN1 and MSN2.

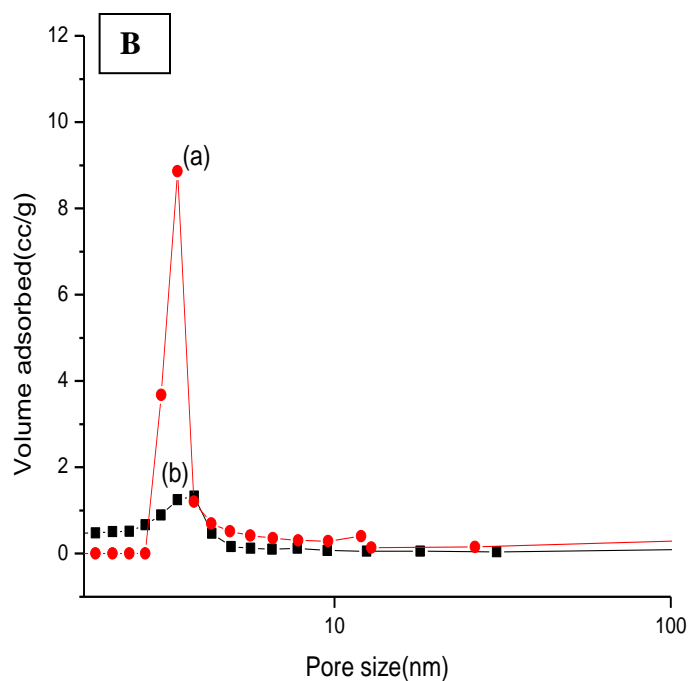


Figure 7.6. (B) Pore size distribution of (a) MSN1 and (b) MSN2

Table 7.1. show the BET surface area, pore volume and pore size for MSN1 and MSN 2 particles. The parameters obtained show that MSN1 presents a mean pore diameter of 3.4nm with a narrow pore distribution, while MSN2 has two distributions of pores: a narrow one centered at 3.4nm and a broad one around 12nm. Surface area measured for MSN 2 particles are higher than that of MSN1. This can be explained based on concentration of surfactants to TEOS ratio. With low concentration of surfactant, the amount of silica per surfactant will be higher and this leads to increase in thickness of the silica pore walls. The opposite is true with high concentration of surfactant, where amount of silica drastically reduces per surfactant molecule, which tends to form thin silica layer at the interface of organic surfactant molecule.

Table 7.1. Structure parameters of mesoporous silica nanoparticles (MSN1 and MSN2)

Sample	Surface area(m ² /g)	Pore volume(cm ³ /g)	Pore size(nm)
MSN1	649	0.53	3.4
MSN2	947	2.19	3.4

N₂ adsorption-desorption isotherms and the corresponding BJH pore size distribution of MSN1 and MSN2 after drug loading were shown in Table 7.2. After drug loading, the pore size distribution of the particles remains the same. However, the measured pore volume and surface area decreases for both the samples after drug loading. The reduction in pore volume and surface area could be attributed to loading of drug in the pores.

Table 7.2. Structure parameters of mesoporous silica nanoparticles (MSN1 and MSN2) after drug loading.

Sample	Surface area(m ² /g)	Pore volume(cm ³ /g)	Pore size(nm)
MSN1	274	0.33	3.4
MSN2	220	1.36	3.4

The drug release profile was measured for both the samples, MSN1 and MSN2. Both the systems exhibited sustained release property, however the measured drug release rate was different. Figure 7.7. shows the drug release profile for MSN1 and MSN2. For MSN1 system, there was fast release of the drug reaching 26% in first 3 h duration. Then, the drug release remains more stable for the remaining long release period, where 36 to 45% release was achieved for remaining 8 h duration. This property of sustained fast and slow release could be beneficial for maintaining the drug concentration and for meeting the requirement of a long-term treatment

effect. In contrast, for MSN2 sample, the total drug release % achieved for same period of 11h duration is ~60%. This in effect 15% higher release than MSN1 samples. However, the initial drug release for first 3 h duration remains the same reaching ~25%. The main reason for faster drug release could be attributed to increased pore volume and surface area. This property allows for closed packing of drug molecules within the pores and allows for further release of drug during the diffusion of dissolution medium in to the pores. However, further studies need to be done to get a much better understanding on the drug release kinetics and to study the influence of texture properties on drug release.

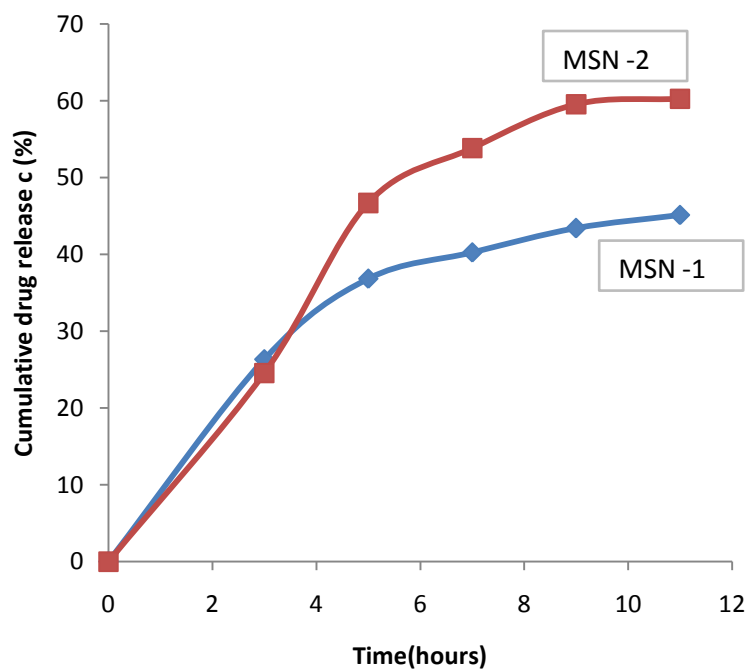


Figure 7.7. Cumulative Release Profiles for ciprofloxacin loaded on mesoporous silica particles of MSN1 and MSN2.

Confocal analysis

The MSN particles were successfully loaded with FITC. Confocal fluorescence images of macrophage cells (Figure 7.8.) clearly show the efficient uptake of the MSN-FITC, after 1 h of incubation.

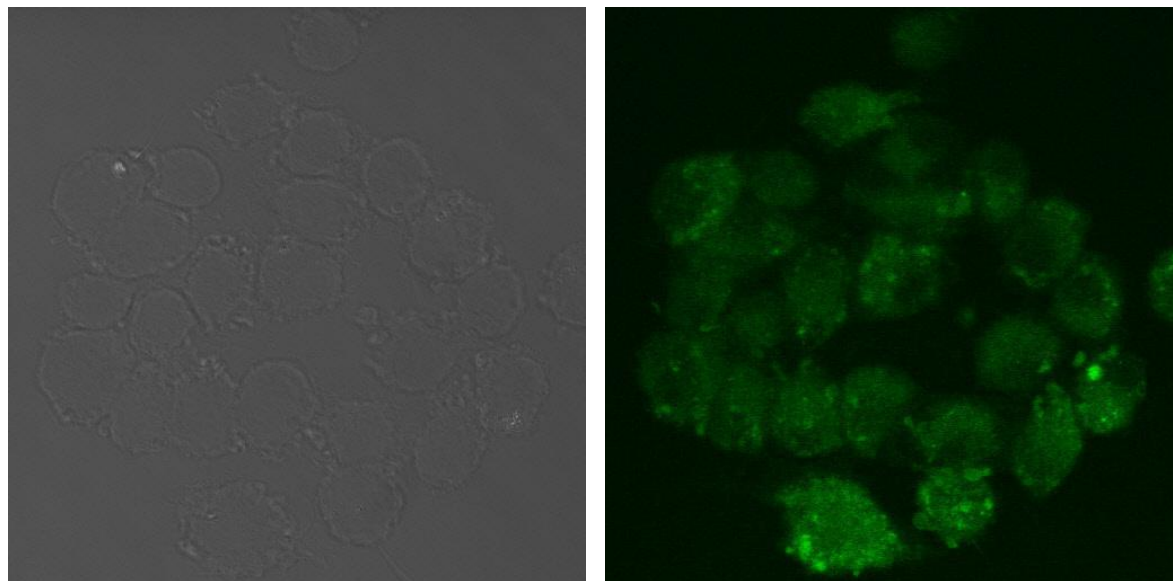


Figure 7.8. (Left) transmitted image of cell lines, (Right) endocytosed green fluorescent image of MSN/FITC.

7.5 CONCLUSION

The mesoporous silica particles, MSN1 and MSN2, were prepared using different surfactant concentrations. The texture properties, specifically the surface area and pore volume increases with template concentration. This allows for high loading of drug molecules. In addition to that, the drug delivery rate measured increases with high pore volume and surface area. This study shows the influence of surfactant concentration in improving the texture properties, which in turn affects the drug loading and drug release. This study also demonstrates the possibility of controlling the drug release velocity by choosing the adequate pore volume and surface area. Initial cell culture studies have shown the efficacy of the MSN particles to penetrate through the cell membrane.

7.6 REFERENCES

- [1] Y. Wan and D. Zhao. 2007. On the Controllable Soft-Templating Approach to Mesoporous Silicates. *Chem.Rev.* **107**: 2821-2860.
- [2] L. Hu, Z. Mao, C. Gao. 2009. Colloidal particles for cellular uptake and delivery. *J. Mater. Chem.* **19**: 3108-3115.
- [3] F. Qu, G. Zhu , H. Lin, W. Zhang, J. Sun, S. Li, S. Qiu. 2006. A controlled release of ibuprofen by systematically tailoring the morphology of mesoporous silica materials. *Journal of Solid State Chemistry.* **179**: 2027-2035.
- [4] S. Jin and K. Ye. 2007. Nanoparticle-Mediated Drug Delivery and Gene Therapy. *Biotechnol. Prog.* **23**: 32-41.
- [5] J.M. Rosenholm, A. Meinander, E. Peuhu, R. Niemi, J.E. Eriksson, C. Sahlgren, M. Linde. 2009. Targeting of Porous Hybrid Silica Nanoparticles to Cancer Cells. **3**: 197-206.
- [6] S. Perrault, C. Walkey, T. Jennings, H.C. Fischer, W.C.W Chan. 2009. *Nano Lett.* **9**: 1909-1915.
- [7] L. Wang, B. Yu, L. Sun, L. Ren, Q. Zhang. 2008. *Front. Mater. Sci.* **2(2)**:172-178.
- [8] C. Leca'roz, M.J. Blanco-Prieto, M.A. Burrell Gamazo. 2006. *Journal of Antimicrobial Chemotherapy.* **58**: 549–556.
- [9] A.R. Bender, H. von Briesen, J. Kreuter, I.B. Duncan, H. Rubsamen-Waigmann. 1996. Efficiency of nanoparticles as a carrier system for antiviral agents in human immunodeficiency virus-infected human monocytes/macrophages in vitro. *Antimicrob. Agents Chemother.* **40**: 1467–1471.

- [10] R. Löbenberg, L. Araujo, H. von Briesen, E. Rodgers, J. Kreuter. 1998. Body distribution of azidothymidine bound to hexyl-cyanoacrylate nanoparticles after i.v. injection to rats. *J. Control. Release.* **50**: 21–30.
- [11] D. Avnir, T. Coradin, O. Lev, J. Livage. 2006. Recent bio-applications of sol–gel materials. *J. Mater. Chem.* **16**: 1013-1030.
- [12] T. Coradin, M. Boissière, J. Livage. 2006. Sol-gel Chemistry in Medicinal Science. *Current medicinal chemistry.* **13**: 99-108.
- [13] H. Podbielska and A. Ulatowska-Jar'za. 2005. Sol-gel technology for biomedical engineering. *Bulletin of the polish academy of sciences technical sciences.* **55**: 261-271.
- [14] I. Slowing, B. G. Trewyn, V.S.-Y. Lin. 2006. Effect of Surface Functionalization of MCM-41-Type Mesoporous Silica Nanoparticles on the Endocytosis by Human Cancer Cells. *J. AM. CHEM. SOC.* **128**: 14792-14793.
- [15] I. I. Slowing, B. G. Trewyn, V.S.-Y. Lin. 2007. Mesoporous Silica Nanoparticles for Intracellular Delivery of Membrane-Impermeable Proteins. *J. AM. CHEM. SOC.* **129**: 8845-8849.
- [16] J. Lu, M. Liong, J.I. Zink, F. Tamanoi. 2007. Mesoporous Silica Nanoparticles as a Delivery System for Hydrophobic Anticancer Drugs. *Small.* **3**: 1341-1346.
- [17] W. Xu, Q. Gao, Y. Xu, D. Wu, Y. Sun, W. Shen, F. Deng. 2009. Controllable release of ibuprofen from size-adjustable and surface hydrophobic mesoporous silica spheres. *Powder Technology.* **191**: 13-20.
- [18] F. Qu, G. Zhu, H. Lin, W. Zhang, J. Sun, S. Li, S. Qiu. 2006. A controlled release of ibuprofen by systematically tailoring the morphology of mesoporous silica materials. *Journal of Solid State Chemistry.* **179**: 2027–2035.

- [19] R. P. Bagwe, L. R. Hilliard, W. Tan. 2006. Surface Modification of Silica nanoparticles to Reduce Aggregation and Nonspecific Binding. *Langmuir*. **22**: 4357-4362.
- [20] P. Zhang, Z. Wu, N. Xiao, L. Ren, X. Meng, C. Wang, F. Li, Z. Li, F.S. Xiao. 2009. Ordered Cubic Mesoporous Silicas with Large Pore Sizes Synthesized via High-Temperature Route. *Langmuir*. **25**: 13169-13175.

CHAPTER 8

MULTIFUNCTIONAL SILICA NANOCOMPOSITES FOR DRUG DELIVERY APPLICATIONS

A manuscript to be submitted to Journal of Biomaterials

8.1 ABSTRACT

The mesoporous silica/calcium/iron core-shell nano-composites were synthesized by the CTAB template based sol-gel procedure. The core-shell structure was successfully synthesized by coating silica/calcium/iron (70-25-5 wt %) on the surface of silica/calcium/iron (50-45-5 wt %) by a simple sol-gel process. The presence of silanol groups on the surface of the silica/calcium/iron (70-25-5) particles facilitates coating of silica/calcium/iron (70-25-5). The obtained core-shell structure maintains the mesoporous structure and size after surface coating. These particles were investigated as new drug delivery system using gentamicin as the model drug. Further characterization included Fourier transform infra-red spectroscopy (FTIR), N₂ adsorption-desorption measurements, and particle size measurements. The results indicated that the solubility rate of the shell and the core layer were different as anticipated. The solubility of these nano-composites can be adjusted by application of magnetic field. In addition to the presence of calcium, the mesoporous structure has the magnetic property which upon exposure to magnetic field further destabilizes the silica network. These observations were confirmed by size measurements. In addition, the silica/calcium/iron particles exhibit a stimuli-response drug release property, where upon application of a magnetic field, the iron particles undergo a reorientation within the network that allows for opening up of the pores and a faster release of the drug molecules.

8.2 INTRODUCTION

Recently, different nanomaterials are being widely investigated for drug delivery applications. Some of them include polymers, virus nanoparticles, and inorganic nanoparticles (silica, gold, etc) [1-5]. Each of these materials possesses unique properties. Among them, silica nanoparticles are attractive due to their versatile properties for drug delivery applications [6-10]. The porous silica particles can possess better control of the drug administration due to their tunable texture properties like surface area, pore volume and pore size. This allows for high loading of different biomolecules, enzymes or proteins [11-13]. One of the strong criteria for any materials to be used as a drug delivery carrier is the requirement that the material be non-toxic to the cells with long term exposures being limited by the potential degradability. This eliminates the problem of the accumulation of drug delivery materials inside the body. It is well documented that silica particles degrade as silicic acid in the presence of low pH conditions and cleared efficiently by the kidney with minimal toxicity [14]. Another important criterion for any material to be used as drug delivery carrier is the controlled rate of release of the drug.

Magnetic field controlled drug release:

To achieve controlled drug release, many different stimuli-response concepts have been developed including photo-controlled and reversible intermolecular dimerization of couamin derivatives, pH stimuli response controlled drug release system, ultrasound and organic modification of surface functional groups [15-18]. Among them, magnetic field controlled drug release is particularly attractive due to its ability of localizing the particles to reach the target site and then controlling the drug release rate by the application of a magnetic field. The magnetic field controlled drug release is an important property specifically for targeting and treating intracellular bacteria such as salmonella, brucella and mycobacterium [19, 20]. Since these

organisms have the ability to hide inside the host cells and by normal therapeutic delivery it is nearly impossible to localize the entire injected drug towards the required target site [21-23].

Solubility:

Since most of the magnetic silica nanomaterials have to be used inside the body, there could be a problem with large accumulation of the drug delivery carrier within the body. This could lead to the problem of surgical removal of drug carrier at different periods of time. Silica is known to have non-toxic degradable properties. Silica dissolves with time at different rates as silicic acid and gets excreted through the kidney. However, the rate at which silica dissolves is low and this may lead to have accumulation of the particles in long term treatment plans. A potential way of overcoming this problem is to modify the structural properties of the silica. We have shown that the addition of calcium within the silica network destabilizes it [24, 25]. This allows for a faster degradation and the rate of dissolution can be modified by the chemical composition of silica.

We propose a novel process to obtain core-shell silica/calcium/iron nano-composites via a simple sol-gel process. Gentamicin sulfate was used as the model drug and a novel drug storage/release system was fabricated by incorporating gentamicin into the channel of the nano-composites. To prevent the leakage of drug molecules, the outer surface was coated with degradable silica/calcium/iron composition which acts as a gate-keeper. Furthermore, the solubility and drug release properties of the system were also investigated with respect to the composition of the silica and the applied magnetic field.

8.3 EXPERIMENTAL SECTION

Materials

Chemicals: Tetraethylorthosilicate (TEOS), cetyltrimethylammoniumbromide (CTAB), Iron nitrate $\text{Fe}(\text{NO}_3)_2$ calcium nitrate $\text{Ca}(\text{NO}_3)_2$ and sodium hydroxide (NaOH) were purchased from Aldrich and used without further purification. Deionized water was used for all our experiments.

8.3.1 Synthesis of silica/calcium/iron nano-composites

The porous silica/calcium/Iron particles were prepared by a base-catalyzed sol-gel process. The silica/calcium/iron particles in the weight (%) ratio of 50-45-5 were prepared using CTAB as the template. As a first step in the synthesis, 480 ml of water was heated at 80° C for 10 min followed by addition of 1g of CTAB powder. The above solution was stirred until all CTAB was completely dissolved. To this solution 3.5 ml of NaOH (2 M) was added. After 2 h of stirring 9 ml of TEOS was added. After the TEOS addition, the solution started turning milky white which indicates the self-assembly of silicate within the CTAB template. To this solution, calcium and iron nitrate salts dissolved in 5 ml water was added. After addition of iron nitrate, salt the milky white solution turned to an orange colored solution. This solution was further stirred for another 2 h. Finally, the silica/calcium/iron nano-composites were isolated by centrifugation and the obtained orange precipitate was washed three times with water to remove excess unreacted material. The silica/calcium/iron nano-composites are further named as MSN1 in the upcoming sections.

8.3.2 Synthesis of core-shell silica/calcium/iron nano-composite

The core-shell nanostructures of silica/calcium/iron (50-45-5)-silica/calcium/iron (70-25-5) was prepared as follows: The calcium and iron nitrate salts were dissolved in water and stirred for 10 min at 80° C. To the above solution, ethanolic TEOS was added as the silica precursor which rapidly hydrolyzes and reacts with Ca and Fe cations. The pH of the above solution was maintained around 2 by the addition of concentrated NaOH. With the addition of NaOH, the orange colored solution turns brown in color. The above solution was stirred continuously for another 2 h at 80° C. To this solution, the template synthesized silica/calcium/iron (50-45-5) was impregnated. The stirring was continued until the evaporation of the ethanol from the suspension was sufficient to form the silica, calcium and iron nitrate coated porous silica/calcium/iron nano-composite. The resultant core-shell precursor powders were dried at 110° C to remove the residual ethanol and water. The dry precursor was calcined in air at 600° C for 5 h with a heating rate of 1° C/min to pyrolyze metal nitrates and remove the CTAB template. The core-shell silica/calcium/iron nano-composites are referred as MSN2 throughout the remainder of this document.

8.3.3 Drug loading studies

The gentamicin sulfate was used the model drug for drug loading and release studies. The drug loading was achieved by an impregnation technique. Initially, a certain amount of gentamicin sulfate was dissolved in water, and to this solution equal amount of silica particles were added and allowed to stand for 48 h under free flow of air. The drug gets adsorbed into the pores of the particles by diffusion. Finally the samples were dried in air. The thermal gravimetric (TGA) analysis was used to characterize the amount of drug loading.

8.3.4 Magnetic field controlled drug release studies

The *in-vitro* gentamicin drug release from the core-shell nano-composites were performed as follows: Initially, the sample with the concentration of 1mg/ml was immersed in to a glass vial containing phosphate buffer saline (PBS) solution. This particles immersed in the PBS solution was kept inside the magnetic field setup (Helmholtz coil). The setup was switched off in-between for 10 min to reduce the heat generated by the heating coils. At predetermined time intervals 3 ml of the dissolution medium was withdrawn. To maintain the equal volume of dissolution solution, the same amount of PBS was injected immediately. The UV-Vis spectrometry method was utilized to determine the drug release amount into the release media. For comparison, the drug release was also measured from particles not exposed to magnetic field and a similar procedure was followed as for magnetic field controlled drug release studies.

8.3.5 Magnetic field controlled solubility studies

The addition of iron within the silica/calcium allows the particles to be susceptible to a magnetic field. With application of the magnetic field, the particles could be heated. For the generation of the magnetic field a Helmholtz coil experimental setup was constructed. Currents were supplied by AC voltage supply. The magnetic field strength was calculated using the equation mentioned below. For solubility measurements the particles at a concentration of 1 mg/3 ml were used. For particle size measurements, the magnetic field was switched and 1 ml of the sample solution was used for particle size measurements.

The field value for a standard Helmholtz coil can be calculated from the simple equation:

$$B = \frac{\mu NI}{R}$$

where:

B is magnetic flux density in gauss,

μ is permeability, where $\mu = \kappa \mu_0$

κ is relative permeability and μ_0 is magnetic permeability in air

N is number of turns in each one of the two coils,

I is the current (amperes) in series (aiding) connected coils, and

R is the coil radius in centimeters.

The magnetic flux density (B) or field strength (H) is directly proportional to the applied current in the coils. Thus, the field can be accurately defined as a function of the current.

8.3.6 Characterization of magnetic mesoporous silica/calcium/iron nano-composite

The following techniques were used for characterizing the magnetic mesoporous silica/calcium/iron nano-composite. The chemical composition of the nanocomposites was characterized using FTIR analysis. For the FTIR analysis, the particles were used in powder form. The FTIR analysis is useful to determine any bond linkages within metallic cations and silica. The solubility of the outer coating silica/calcium/iron layer was characterized using particle size measurements. The solubility of the particles was measured both with and without applying magnetic field. The initial size of the particles and thickness of outer layer coating were measured using particle size analyzer. The porosity was measured using N₂ adsorption-desorption technique for the particles before and after coating. Before N₂ adsorption-desorption measurements the

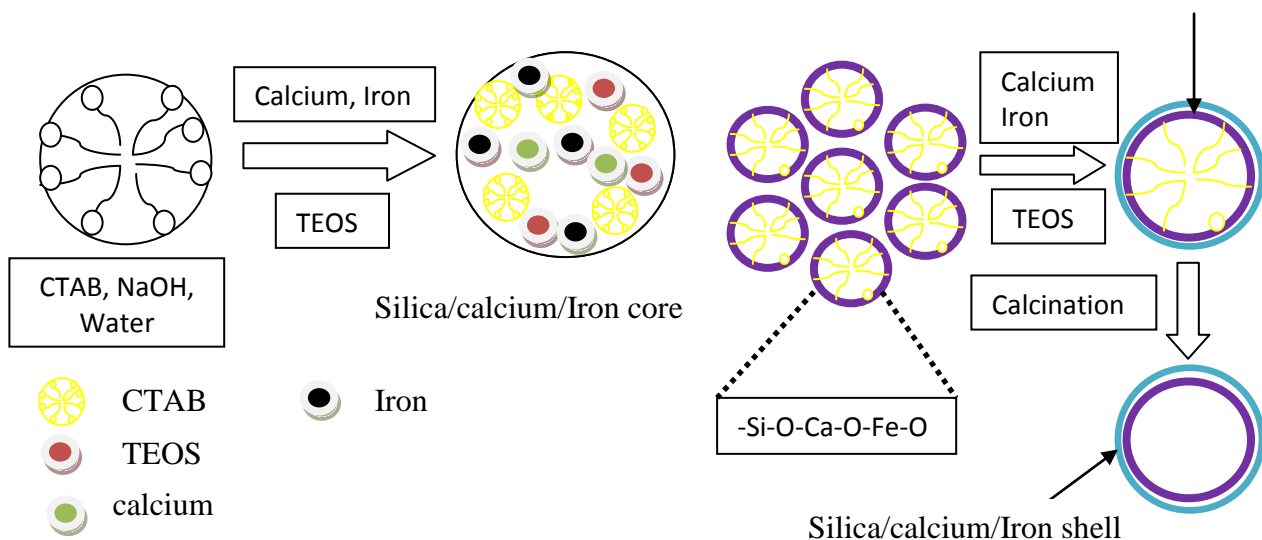
particles were degased at 200°C for 7h to remove and residual water in the pores. The magnetic field measurements were performed using homemade Helmholtz coil which can generate up to 50-100kA/m.

8.4 RESULTS AND DISCUSSION

Mechanism of formation of mesoporous silica/calcium/iron nano-composites

The Figure 8.1. shows the mechanism of formation of mesoporous silica/calcium/iron nano-composites. Initially, the surfactant CTAB molecules undergo a self assembly process to form a self-assembled micelle under basic sol-gel condition. Upon addition of TEOS, the forming silica polymer chains self-assemble within the formed CTAB micelle. Additionally, nitrate salts of calcium and iron present in the solution undergo a hydrolysis process and breaks down to Fe^{2+} and Ca^{2+} . The silica polymer chains which self-assembled on the CTAB micelle provides a large number of surface OH groups which favors the molecules of calcium and iron to get reacted on to the silica network. This mechanism allows for formation of Si-O-Ca-O-Fe-O-Si- bond linkages under basic condition and the clusters of calcium and iron are incorporated in the silica chain network. Hence addition of calcium and iron acts as a network modifier and based on the amount of dopants (Ca, Fe) included, the mesoporous structure formed within the silica will be affected. The FTIR analysis confirms the process of formation and existence of Si-O-Fe and Si-O-Ca bonds and is in good agreement with this mechanism. Therefore, the sol-gel techniques allow for incorporation of the dopants in the silica walls.

Furthermore, the surface coating (core) layer of silica/calcium/iron was achieved by an additional sol-gel step process. The core layer of the silica/calcium/iron with CTAB template has a negatively charged surface due to the base catalyzed sol-gel process. These particles up on immersion in the solution containing TEOS, calcium and iron nitrate along with NaOH, gets precipitated as Ca^{2+} and Fe^{2+} with $[\text{SiO}_4]^{4-}$ and OH^- in parallel. Finally, during the calcinations process, for removal of CTAB template, the surface attached calcium and iron cations undergoes dehydration and structural rearrangement process for forming -Ca-O-Fe-O on the silica surface.



Scheme 8.1. A schematic on the Mechanism for the formation of mesoporous silica/calcium/iron nano-composites. Step 1: Surfactant molecules cluster together to form micelles, as their hydrophobic tails tend to congregate and their hydrophilic heads provide protection in water, Step 2: Addition of inorganic precursor materials (TEOS, calcium and iron) gets deposited on surfactant micelles and condense to form $-\text{Si-O-Ca-O-Fe-O}$ inorganic network. Step 3: Surface coating of mesosphere silica/calcium/iron with another layer silica/calcium/iron. The presence of silanol groups on the core particles facilitates further coating on the surface of core particles.

FTIR analysis

The FTIR spectra for MSN2 particles before and after loading of gentamicin drug are shown in Figure 8.2. For comparison the pure mesoporous silica particles and gentamicin drug is also provided. Other than pure gentamicin, all of the spectra show the characteristic stretching vibration ($900\text{-}1300\text{cm}^{-1}$), and Si-O bending vibration around 800cm^{-1} . The mesoporous silica/calcium/iron nano-composites before and after drug loading showed Si-O-Si asymmetric stretching vibration at a range of $\sim 1070\text{-}1080\text{ cm}^{-1}$. This is lower in wave-number compared to

pure silica, where intense bands are observed in the range of 1000-1300 cm^{-1} and with an intense absorption band centered at 1100 cm^{-1} and a shoulder around 1220 cm^{-1} . Similar results were reported by Serra et.al where they have observed $-\text{Si-O-Si}-$ adsorption with maximum intensity at 1055 cm^{-1} and formation of a new band at 890-975 cm^{-1} . Hence it is possible that, addition of alkali and alkaline earth oxides could modify the silica network in such a way that Si-O groups are involved in forming the network structure by influence of bridging and non-bridging oxygen via $[\text{SiO}_4]$ tetrahedral structure.

Therefore, the presence or addition of the metallic cations during the formation of the silica network leads to formation of SiO- groups which then tends to increase the number of non-bridging oxygen and shifting of the Si-O-Si adsorption band to longer wavelength occurs. Additionally, the reason behind the band shift of Si-O-Si symmetric stretching vibration can be related to the change in Si-O-Si bond angle, which depends on the effect of the metal cations in the silica structure. As a further confirmation, an additional band is observed $\sim 857\text{cm}^{-1}$ and 962cm^{-1} and can be assigned to the Si-O-Ca vibration band and Si-O-Fe bands, which represents replacement of silicon atoms with iron and calcium atoms. These results indicate the formation of $-\text{Si-O-Ca-O-Fe-O}$ inorganic network.

The Figure 8.2. (b) shows the FTIR spectra for drug loaded silica/calcium/iron samples. It is very clear that additional bands at 850 and 970 cm^{-1} appear for gentamicin loaded nanocomposites. This corresponds to the loading of gentamicin within the porous channels. Furthermore, the intense absorption bands at 1220 cm^{-1} of pure silica and silica/calcium/iron diminished after loading gentamicin suggesting the formation of hydrogen bonds between the functional groups of gentamicin and silanol groups of mesoporous silica. The additional peaks

observed at $1400\text{-}1600\text{cm}^{-1}$ and C-H peaks at $\sim 3000\text{cm}^{-1}$ confirms that gentamicin has been loaded in the mesoporous silica/calcium/iron system.

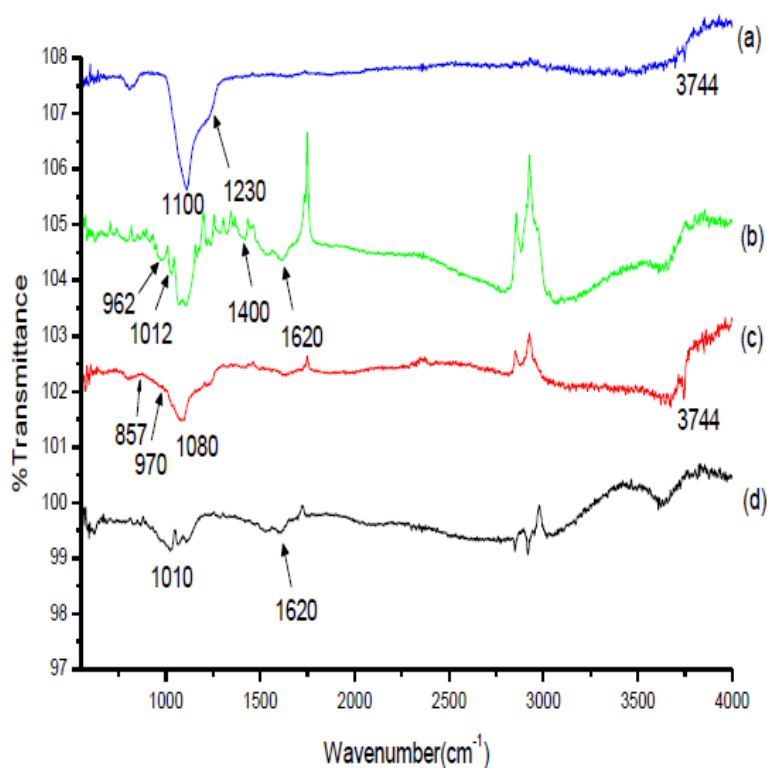


Figure 8.2. FTIR spectra for silica/calcium/iron nano-composites mesoporous silica (a), mesoporous silica/calcium/iron-gentamicin (b), mesoporous silica/calcium/iron (c), and free gentamicin (d).

Texture properties of silica/calcium/iron

Figure 8.3. shows the N_2 adsorption-desorption isotherms for MSN1, MSN2 and MSN1 after drug loading and the inset shows the pore size distribution of MSN1 and MSN2. According to (International Union of Pure and Applied Chemistry) IUPAC nomenclature, the isotherms observed for all the samples can be classified as type IV. The hysteresis loop observed is of H1 types which relates to the hexagonal cylindrical channels. The MSN1 possesses high surface area

and large pore volume. Furthermore a well defined sharp step-up observed in the adsorption curve at a relative pressure (P/P_0) of 0.2-0.3 for MSN1 and MSN2. This could be attributed to the filling of the framework-confined mesoporous structure. From the N_2 adsorption-desorption measurements, it is evident that coating of silica/calcium/iron on the surface of silica and incorporation of the gentamicin did not modify the basic pore structure of the mesoporous inner core particles. Figure 8.3 (inset) shows the pore size distribution for the MSN1 and MSN2 particles. The MSN1 and MSN2 samples exhibit a broad pore size distribution with a sharp peak maximum at 3.4 nm. Additionally, there were no change in the N_2 adsorption-desorption curves for MSN1 samples before and after drug loading and this corresponds to encapsulation of drug molecules inside the channel of mesoporous silica carrier. This observation was consistent with the results of FTIR spectra.

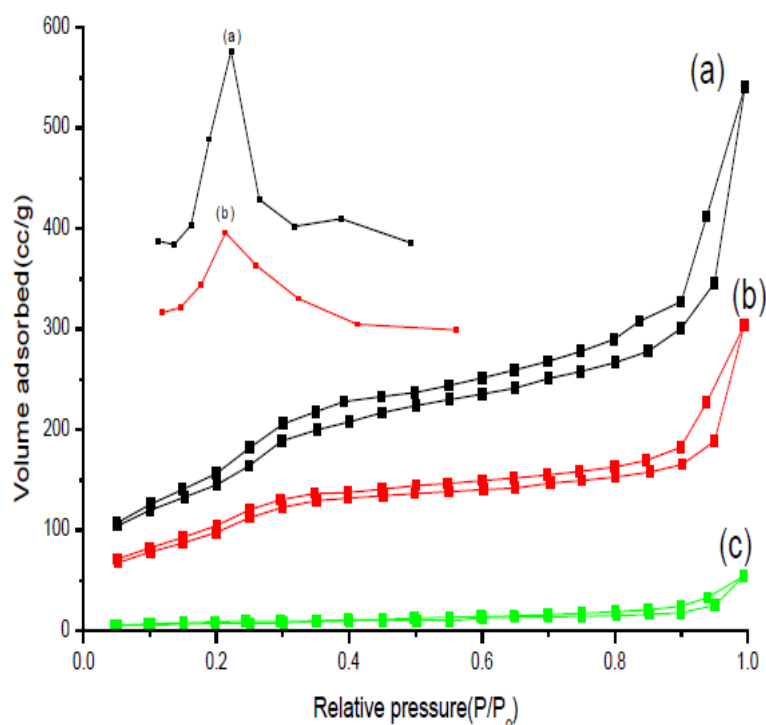


Figure 8.3. Nitrogen adsorption/desorption isotherms of (a) MSN1, (b) MSN2 and (c) drug-loaded MSN1 samples. Inset- Pore size distribution of (a) MSN1, and (b) MSN2.

The textural properties of the samples are summarized in Table 8.1. MSN1 samples had a high surface area ($161\text{m}^2/\text{g}$) and large pore volume (cm^3/g). The pore size measured was unchanged for MSN1. Coating or loading of the drugs in MSN1 or MSN2 doesn't block the open pore channels. As expected, loading of the gentamicin leads to a decrease in the surface area and the pore volume which confirms that the majority of the pores are being loaded with drug molecules. However, the surface area and pore volume decrease after coating and this could be attributed to the covering of the surface or by partial filling of the pores.

Table 8.1. Textural parameters of MSN1, MSN2 and gentamicin drug loaded MSN1 particles.

Samples	Surface area(m ² /g)	Pore volume(cm ³ /g)	Pore size(nm)
MSN1	161	0.6	3.4
MSN2	54	0.29	3.4
MSN1-drug	12	0.09	3.4

Solubility of silica/calcium/iron (50-45-5)-silica/calcium/iron (70-25-5) with and without magnetic field

The solubility of the surface coating (70-25-5) with and without magnetic field was measured. Figure 8.4. show the solubility of the surface coating layer with application of magnetic field. For comparison, the solubility of surface layer was also determined without application of the magnetic field. For measuring the thickness of coating layer a size comparison was made between coated and uncoated particles. In comparison to the uncoated particles (size – 120-125nm), the measured coated particle size was in the range of 170 nm. Hence, the thickness of coated layer was between 40-45 nm. For the magnetic field exposed particles, the size decreases from 170nm to 110 nm in 7 h duration. While for unexposed particles, the reduction in size is about 30nm for the same period of dissolution. From our previous studies, we observed the solubility of the silica nanoparticles can be altered by addition of the Ca²⁺ ions. With increase in the calcium content, the –Si-O-Si bond network is modified to –Si-O-Ca-O which destabilized the silica network and allows for solubility of the particles. Similarly, addition of Fe²⁺ within the silica/calcium network allows for having magnetic susceptible particles. Hence, with the application of the magnetic field, the –Si-O-Ca-O-Fe- bond network undergoes vibrational motion along with the magnetic

field. In addition to that, application of the magnetic field induces a heat effect within the particles which allows for increased solubility of the particles.

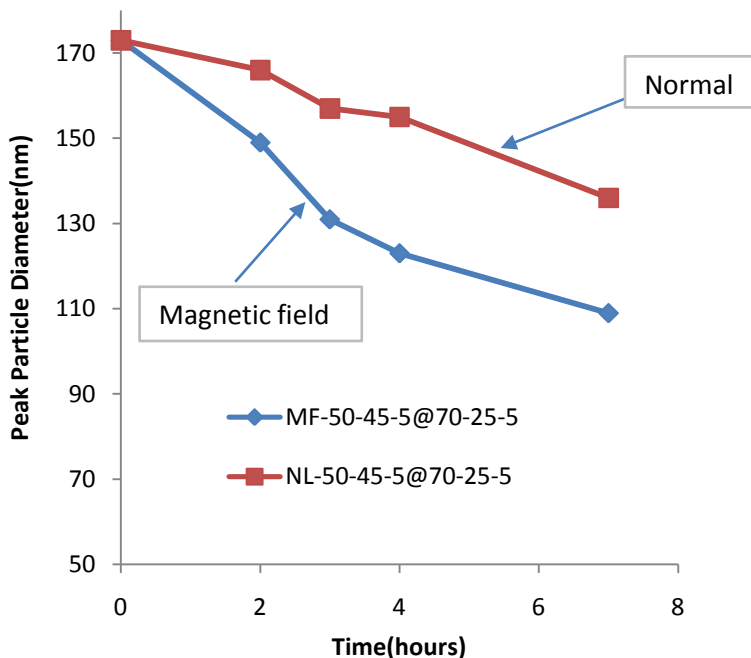


Figure 8.4. Particles size measurements for MSN2 particles. The solubility of the particles was investigated with and without exposure to magnetic field.

Drug release studies for silica/calcium/iron (50-45-5) @ silica/calcium/iron (70-25-5) with and without magnetic field

The drug release measurements were performed under *in-vitro* conditions. Two sets of particles were used for drug release measurements, one exposed to magnetic field without any stirring or heating. The other set of particles were immersed in dissolution medium and undergoes stirring process without application of magnetic field until the end of the experiment. To maintain *in-vitro* conditions, for particles unexposed to the magnetic field, the temperature was set to 37°C for the

whole set of experiments. Figure 8.5 shows the drug release profile for the particles exposed and unexposed to the magnetic field. For the particles unexposed to the magnetic field, there was no or minimal concentration of drug release for the first 3 h. After that the drug release rate started to increase, reaching ~35% in 22h. In comparison, the particles exposed to the magnetic field show a high drug release rate. There was no drug release for the first 2 h then there was a burst release reaching 30%. This possibly might be due to the release of drug molecules very near the pore entrance. Then the drug release rate stabilized with a final concentration of 50% drug release in 22h of time at the end of the experiment. This suggest that the presence of magnetic field allows for a much faster drug release than without the magnetic field. This could be explained by the formation of siloxane bonds with the inclusion of calcium and iron cations in the silica network. In addition to destabilization of the silica network with addition of calcium, the presence of iron makes the particles susceptible to magnetic field. This leads to increased solubility by breakage of -Si-O-Si bonds. Similarly by applying magnetic field, the silica bonds linkage undergoes a reorientation motion which may also allow to open up the pores within the silica network. This acts like an open channel for faster drug release. However, without magnetic field, the silica network breaks down at its own rate due to diffusion of dissolution medium without application of any external stimuli forces in this case magnetic field. The outer shell coating proves to be useful in triggering the drug release rate. The coating of the silica/calcium/iron over the particles allows stopping the drug release from the core particles. Additionally, this composition can be modified accordingly ranging from slow solubility up to very high solubility based on the composition of the particles. In our studies, we used silica/calcium/iron composition of 70-25-5 which allows for drug release after 3 h of duration for particles unexposed to the

magnetic field. Another advantage with this process is that addition of iron in the outer coating allows for controlling the solubility of the outer shell by exposure to magnetic field.

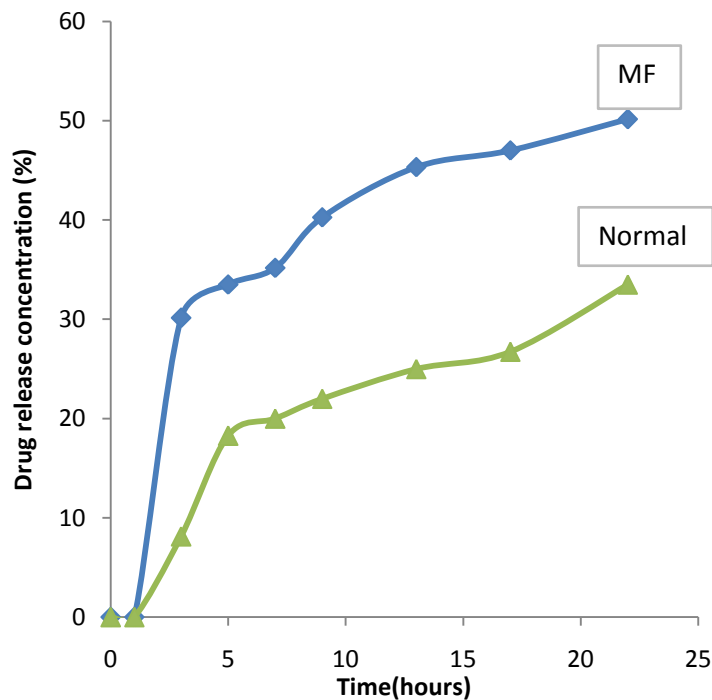


Figure 8.5. Cumulative release of gentamicin drug from mesoporous silica/calcium/iron nanocomposites. The drug release rate was altered by exposing the magnetic field to the particles. As a control group, the same particle without magnetic simulation was shown. The particles exposed to magnetic field shows faster drug release.

8.5 CONCLUSIONS

A new core-shell structured silica/calcium/iron nano-composites system was designed and synthesized for controlled solubility and stimuli-response drug release behavior. Some of the important properties of this core-shell nano-composite include ordered meso-pores for high drug loading, controlled degradation and magnetic field controlled drug release. One of the exciting developments in this research is that the leakage of drug molecules before reaching the target site can be controlled by adding a coating (shell layer) on surface of the porous inner core. This core layer acts as a gate-keeper which degrades at a controlled rate based on the composition of silica. Furthermore, the rate of dissolution of the shell can be tuned by the application of a magnetic field. Additionally, this multifunctional system provides a magnetic field-controlled drug release, which will be potentially useful for intracellular and targeted drug delivery applications. Considering the potential of this multifunctional controlled drug release system, the extension of the presented technique would be to investigate other silica/calcium/iron compositions that possess the property of controlled degradation and sustained drug release for bio-medical applications. The outer shell layer surface can further be coated with biocompatible natural polymers that would be useful for improving the biocompatibility of the particles specifically for *in-vivo* drug delivery applications.

8.6 REFERENCES

- [1] E. Nakamura, H. Isobe. 2003. Functionalized fullerenes in water. The first 10 years of their chemistry, biology, and nanoscience. *Accounts of Chemical Research*. **36**: 807–815.
- [2] E. Nakamura, H. Isobe, N. Tomita, M Sawamura, S Jinno, H Okayama. 2000. Functionalized fullerene as an artificial vector for transfection. *Angewandte Chemie International Edition*. **39**: 4254–4257.
- [3] E.E. Connor, J. Mwamuka, A. Gole, C.J. Murphy, M.D. Wyatt. 2005. Gold nanoparticles are taken up by human cells but do not cause acute cytotoxicity. *Small*. **1**: 325–327.
- [4] M.C. Garnett. 2004. Gene-delivery systems using cationic polymers. *Critical Reviews in Therapeutic Drug Carrier Systems*. **16**: 147–207.
- [5] T. Nowling, M. Desler, C. Kuszynski, A. Rizzino. 2002. Transfection of embryonal carcinoma cells at efficiency using liposome-mediated transfection. *Molecular Reproductive Devices*. **63**: 309–317.
- [6] D. Luo, E. Han, N. Belcheva, W.M. Saltzman. 2004. A self-assembled, modular DNA delivery system mediated by silica nanoparticles. *Journal of Controlled Release*. **95**: 333–341.
- [7] D.R. Radu, C.-Y. Lai, K. Jeftinija, E.W. Rowe, S. Jeftinija, V.S.-Y. Lin. 2004. A polyamidoamine dendrimer-capped mesoporous silica nanosphere-based gene transfection reagent. *Journal of the American Chemical Society*. **126**: 13216–13217.
- [8] S.G. Zhu, J.J. Xiang, X.L. Li, S.R. Shen, H.B. Lu, J. Zhou, W. Xiong, B.C. Zhang, X.M. Nie, M. Zhou, K. Tang, G.Y. Li. 2004. Poly (L-lysine)-modified silica nanoparticles for the delivery of antisense oligonucleotides. *Biotechnology of Applied Biochemistry*. **39**: 179–187.
- [9] F. Lu, S.H. Wu, Y. Hung, C.Y. Mou. 2009. Size Effect on Cell Uptake in Well-Suspended, Uniform Mesoporous Silica Nanoparticles. *Small*. **5**:1408-1413.

- [10] I.I. Slowing, J.L. Vivero-Escoto, C.W. Wu, V.S.-Y. Lin. 2008. Mesoporous silica nanoparticles as controlled release drug delivery and gene transfection carriers. *Advanced Drug Delivery Reviews*. **60**: 1278–1288
- [11] H. Frenkel-Muller and D. Avnir. 2005. Sol–Gel Materials as Efficient Enzyme Protectors: Preserving the Activity of Phosphatases under Extreme pH Conditions. *J. Am. Chem. Soc.* **127**:8077.
- [12] M.L. Ferrer, F. del Monte, D. Levy. 2002. A Novel and Simple Alcohol-Free Sol–Gel Route for Encapsulation of Labile Proteins. *Chem. Mater.* **14**: 3619.
- [13] N. Nassif, C. Roux, T. Coradin, O. M.M. Bouvet, J. Livage. 2004. Bacteria quorum sensing in silica matrices. *J. Mater. Chem.* 2004. **14**: 2264.
- [14] S. Radin, S. Falaize, P. Ducheyne. 2002. In vitro bioactivity and degradation behavior of silica xerogels intended as controlled release materials. *Biomaterials*. **23**: 3113–22.
- [15] Z.Y. Zhou, S.M. Zhu, D. Zhang. 2007. Grafting of thermo-responsive polymer inside mesoporous silica with large pore size using ATRP and investigation of its use in drug release. *J Mater Chem*. **17**: 2428–33.
- [16] Q. Yang, S.H. Wang, P.W. Fan, L.F. Wang, Y. Di, K.F. Lin. 2005. pH-Responsive carrier system based on carboxylic acid modified mesoporous silica and polyelectrolyte for drug delivery. *Chem Mater* 2005. **17**: 5999–6003.
- [17] N.K. Mal, M. Fujiwara, Y. Tanaka. 2003. Photo-controlled reversible release of guest molecules from coumarin-modified mesoporous silica. *Nature*. **421**: 350–3.
- [18] H.J. Kim, H. Matsuda, H.S. Zhou, I. Honma. 2006. Ultrasound-triggered smart drug release from a poly (dimethylsiloxane)-mesoporous silica composite. *Adv Mater*. **18**: 3083.

- [19] E. Briones, C.I. Colino, J.M. Lanao. 2008. Delivery systems to increase the selectivity of antibiotics in phagocytic cells. *Journal of Controlled Release*. **125**: 210–227.
- [20] B. Holmes, P.G. Quie, D.B. Windhorst, B. Pollara, R.A. Good. 1966. Protection of phagocytized bacteria from the killing action of antibiotics. *Nature*. **210**: 1131–1132.
- [21] M.C. Garnett. 2004. Gene-delivery systems using cationic polymers. *Critical Reviews in Therapeutic Drug Carrier Systems*. **16**: 147–207.
- [22] Z.P. Xua, Q. H. Zeng, G.Q. Lu, A. Bing Yu. 2006. Inorganic nanoparticles as carriers for efficient cellular delivery. **61**: 1027-1040.
- [23] G.P.H. Dietz, M. Bahr. 2004. Delivery of bioactive molecules into the cell: the Trojan horse approach. *Molecular and Cellular Neuroscience*. **27**: 85–131.
- [24] P. Munusamy, C. Suchicital, N. Sriranganathan, G. Pickrell. 2010. In-vitro Solubility Behaviour of Mesoporous Silica/Calcium Nano-composites for Drug Delivery. (Manuscript in preparation)
- [25] M.Vallet-Regí, C. Victoria Ragel, A. J. Salinas. 2003. Glasses with Medical Applications. *Eur. J. Inorg. Chem*. **6**: 1029-1042.

CHAPTER 9

GENERAL CONCLUSIONS

The research presented in this dissertation provides details about design and development of porous silica as a drug delivery carrier for treatment of salmonella infection. To study the suitability of the porous silica particles for intracellular drug delivery, sol-gel derived acid-catalyzed and acid-base catalyzed silica particles were designed. The sol-gel synthesis conditions and pore surface modification allows for control over the porosity, drug loading and drug release kinetics. Efficacy of the particles was tested in *in-vivo* studies, where these particles are successful in achieving high log reduction of bacteria in liver and spleen compared to untreated controls.

The application of delivering pharmaceutical cargo using nanocarriers may be further facilitated by designing site-specific stimuli response drug delivery systems. In this research work a magnetic field a controlled “ON-OFF” drug release system was developed. This new ON–OFF process of drug release methodology provides numerous possibilities in treating chronic diseases by intracellular pathogens where the particles could be designed for uncontrolled slow diffusion to a regulated release of (therapeutically effective) curative dosage after reaching the intracellular location in organs(liver and spleen) and where the pathogens reside.

To improve the degradability of the magnetic silica particles (silica/Fe), the biocompatible calcium cations were included within the silica network. The inclusion of calcium destabilizes the particle network and allows for controlled solubility of silica. The silica particle that contains a higher content of calcium degrades faster under *in-vitro* conditions. In comparison, the same particles with low calcium content possess very low solubility.

As a further advancement, novel core-shell silica/calcium/iron nano-composites were designed. These particles possess a special property of controlled drug release using “ON-OFF”

mechanism and solubility based on the concentration of calcium and iron. Furthermore, the addition of a shell layer with appropriate concentration of calcium and iron allows for blocking the drug leakage until reaching the target site. These attractive properties of controlled solubility and controlled drug release provide enormous potential specifically in intracellular drug delivery applications.

Furthermore, the work presented in this dissertation could shed some light for further development of stimuli-response porous silica nanoparticles as ideal intracellular drug delivery carrier. Additionally, there are several new properties can be included, such as appropriate surface functionalization for attachment of targeting ligands to reach required target site. Inclusion of optical probes within the outer surface of porous silica for intracellular trafficking applications.

Scientific contributions

1. Influence of sol-gel synthesis conditions in preparation of silica xerogel particles and its efficacy in killing of intracellular Salmonella is demonstrated.
2. A novel magnetic field “ON-OFF” switching mechanism has been developed for controlled intracellular drug release. This new phenomenon of magnetic drug targeting allows the release of drugs at a specific target site and has the potential to be applied to organs using magnetic field.
3. In addition to sol-gel synthesis conditions, the influence of template concentration on modifying the texture properties has been studied. This property should allow for high drug loading capacity by which we can minimize the drug dosage frequency and make use of toxic but potentially useful antibiotics.

A novel porous silica based core-shell nanostructure has been designed and developed for controlled solubility and intracellular drug release applications. This nanostructure provides the essential property of controlling or stopping the drug release until reaching the target site. Furthermore the silica particles have been designed to have controlled solubility rates based on the silica composition. This is a significant advancement because it combines the important properties of high drug loading, controlled drug release rate and controlled solubility of the drug delivery carrier, and this has not been reported in the literature.

Appendix: List of Abbreviations

Λ	Wavelength
S	Surface area
V	Volume
D	Diameter
N ₂	Nitrogen
Si	Silica
Ca	Calcium
Å	Angstrom
μ	micro
SiO ₂	Silicon-dioxide
P/P ₀	Relative pressure
HCl	Hydrochloric acid
HNO ₃	Nitric acid
NH ₄ OH	Ammonium hydroxide
Cu	Copper
TMOS	Tetramethyl Orthosilicate
TEOS	Tetraethyl Orthosilicate
PEG	Poly (ethylene glycol)
IUPAC	International Union of Pure and Applied Chemistry
BET	Brunauer-Emmett-Teller
BJH	Barrett-Joyner-Halenda
PSD	Pore Size Distribution
TEM	Transmission Electron Microscopy
TGA	Thermal Gravimetric Analysis
NMR	Nuclear Magnetic Resonance
IR	Infrared Spectrum
PBS	Phosphate Buffer Saline
Rpm	Rotations per minute
MSN	Mesoporous silica nanoparticles
BDDT	Brunauer, Deming, Deming, Teller

FITC	Flourescin iso-thiocyanate
CTAB	Cetyl (trimethyl ammonium bromide)
EDX	Energy dispersive X-ray analysis
SUV	Small Unilamellar Vesicles
LUV	Large Unilamellar Vesicles
PLA	Polylactic acid
PGA	Polyglycolic acid
PLGA	Polylactic-glycolic acid
PMMA	Polymethyl methacrylate
DNA	Deoxyribonucleic acid
LD	Lethal dose
QD	Quantum dots
TGF	Transforming growth factors
CdS	Cadmium sulfide
CFU	Colony forming unit
UV-Vis	Ultraviolet-Visible
TSB	Trypic soy bath
TSA	Trypic soy agar
MTT	3-(4,5-Dimethylthiazol-2-yl)-2,5-diphenyltetrazolium bromide, a yellow tetrazole
PMS	Phenazine Methosulfate
CD-1	Family of glycoprotein's expressed on the surface of various human antigen-presenting cells
FBS	Fetal bovine serum
DMEM	Dulbecco's modified Eagle's medium (DMEM), which contains approximately four times as much of the vitamins and amino acids present in the original formula and two to four times as much glucose.